Aberrant expression of miR-133a in endothelial cells inhibits angiogenesis by altering the expression of key angiogenic genes.

Suhail Ahmed

A thesis submitted in fulfilment of the requirement of the University of Wolverhampton for the degree of Doctor of Philosophy

Research Institute in Healthcare Sciences

Faculty of Science and Engineering

University of Wolverhampton

DECLARATION

This work or any part hereafter has not previously been presented in any form to the University or to any other body whether for the purposes of assessment, publication or for any other purposes (unless otherwise stated). Save for any express acknowledgements, reference and/or bibliographies cited in the work, I can confirm that the intellectual content of the work is the result of my own efforts and no other person

The right of Suhail Ahmed to be identified as the author of this work is asserted in accordance with ss.77 and 78 of the Copyright, Designs and Patents act 1988. At this date copyright is owned by the author

SUHAIL AHMED

Abstract

Angiogenesis is a physiological process involved in the formation of blood vessels from pre-existing ones and is tightly regulated by a balance between pro- and anti- angiogenic signals. Disturbance to this balance is associated to human diseases characterised by excessive or insufficient angiogenesis. MicroRNA (miRNA) are small non-coding RNA molecules, which inhibit gene expression by inducing mRNA degradation or suppressing protein translation. Emerging evidence highlights a novel role for miRNAs as regulators of angiogenesis. In endothelial cells miR-133a is expressed at very low levels in physiological conditions however, increased expression of this microRNA in the endothelium has been strongly associated with cardiovascular disease. Previous studies have reported conflicting results regarding the effect of miR-133a expression in endothelial cells during blood vessel formation. The study involved assessing the specific effect of mature miR-133a strands in angiogenesis and the expression of endothelial angiogenic genes. The study evaluated the consequences of aberrant expression of miR-133a in endothelial cells via transfection of miR-133a-3p, -5p, or negative control mimics in primary endothelial cells. This significantly inhibited endothelial cell proliferation, migration, and tubular morphogenesis. The screened gene arrays were performed to identify genes involved in the regulation of signalling pathways, which play a key role in angiogenesis. The results have been further validated by qPCR, which revealed that aberrant expression of miR-133a-3p led to a decrease in the expression of genes encoding pro-angiogenic molecules, whilst increasing those with anti-angiogenic functions. Ingenuity Pathway Analysis of a network of genes differentially expressed in cells harbouring miR-133a-3p, predicted decreased cellular functions related to vasculature branching and cell cycle progression, underlining the inhibitory role of miR-133a-3p in angiogenic cellular processes. The results indicate that enhanced expression of miR-133a-3p in endothelial cells during cardiovascular disease impairs pro-angiogenic cellular processes by altering the expression of specific target genes. Therefore, the results suggest that controlled delivery of miR-133a-3p mimics in diseased endothelial cells may open new therapeutic interventions to treat

patients suffering from cardiovascular pathologies associated with excessive or insufficient blood vessel formation.

TABLE OF CONTENTS

ABBREVIATIONS

AGO- Argonaute

AMD- Age-related macular degeneration

ANG- Angiopoietin

BAD- Bcl-2 associated death promotor

bFGF- Basic fibroblast growth factor

CAD- coronary artery disease.

CDKs- Cyclin dependent kinase

CK- Creatine phosphokinase

CLI- Critical limb ischemia.

COX-2- Cyclooxygenase-2

CTD- Carboxyl terminus domain

cTnT- Cardiac troponin

CVD- cardiovascular disease

DAG- Diacylglycerol

DGCR8- DiGeorge syndrome chromosome region 8

***DLL4*- Delta like ligand 4**

DMEM- Dulbecco's modified eagle medium

DMSO- Dimethyl sulfoxide

EC- endothelial cells.

ECFCs- endothelial colony-forming cells

ECGM- Endothelial cell growth medium

ECM CAM- extracellular matrix and cell adhesion molecules

ECM- Extracellular matrix.

EGF- Epidermal growth factor

EGFR- Epidermal growth factor receptor

eNOS- endothelial nitric oxide synthase

EtBr- Ethidium bromide

ETCs- Endothelial tip cells.

FBS- Fetal bovine serum

FDA- Food and drug Administration

FGF- Fibroblast growth factor.

Flk-1- Foetal liver kinase 1

Flt-1- fms-like tyrosine kinase 1

gDNA- Genomic DNA

HDFa- Human dermal fibroblast adult

HEK293A- Human embryonic kidney 293

HGF- Hepatocyte growth factor.

HGFR- Hepatocyte growth factor receptor

HIF-1α- Hypoxia-inducible factor 1 alpha

HMEC-1- Human dermal microvascular endothelial cells

HSPG- Heparin sulfate proteoglycan

HUVEC- Human umbilical vein endothelial cell

IA- Intussusceptive angiogenesis.

IAR- Intussusceptive arborisation.

IBR- Intussusceptive branching remodelling.

IGF- Insulin like growth factor

IgG- Immunoglobin G

IL- Interleukin

IMG- Intussusceptive microvascular growth.

IP3- Inositol 1,4,5-trisphosphate

IPA- Ingenuity pathway analysis

IS- Ischemic stroke.

IV- intravenous.

Jag1- Jagged 1

KDR- kinase insert domain

LB- Luria broth

LVEF- Left ventricular ejection fraction.

MAPK- Mitogen-activated protein kinase

MCS- multiple cloning site

MI- Myocardial infarction

miRNAs- MicroRNAs

MMPs- Matrix metalloproteinases.

MT-MMPs- Membrane-type matrix metalloproteinases

MVO- Microvascular occlusion

NICD- Notch receptor intercellular domain

NO- Nitric oxide

NRARP- Notch-regulated ankyrin repeat protein.

NRPs- Neuropilins

PAD- Peripheral artery disease.

PAI-1- Plasminogen activator inhibitor-1

PBS1x- Phosphate buffered saline 1x

PDGF- Platelet derived growth factor.

PDGFR- Platelet derived growth factor receptor

PDR- Proliferative diabetic retinopathy

PGs- Proteoglycans

PHD2- Prolyl hydroxylase domain 2

PIP2- Phosphatidylinositol (4,5)- bisphosphate

PKB- Phosphorylate and activate protein kinase B

PLCγ- Phospholipase C-γ

PLGF- Placental growth factor

Pre-miRNAs- Precursor microRNAs

Pri-miRNAs- Primary microRNAs

RA- Rheumatoid arthritis

Rb- Retinoblastoma

RBP- RNA-binding protein

RISC- RNA-induced silencing complex

RLU- Relative light unit

RTKs- Receptor tyrosine kinase

SA- Sprouting angiogenesis.

SCF- Stem cell factor

SCs- Stalk cells

shRNA- Short hairpin RNA

siRNA- Short interfering RNA

STEMI- ST segment elevation myocardial infarction

STZ- Streptozotocin

svVEGF- Snake venom Vascular endothelial cell growth factor

TAE- Tris acetate-EDTA

TAM- Tumor-associated macrophages

TGF-α- Transforming growth factor alpha.

TGFβ-1- Transforming growth factor beta 1.

TIMPs- Tissue inhibitors of MMP

TNF-α- Tumour necrosis factor alpha

TSP-1- Thrombospondin 1

TSR- Thrombospondin type 1 repeats

uPA- urokinase-type plasminogen activator

VBM- Vascular basement membrane.

VEGF- Vascular endothelial growth factor.

VEGFR- Vascular endothelial cell growth factor receptor

VPF- Vascular permeability factor

VSMCs- Vascular smooth muscle cells

LIST OF FIGURES

i

LIST OF TABLES

Publications from this thesis

Publication of this study in Scientific Reports

Ahmed S, Kurusamy S, David ELS, Khan K, Kalyanakrishnan K, Ian-Gobo M, Kola TM, Wilkinson RN, Kannappan V, Wang W, Gómez MJ, Redondo JM, Cotton J, Armesilla AL. Aberrant expression of miR-133a in endothelial cells inhibits angiogenesis by reducing pro-angiogenic but increasing anti-angiogenic gene expression. Sci Rep (2022) Aug 30;12(1):14730. doi: 10.1038/s41598-022-19172-x.

Conference Abstracts

Suhail Ahmed[1], Satishkumar Kurusamy[1], Angel L Armesilla[1], James M Cotton[2] (2019) Functional and molecular analysis of aberrant expression of microRNA-133a in endothelial cells during cardiovascular disease **British society for cardiovascular research conference 3rd – 4th June 2019**

Suhail Ahmed[1], Ezra Leander Santhosh D[1], Sathishkumar Kurusamy[1], Angel L Armesilla[1], James M Cotton[2] (2019) MicroRNA 133a targets angiogenic gene expression in endothelial cells **Northern Vascular Biology Forum, which was held at Sheffield Hallam University on the 4th of December 2019**

Suhail Ahmed[1], Ezra Leander Santhosh D[1], Sathishkumar Kurusamy[1], Angel L Armesilla[1,*], James M Cotton[2,*] (2021) ABERRANT EXPRESSION OF MIR-133A IN ENDOTHELIAL CELLS ATTENUATES ANGIOGENESIS AND ALTERS THE EXPRESSION OF GENES RELATED TO NOTCH SIGNALLING, CELL MOTILITY, CELL ADHESION AND EXTRACELLULAR MATRIX BIOLOGY**. 71st Annual British Microcirculation & Vascular Biology Society Conference 2021.** I had the opportunity to perform a 10-minute oral presentation, however this was cancelled due to the COVID-19 pandemic.

ACKNOWLEDGEMENT

It is an honour and my pleasure to say that I was blessed to get this great opportunity to work with such an experienced and knowledgeable person who I am so grateful to have as my PhD supervisor Prof Angel Armesilla. His vast wisdom and wealth of experience have inspired me throughout my studies. This research would have not been completed without his support. He has stood by me from day one of this project and help me grow and fulfil this research. He is an Angel (by his name) who has been by my side throughout this journey and made me accomplish this research and got it published in the 5th most cited journal in the world, scientific reports. I would like to thank him from the bottom of my heart by giving me so much encouragement and trusting me to do this research. He has worked very hard to help me complete this thesis.

I would also like to thank my second supervisor Prof James Cotton for his kind support and guidance in helping me succeed. In addition, I would like to thank Manuel J Gomez for performing ingenuity pathway analysis experiment and allowing me to present it in my thesis. To my colleagues and all the laboratory staff who have always been there and supported me throughout this project. I say thank you so much for your never-failing assistance to me.

I would also like to thank all the research technical staff at the Research Institute in Healthcare Science (RIHS), University of Wolverhampton for all their support.

I thank my family and friends who have supported me in every way possible so that I can fulfil this research, I don't know how to thank them, but I promise to look after them all my life as whatever I am today is due to their support and encouragement in making me accomplish this dream.

I am grateful to the Almighty God, to give me such wonderful people who have been there for me throughout this research and supported me through my life. Thank you, Allah!!

Suhail Ahmed

Chapter 1

Introduction

Chapter 1 Introduction

1.1 Angiogenesis

Blood vessels formed from pre-existing vessel is a process known as angiogenesis. To effectively treat human problems such as cancer, ischemic cardiovascular diseases, and ocular diseases, new therapies must target angiogenesis (Zachary and Morgan, 2010). Capillary development is crucial to the remodelling of tissues during growth and adaptation. These responsibilities include controlling the movement of nutrients, oxygen, and waste. (Egginton and Bicknell, 2011). Both physiological and pathological conditions can lead to angiogenesis. In the following sections, it is demonstrated that in healthy conditions, angiogenesis is crucial for organ regeneration, wound healing, placenta growth, and embryogenesis. The strictly controlled process of angiogenesis involves balancing the activity of both positive and negative regulatory mechanisms. (Kazerounian and Lawler 2018). Blood vessel development and pro- and anti-angiogenic substances work together to control the physiological balance between inhibitory and stimulatory impulses. (Carmeliet and Jain, 2011). As shown in figure 1 when this equilibrium is altered pathological angiogenesis occurs, leading to abnormal blood vessel creation in numerous human disorders, which include diabetic retinopathy, rheumatoid arthritis, and psoriasis. Although there are several pro-angiogenic agents, the most prevalent and significant one is VEGF, a strong cytokine that regulates both physiological and pathological angiogenesis (Shibuya, 2012).

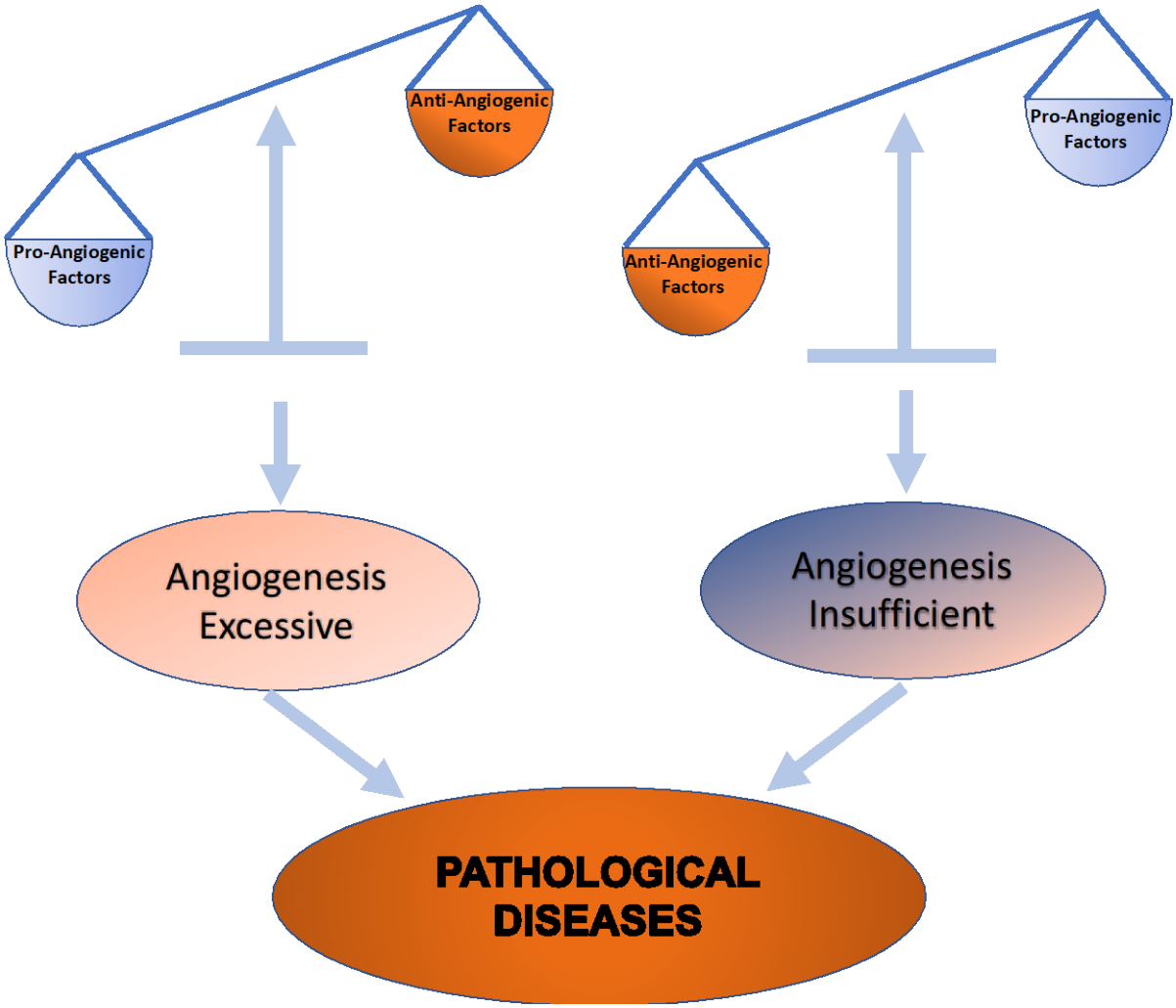

Figure 1: An example of how the imbalance of pro- and anti-angiogenic factors may lead to either excessive or insufficient angiogenesis, which in turn can lead to pathological diseases, that require angiogenesis to be enhanced or reduced.

1.1.1 Physiological Angiogenesis

1.1.1a Embryogenesis and Vasculogenesis

The initial vascular structures, or primitive blood islands, are made during development by mesodermal cells differentiating into hemangioblasts. While hemangioblasts from the island's perimeter differentiate into angioblasts, those from the island's centre differentiate into hematopoietic stem cells. The embryonic form of mature endothelium cells are called

angioblasts. The blood islands merge and transform into tubular structures, and the first rudimentary vascular plexus is formed thanks to the migration of newly formed endothelial cells and angioblasts induced by vascular endothelial growth factor (VEGF). The embryo becomes vascularised by a process called vasculogenesis, which changes the tubules into larger blood vessels. Contrary to vasculogenesis, intussusceptive angiogenesis (IA) and sprouting angiogenesis (SA) are two distinct kinds of angiogenesis (Swapna *et al.,* 2018).

1.1.1b Sprouting Angiogenesis

The expansion of a vascular network through sprouting Angiogenesis (SA) process requires many cellular functions such as quiescent endothelial cell activation, cell protrusion, extracellular matrix degradation, cell migration, cell proliferation, deposition of new basement membrane, cell junctions and cell polarity (Rosano *et al.,* 2020). A sophisticated mechanism called SA allows a vascular sprout to generate a new blood vessel from an already-existing channel. The process of sprouting angiogenesis is seen in figure 2 below. Angiogenic growth factors regulate this mechanism, which in a paracrine manner are expressed by hypoxic tissues (Carmeliet, 2005). By enabling proteins to extravasate and break the endothelial basement membrane, sprouting angiogenesis initiates with vessel expansion, enhanced vascular permeability, and builds a temporary scaffold for migratory cells (Carmeliet and Jain, 2011). This procedure enables the endothelial cells to split off and move in the direction of the angiogenic stimulus. A lumen is created because of endothelial cell proliferation. A vascular sprout develops and joins a blood vessel or another sprout. Endothelial cells ultimately reach a point of maturity when they stop proliferating and cling to the basement membrane, each other, and the pericytes surrounding them (Bouis et al., 2006). Three cell types known as tip, stalk and phalanx cells have been thoroughly examined make up angiogenic sprouts (De Smet et al., 2009). An angiogenic sprout is made up of a single tip cell that is located at the apex (tip) of the sprout. Numerous filopodia that make up the tip cell search the surroundings for angiogenic cues and lead the angiogenic sprout in that direction. A trail of stalk cells with a

faster rate of proliferation but no filopodia follow the tip cell. The development and lumenisation of the capillary basement membrane depend heavily on stalks cells. Phalanx cells are created as a consequence of the growth of stalk cells. Even though they multiply more slowly than stalk cells. Phalanx cells can create homogeneous monolayers of endothelial cells and strong barriers between the blood and surrounding tissues. Although they continue to strengthen tight connections and create the basement membrane, phalanx, and stalk cells both exhibit the same physical traits as dormant endothelial cells (De Smet et al., 2009).

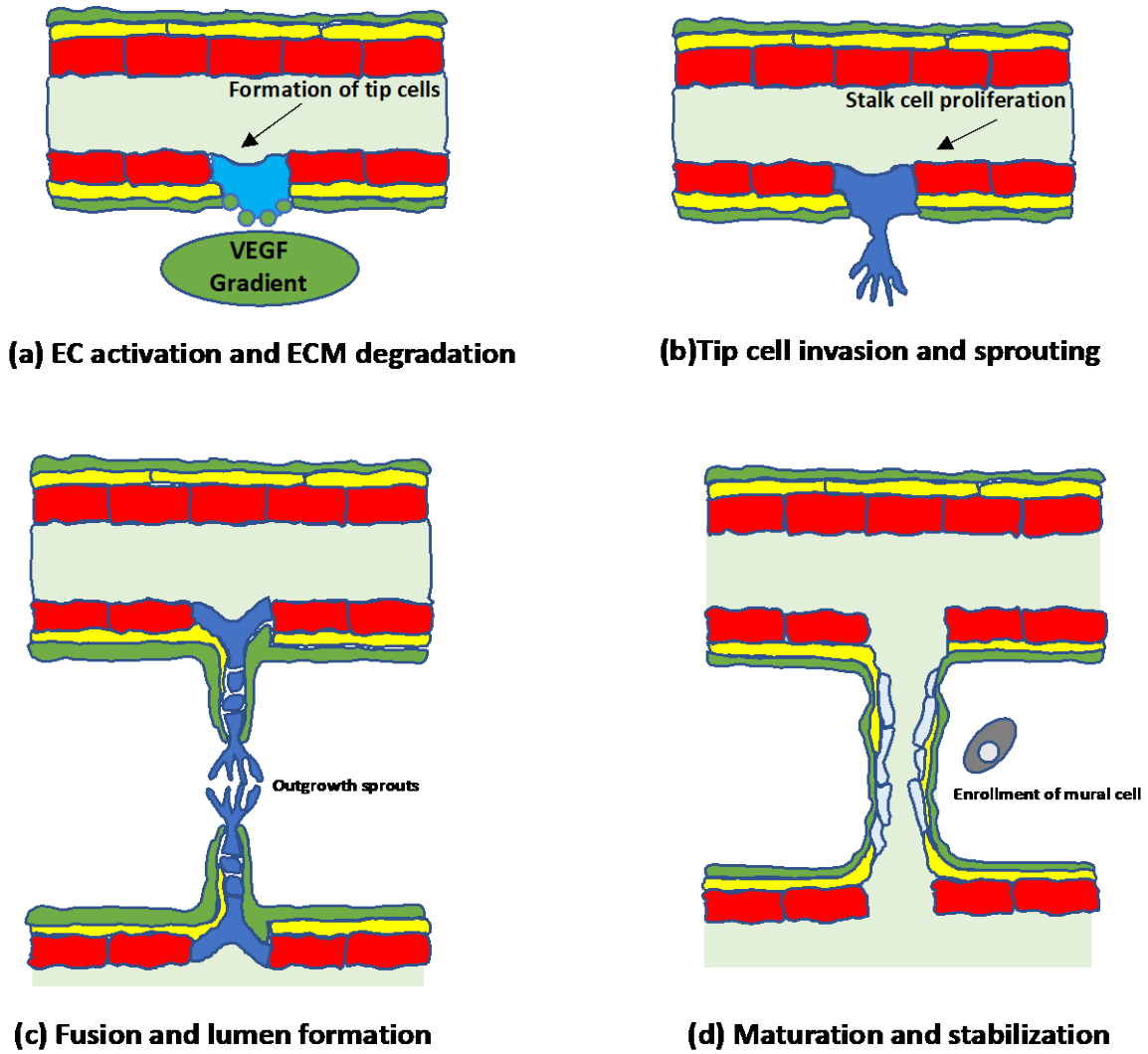

Figure 2: An example of sprouting angiogenesis (adapted from Ahmadi & Rezaie, 2020). (a) The balance of pro- and anti-angiogenic factors governs angiogenesis. For angiogenesis to start, the extracellular matrix must be degraded, and certain endothelial cells must be activated to act as tip cells. (b) As demonstrated, stalk cells that facilitate the development of

new networks are characterised by their strong proliferative capability, while tip cells exhibit filopodia and migrate toward angiogenic agents like VEGF. (c) To create a lumen, many sprouts are connected to one another by their tip cells. (d) Following the development of a new vessel, endothelial cells enter a state of quiescence, It is followed by the extracellular matrix being deposited, the development and stabilisation of mural cells, and so on.

1.1.1c Intussusceptive Angiogenesis

Splitting angiogenesis, also known as intussusceptive angiogenesis (IA), is a mechanism that is well known for creating transluminal tissue pillars and then splitting blood vessels. Intraluminal tissue pillars must be formed by a multistep process. An intraluminal pillar is created by the first migration of the opposing endothelial walls of the channel. (Burri and Djonov, 2002). In the subsequent step, the inter-endothelial connections are reorganised, and a central puncture is made in the centre of the pillar. When this occurs, pericytes and myofibroblasts penetrate the pillar and add extracellular matrix to it. The old capillary can split into two new capillaries in the final step due to continued expansion in pillar size, which fuses with one another (Burri and Djonov, 2002).

IA plays a key role in the formation of tumour vascular beds, tissue regeneration, and inflammatory diseases. (Hlushchuk *et al*., 2008). Different types of IA, which are, intussusceptive branching remodelling (IBR), intussusceptive microvascular growth (IMG), and intussusceptive arborization (IAR), result in subsequent development and remodelling, as shown in figure 3. IMG will cause a pre-existing vascular network to rapidly expand. This is accomplished by the emergence and growth of new pillars within the network, which leads to capillaries of the same size within the network. This kind of action, which is often driven by blood flow, results in the dispersed formation of many pillars. By fusing, splitting, and expanding the capillary network, these pillars will create the organ-specific architecture (Makanya *et al.,* 2009). It is possible to distinguish arterioles, venules, and capillaries thanks

to the IAR process, it allows a hierarchical vascular tree to be formed from a capillary network. IAR is best described as a thick network of capillaries with pillars separating the vessel supply from nearby capillaries in a continuous pattern. IBR, which is the third type of IA, changes the blood vessels' branching patterns or prunes the vascular network to maximise the number of arteries for effective blood delivery to tissues (Lee *et al.,* 2010). IBR happens when a tissue pillar develops at the junction of two blood arteries. With the connective tissues surrounding the arteries, these pillars develop and converge. As a result, the bifurcation becomes more proximally placed and narrows even more (Swapna *et al*., 2018).

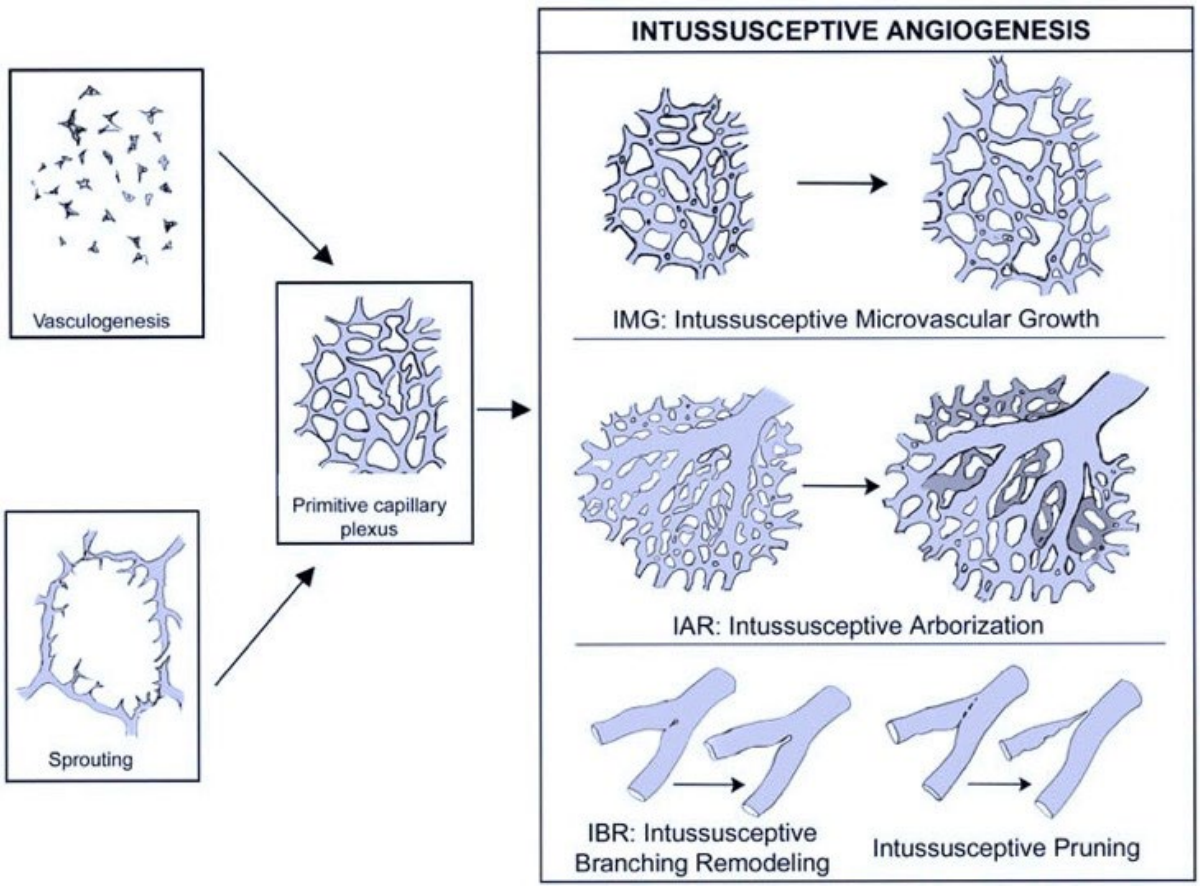

Figure 3: An example of Intussusceptive angiogenesis (adapted from Djonov et al., 2003). Intussusception begins when a primitive capillary plexus is generated by sprouting or vasculogenesis, which is responsible for initiating rapid vascular development and remodelling. Following that, IAR separates feeding veins from the capillary plexus. IBR manages vascular pruning and optimises branching geometry.

1.1.1d Wound healing

For wounds to heal, angiogenesis is essential. Capillary sprouts produced by moving endothelial cells break the vascular basement membrane underneath (VBM) to allow entry into the extracellular matrix (ECM) stroma and create networks of tube-like structures that keep expanding, branching, and forming (Honnegowda *et al.,* 2015). Endothelial cell proliferation causes capillary enhancement in the ECM, and chemotaxis from the target location directs the growth in that direction (Morgan *et al.,* 2007). Extracellular matrix synthesis and remodelling (maturation), inflammation, proliferation (tissue development), and Haemostasis (blood clotting) are the four stages of wound healing. Angiogenesis occurs in the proliferation phase between days 3 and 20 after the formation of a wound (Greaves *et al.,* 2013). The angiogenesis process is essential for supplying oxygen and nutrition to the wounded regions, mending any broken capillaries, and helping to remove any debris from the wound site. (Bauer *et al.,* 2005) (Greaves *et al.,* 2013). Between 3 and 7 days after the initial wound, the quantity of VEGF discovered in injured regions rises, highlighting the significance of this pro-angiogenic agent. When a wound is healing, new capillaries may invade it quickly and create an extensive web of blood vessels that is 2, 3, or even 10 times denser than healthy tissue. Numerous factors positively influence angiogenesis, but VEGF-A is by far the most significant one. Mammals have five members of the VEGF family which are VEGF-A, -B, -C, -D, and placenta growth factor. Numerous reports have shown VEGF-A is a crucial pro-angiogenic factor for wound healing, especially during the response to hypoxia. VEGF-A is a powerful pro-angiogenic mediator in addition to having the potential to increase vascular permeability and cause wound edema (Nagy *et al.,* 2008). Other chemicals that promote wound angiogenesis include cardiac ankyrin repeat proteins, platelet-derived growth factors, fibroblast growth factor-2, and TGF-family members (Shi *et al.,* 2005) (Uutela *et al.,* 2004) (Pardali *et al.,* 2010). Capillary regression occurs in wounds when pro-angiogenic stimuli are lost, and the healing wound produces various inhibitors of angiogenesis, including Sprouty2, CXCR3 ligands, and pigment epithelium-derived factor (Wietecha *et al.,*2011). The maturation

of capillaries is significantly influenced by the pericytes that produce selective capillary covering. Pericytes stabilise and safeguard capillaries from harmful signals (Kelly-Goss *et al.,* 2014).

1.1.2. Pathological excessive Angiogenesis

As mentioned in this thesis, angiogenesis is the formation of blood vessels from pre-existing vessels, which is tightly regulated by a balance of pro angiogenic and anti-angiogenic factors. An imbalance of pro angiogenic and anti-angiogenic factors lead to excessive angiogenesis. This leads to abnormal blood vessel development and blood vessels with leaks. This chapter demonstrates pathological diseases such as retinopathies, rheumatoid arthritis, and psoriasis, where there is more pro angiogenic factors compared to anti-angiogenic factors, leading to excessive angiogenesis.

1.1.2a Retinopathies

It has been known for some time how angiogenesis contributes to retinopathy. Higher amounts of VEGF have been found in the aqueous and vitreous fluid in the retina of retinopathy patients, and this has been shown to trigger abnormal development of new, highly permeable blood vessels in the patients' eyes (Cheung *et al.,* 2010).

Choroidal neovascularization in age-related macular degeneration (AMD) may also lead to aberrant retinal vessel growth (Kourlas and Abrams, 2007). This aberrant growth in AMD leads to vascular leakage and haemorrhage, which causes the retinal pigment epithelium to separate. This condition is more prevalent in older adults.

Diabetic retinopathy, a microvascular complication of diabetes, may result in blindness, haemorrhage, retinal detachment, and neovascular glaucoma (Duh *et al.,* 2017). According to studies, diabetic patients' retinal endothelial cells and pericytes express more VEGF when the

eye's hypoxic environment is present. Endothelial cells in the choroid undergo apoptosis as a result of excessive blood glucose levels, which causes vascular rarefaction and generates an environment that is low in oxygen inside the eye, that promotes the development of new blood vessels with leaks (Shin *et al.,* 2014). Proliferative diabetic retinopathy and non-proliferative are the two phases of the disease. A kind of diabetic retinopathy called proliferative diabetic retinopathy (PDR), which develops gradually and is linked to pathological angiogenesis (Williams *et al.,*2004). Epidermal growth factor (EGF), VEGF, and basic fibroblast growth factor (bFGF) (Ellis et al., 2004; Cross et al., 2001) are key pro-angiogenic molecules, that are essential for pathological angiogenesis which stimulate the migration and proliferation of vascular endothelial cells. A recombinant fusion protein made of Fc fragment antibodies coupled to the extracellular domains of VEGF receptor 1 (VEGFR1) and VEGF receptor 2 (VEGFR2) is being investigated as a therapy for diabetic retinopathy that includes neutralising VEGF. Patients with active PDR have high VEGF levels, which are found early in the illness and may further cause substantial vision loss. Pegaptanib sodium (Macugen), a well-known powerful VEGF inhibitor, is administered intravitreally to treat PDR and avoid severe vision loss as a result of the condition (Goldie et al., 2008). Key anti-VEGF therapies like bevacizumab and ranibizumab diminish neovascular growth and prevent vascular leakage; nevertheless, resistance to these medications is being observed in a number of PDR patients, necessitating the development of novel therapeutic strategies (Wenyi *et al.,* 2020).

1.1.2b Rheumatoid Arthritis

Increased angiogenesis has been linked with inflammatory disorders such as rheumatoid arthritis (RA) and other conditions. When angiogenesis occurs, the complex chronic systemic illness RA can cause synovial proliferation and progressive joint deterioration because it has inflammatory, autoimmune, and fibrovascular components (Szekanecz and Koch, 2008). Trans-endothelial leukocyte infiltration is elevated and encourages synovial inflammation, bone and cartilage degeneration, is made possible by excessive pro-angiogenic factors, which

balance out the angiogenic inhibitors in RA. According to research, synovial fibroblasts and macrophages are crucial for RA angiogenesis. The quantity of synovial macrophages can be used as a marker to track the severity of the disease and how well it responds to treatment. This is correlated with the quantity of myeloid cells in RA, which causes joint discomfort, synovial inflammation, and bone deterioration (Haringman *et al*., 2005). In the lining layer, the contact between RA fibroblasts and macrophages promotes the inflammatory signalling cascades that result in the production of IL-6 and IL-8. The severity of the illness causes the synovium to produce more VEGF (Sone *et al.,* 2001). The synovium grows in size and becomes inflamed during RA, which causes a hypoxic environment that stimulates VEGF gene production and angiogenesis. In addition to carrying nutrition and oxygen to sustain the development of synovial cells, Inflammation of the synovium is brought on by newly formed blood arteries that aggregate inflammation cells in the area (Marrelli *et al.,* 2011).

1.1.2c Psoriasis

An immune-mediated inflammatory condition called psoriasis raises the risk of cardiovascular disease (CVD) (Griffiths and Barker, 2007). Psoriasis may cause microvascular alterations in the plaque, such as substantial capillary dilatation, endothelial proliferation, and increased capillary permeability in the venous limb in the superficial dermis. Numerous minor bleeding points and shredded suprapapillary epithelium, which are thinned and show the papillary capillaries as elongated and dilated, due to the increased upper dermal vascularity. Skin examination reveals that the capillary bed's structural changes are the earliest discernible step of the pathogenesis of psoriasis (Guérard and Pouliot, 2012). Psoriasis patients may experience inflammation as a result of excessive capillary venular dilatation, which causes vascular alterations that signal the clearing of psoriasis plaques. Vascular enlargement in psoriasis plaques is brought on by inflammatory angiogenesis, which also limits vascular enlargement, elongation, and increased tortuosity while creating new development from the current vascular bed (Henno *et al.,* 2010). Research have shown that the variations in VEGF

isoforms inside the skin are a factor in the changes caused by psoriasis (Henno *et al.,* 2010). Microvascular endothelial cells experience a change in cytokine response during psoriasis, simulating the epidermal involvement of certain lesions and the configuration of plaque type. When TGF- enhances VEGF levels in a paracrine manner, keratinocytes are both clinically involved and uninvolved in skin patients with persistent, chronic plaque psoriasis. VEGFR1 and VEGFR2 are overexpressed in the dermal microvascular endothelium, skin wound healing, and hypersensitivity reactions in psoriasis. Patients with erythrodermic psoriasis, according to studies had higher VEGF levels in their plasma. Higher plasma VEGF levels were also seen in patients with mild to serious psoriasis and stable chronic plaque psoriasis (Malecic and Young, 2017).

1.1.3 Cancer-associated angiogenesis

Key separate biological mechanisms that differ across various tumour types and cancer tissues are where tumour vascularization occurs. Apart from endothelial cells, these activities require a variety of secreted substances and signalling pathways that are also present in progenitors or cancer stem cells. The use of tyrosine kinase inhibitors or antibodies in anti-angiogenic therapy, has been approved to treat a variety of cancers. Anti-angiogenic therapy has had only minimal success thus far since it only temporarily slows tumour growth until resistance sets in, with only minor survival advantages. Angiogenesis, which is often started from the capillaries, which is necessary for the development, spread, and upkeep of tumours. Numerous biological processes, including the ones mentioned above in this thesis, such as sprouting angiogenesis and intussusceptive angiogenesis, can cause the formation of blood vessels in tumours (Lugano et al., 2019). Haemangioma is a common benign vascular tumour, which is associated with excessive angiogenesis/vasculogenesis that early emerges from childhood. Apart from only occurring in the skin, it is also involved in other organs (Tang et al., 2021).

Haemangioma affects the appearance and psychology and in some specific functional organs, haemangioma leads to visual impairment, hepatic haemangioma bleeding, congestion heart failure and respiratory failure. Emerging evidence has shown that hypoxia induced vascular endothelial cell proliferation and abnormal angiogenesis are mainly involved in haemangioma. Hypoxia-inducible factor-1*α* (HIF-1*α*) and VEGF play a major role in vascular endothelial cell proliferation and abnormal angiogenesis and are highly expressed in haemangioma. A study by Tang *et al*, has demonstrated proanthocyanidins may be a potential novel way for the treatment of haemangioma. Proanthocyanidins are naturally active substance from plants and fruits, which possess multiple functions such as anti-proliferation, anti-angiogenesis, and anti-tumour. It has been shown in various diseases that proanthocyanidins inhibit the expression of various factors such as HIF-1*α,* VEGF, PI3K and Akt. They hypothesis the following, haemangioma, a common benign vascular tumour, which involves excessive angiogenesis and abnormal vascular endothelial cell proliferation. The main contributors of haemangioma are HIF-1*α* and VEGF, which causes an imbalance of pro-angiogenic and anti-angiogenic factors. HIF-1*α* activates VEGF, whereas proanthocyanidins suppresses HIF-1*α* and VEGF activation, which in turn prevents cell proliferation and angiogenesis. Taking all this together, proanthocyanidins may be a potential novel way for the treatment of haemangioma (Tang et al., 2021)

1.1.4 Pathological insufficient angiogenesis

An imbalance of pro angiogenic and anti-angiogenic factors leads to insufficient angiogenesis. This chapter demonstrates pathological diseases such as Ischemic stroke, coronary artery disease, and peripheral arterial disease, which require angiogenesis to promote blood vessel formation, improve blood flow and supply damage tissues with oxygen and nutrients.

1.1.4a Ischemic Stroke

Ischemic stroke (IS) is the leading global cause of mortality and disability, although there are currently no recognised causes and few effective treatments. IS can be effectively treated with thrombolytic therapy, which is administered intravenously and used to treat and dissolve potentially harmful blood clots in blood arteries, improve blood flow, and avoid damage to tissues and organs. Clot-busting medications like Eminase and Retavase are given right where the blockage is, through an intravenous (IV) line or a lengthy catheter. However, these drugs duration of efficacy is just a brief time, only a few patients can benefit from it, and it is not advised for people who use blood thinners (Zhou *et al.,* 2019). For the treatment of stroke, heart attack, and pulmonary embolism, healthcare professionals use this procedure as an emergency. Low blood pressure and internal bleeding are risks of thrombolytic treatment. While this therapy reduces the damage caused by a heart attack, pulmonary embolism, stroke, and frequently dissolves blood clots, more surgery may be necessary to address the underlying reasons (Baig and Bodle, 2022). Angiogenesis is crucial to IS because it can restore cerebral blood flow, which maintains the neurons and damaged tissues by supplying oxygen and nutrients. Occlusion or cerebral stenosis in a stroke result in focal cerebral ischemia. Blood flow in the brain tissue's cerebrovascular region abruptly decreases, which reduces the availability of nutrients and oxygen and causes damage or even death to tissue cells. The creation of new arteries is one possible method to increase the oxygen flow to ischemic brain tissue. Brain blood flow, regeneration, and neuron repair are controlled by

neovascularisation in the region of ischemic infarction (Pan *et al.,* 2010). The opening of the pre-existing vascular network is the initial step of IS, and new blood vessels are then developed after that. 3 days after IS, new blood vessel formation begins, and steady growth continues for at least 21 days (del Zoppo and Mabuchi, 2003). After a stroke, angiogenesis offers possible therapies. Studies on the brain tissue of stroke victims with varying levels of survival time have shown that the infarcted region's microvascular density is substantially higher than that of the hemisphere on the opposite side. New blood vessel growth around the infarcted area is favourably correlated with stroke patients' time to recovery, survival rate, and restoration of their neurological function (Krupinski *et al.,* 1994). Further studies have shown that dementia patients have lower cerebral blood flow in regions that are not infarcted, suggesting that angiogenesis increases cerebral blood flow to enhance patient everyday activities (Schmidt *et al.,* 2000).

1.1.4b Coronary artery disease

The main factor contributing to death and morbidity worldwide is coronary artery disease (CAD) (Wen *et al.,* 2018). Plaque build-up in the coronary arteries is the primary cause of CAD, which leads to damage or illness of a major blood vessel that provides the heart with blood, oxygen, and nutrients. Chest pain and myocardial infarction are caused by this build-up, which narrows these arteries and reduces blood flow to the heart (Hajar, 2017). Angiogenesis and CAD are related in both directions. Plaque angiogenesis is responsible for promoting plaque vulnerability and growth, which results in intraplaque bleeding. A plaque rupture is brought on by inflammatory cells, an excess of erythrocytes, and inflammatory cells inside a plaque, which leads to acute coronary syndrome. Inhibiting intraplaque angiogenesis would then be a viable therapeutic target for CAD. In individuals with CAD, encouraging angiogenesis has been employed as a therapeutic approach to encourage reperfusion to the ischemic myocardium and to increase the cardiac microvascular network. Protein therapy, which administers angiogenic growth factor directly, is one of the available treatments. To

boost the expression of angiogenic genes in vivo by gene therapy. To administer stem cells or exosomes, use cell therapy or cell-free therapy (Wen *et al.,*2018).

1.1.4c Peripheral arterial disease

After coronary artery disease and stroke, the third most common factor contributing to atherosclerotic cardiovascular morbidity is peripheral arterial disease (PAD). Age, hypertension, diabetes mellitus, elevated cholesterol, and smoking are risk factors for PAD. Walking with leg pain may be a sign of PAD (Fowkes *et al.,*2013). The term "critical limb ischemia" (CLI) refers to the most severe form of PAD, which is characterised by persistent rest discomfort or gangrene of the lower extremity and results in limb amputation and cardiovascular death in PAD patients (Farber and Eberhardt 2016; Fowkey et al., 2017). Examples of angiogenic cytokines that have been demonstrated to enhance limb blood flow and angiogenesis in animal models of PAD include angiopoietins, VEGF, hepatocyte growth factor (HGF), platelet-derived growth factor (PDGF), and fibroblast growth factor (FGF) (Morishita *et al*., 1999; Qian *et al.,* 2006; Ferraro *et al.,* 2010; Banfi *et al.,* 2012; Lekas *et al.,* 2012). The best well-researched pro-angiogenic factors mentioned previously is VEGF, which is essential for the migration, proliferation, and formation of endothelial lumens and is regulated by the receptors VEGFR-1 and VEGFR-2 (Ferrara *et al.,* 2003).

1.1.5 Cellular biology of angiogenesis

A successful angiogenesis as shown in figure 4 below involves key cellular events such as extensive interplay between extracellular matrix components (ECM), cells and soluble factors (Ribatti *et al.,*2012). Endothelial cells that line the luminal surface of stable vessel tubes create a monolayer of dormant cells when they are in a quiescent condition (Mazzone *et al.,* 2009). The connections between cells Pro-angiogenic substances cause the loosening of endothelial cell connections. This causes the existing artery to lose pericytes and/or smooth muscle cells.

This process results in the initiation of proteases such matrix metalloproteinases (MMPs) and plasmin, which promotes the endothelial cells to exit the surrounding tissue due to a rupture of the basement membrane and can then react to external signals (Carmeliet and Jain, 2011). The angiogenic stimulation, which results in the development of newly sprouting blood arteries, can be sensed by endothelial tip cells (ETCs). Filopodial extension, supported by certain pro-angiogenic growth factors, ephrin's, and semaphorins, encourages ETCs to sprout further (De Smet *et al.,* 2009). VEGF, bFGF, cytokines, chemokines, angiopoietins, and other pro-angiogenic inducers, all promote endothelial cell proliferation (Ucuzian *et al.,* 2010). Behind the ETCs, there is a trail of endothelial "stalk cells" (SCs), which help sprouting vessels elongate, form the vessel's trunk, and allow the parental vessel to be connected to the sprout (Iruela-Arispe *et al.,* 2009). When ETCs come into contact with another vessel, the anastomosis process causes them to lose their motility and fuse with the tip cell of the other vessel (Kamei *et al.,* 2006). Anastomosis mechanism still remains unknown; however, it is thought the anastomotic process is considered to be impacted by myeloid cells and some kinds of macrophages (Fantin *et al.,* 2010). For the last stage of angiogenesis to produce new capillaries, smooth muscle cells and pericytes must be recruited. These cells are stimulated by growth hormones including transforming growth factor-1 (TGF-1) and platelet-derived growth factor-B (PDGF-B), among others. Endothelial development, vascular permeability, and migration are inhibited by the formation of the endothelial basement membrane and the stability of the cell-cell junction, reconstructing a quiescent state (Herbert and Stainier, 2011).

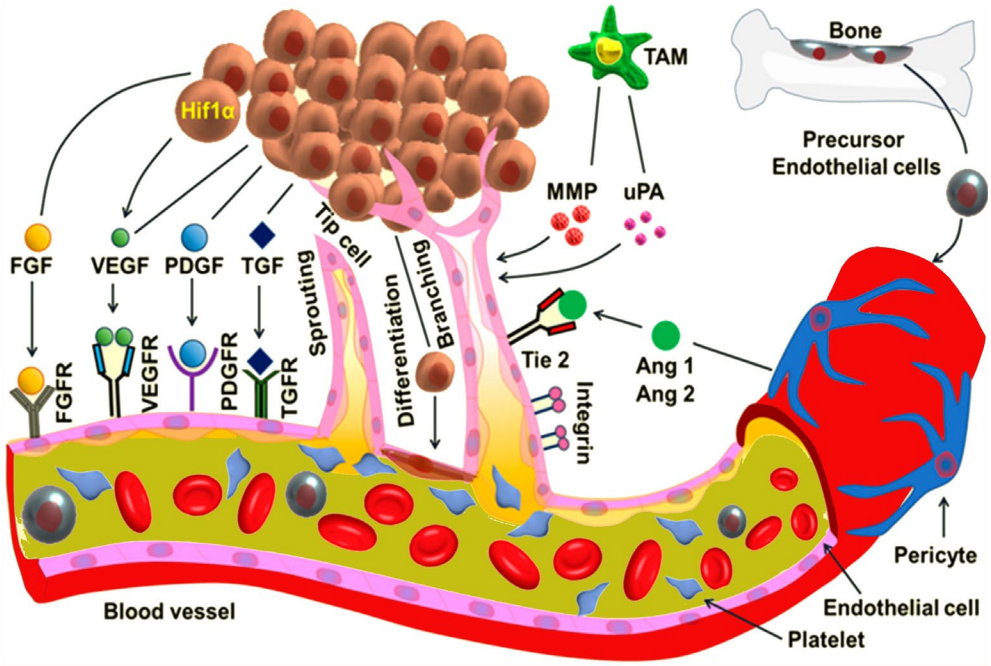

Figure 4: Angiogenic signalling pathway and angiogenesis (adapted from Mukherjee et al., 2020). Angiogenesis is a result of a complicated series of angiogenic signalling processes that are activated in a variety of cell types, particularly endothelial cells. Pro-angiogenic factors include platelet-derived growth factor (PDGF), VEGF, angiopoietin (Ang 1, 2), transforming growth factor-alpha/beta (TGF α/β), and the associated receptors. Once the perivascular cells detach from the mature blood vessels, vascular remodelling and endothelial cell proliferation begin. At the locations where the exposed basement membrane is present, platelets are activated and drawn there. VEGF, MMPs, and urokinase-type plasminogen activator are angiogenic factors that are produced by tumor-associated macrophages (TAM) (uPA). Precursor endothelial cells travel to the alleged site of the wound and release angiogenic factors. The extracellular matrix (ECM) is remodelled as a result of the stimulated endothelial cells' release of proteases, which is followed by directed sprouting. Following vessel arterio-venous patterning and maturation, the signalling cascades activate tube development and branching.

1.1.6 Molecular biology of angiogenesis

1.1.6a molecular regulators and clinical applications of angiogenesis

Key molecular regulators, such as pro- and anti-angiogenic substances, carefully regulate angiogenesis. Angiogenic inducers are proteins, typically growth factors, that promote endothelial cell migration and proliferation in the direction of angiogenic stimuli. Some of the main inhibitors that suppress angiogenesis are endostatin, thrombospondin 1 (TSP-1), and angiostatin. Some of the most important pro- and anti-angiogenic factors that control angiogenesis are included in the table below.

Table 1: Pro and anti-angiogenic factors of angiogenesis

Pro-angiogenic factors (Activators)	Anti-angiogenic factors (Inhibitors)
Tumour necrosis factor-α (TNF-α)	Tissue inhibitors of MMP (TIMPs)
Interleukin-B (IL-B)	Endostatin
Plasminogen activator	Angiostatin
Metalloproteinase (MMP's)	Vasostatin
Hypoxia-inducible factor 1α (HIF-1α)	Thromospondin-1 (TSP-1)
Fibroblast growth factor (bFGF)	Platelet factor 4
Vascular endothelial growth factor (VEGF)	Anti-thrombin III fragment
Platelet-derived growth factor (PDGF)	
Cyclooxygenease-2 (COX-2)	
Nitric oxide synthase	
Angiopoietin-1 and 2	
Insulin like growth factor (IGF)	

Studies into the molecular processes of angiogenesis have been very popular since the successful creation of anti-angiogenic drugs, which will be covered further in this thesis. Recent clinical and pre-clinical studies have revealed new molecular targets, increasing the therapeutic effects of anti-angiogenic tactics. Important molecular players are engaged in vessel branching, maturation, and quiescence, as illustrated in table 1. Due to their extremely lengthy half-lives, quiescent endothelium cells may be protected from the autocrine effects of maintenance signals such VEGF, fibroblast growth factors (FGFs), Notch, and angiopoietin-1 (ANG-1). Prolyl hydroxylase domain 2 (PHD2) and hypoxia inducible factors like HIF-2, which are oxygen sensors, allow endothelial cells to modify the geometry of blood arteries to improve blood flow. The junctional molecules VE-cadherin and claudins work together to enable dormant cells to organise into a monolayer of phalanx cells. Pericytes surround these endothelial cells, preventing them from proliferating and causing the release of ANG-1 and VEGF, two substances that help cells survive. When at rest, pericytes and endothelial cells both create a comparable basement membrane. A quiescent vessel detects the release of angiogenic signals from an inflammatory, hypoxic, or malignant cell, which include chemokines, VEGF, FGFs, and ANG-2. By using MMP-mediated proteolytic degradation, ANG-2 will cause the pericytes to separate from the vessel walls and release themselves from the basement membrane. In response to VEGF, endothelial cell connections loosen, arteries expand, and the endothelial cell layer's permeability rises, enabling plasma proteins to escape and creating a transient extracellular matrix (ECM) scaffold. Endothelial cells move to this ECM surface in response to integrin signalling. Proteases allow for the remodelling of the ECM by releasing angiogenic substances like FGF and VEGF from the ECM. The tip cell is guided toward the angiogenic stimuli by neuropilins (NRPs), notch ligands (*JAGGED 1* and *DLL4*) and VEGF receptors. The tip cell is followed by a trail of stalk cells. placental growth factor (PIGF), Notch-regulated ankyrin repeat protein (*NRARP*), FGFs, and WNTs all promote the mechanism of stalk cell elongation. In order to encourage stalk cell elongation, the ECM will receive information about the neighbours thanks to the release of *EGFL7* from stalk cells. Hedgehog, VEGF, VE-cadherin, VEGF, *CD34*, and sialomucins all have a role in lumen

development. The tip cells with filipodia use semaphorins and ephrins to search the environment for angiogenic triggers. A hypoxia inducible programme controlled by HIF-1 is responsible for endothelial cells responding to angiogenic signals. Important molecular factors including transforming growth factor- (TGF-), platelet-derived growth factor B (PDGF-B), ephrin-B2, NOTCH, and ANG-1 allow endothelial cells to be covered in pericytes when they are in their quiescent phalanx condition. The creation of a basement membrane is induced by protease inhibitors, such as plasminogen activator inhibitor-1 (PAI-1) and tissue inhibitors of metalloproteinases (TIMPs), which also promote appropriate flow distribution by re-establishing connections. The most well researched pro-angiogenic factor among the ones named above is VEGF, whose importance in both pathological and physiological angiogenesis has been amply proven (Carmeliet and Jain, 2011). VEGF has been the main pro-angiogenic factor used in this work, for this reason, the VEGF family features, and mechanism of action will be further explained in this thesis.

1.2 The vascular endothelial growth factor (VEGF) protein family

1.2.1 VEGF family

It is surprising that VEGF a single type of growth factor, that monitors angiogenesis, a complex process, so predominately (Carmeliet and Jain, 2011). As illustrated in figure 5 below, this family has seven members: placental growth factor (PLGF), VEGF-A, -B, -C, -D, -E, and snake venom VEGF (svVEGF) (Takahashi and Shibuya, 2005). Three structurally distinct tyrosine kinase receptors called VEGFR-1, VEGFR-2, and VEGFR-3, also known as Flt-1, KDR/Flk-1 and Flt-4 respectively, bind to VEGFs (Holmes *et al.,* 2007). VEGF-A regulates vascular permeability, inflammation, and angiogenesis via interacting with VEGFR-1 and VEGFR-2. By interacting with VEGFR-1, VEGF-B can control angiogenesis, apoptosis, and redox. VEGF-C regulates lymphangiogenesis, inflammation, apoptosis, fibrogenesis, and angiogenesis through interacting with VEGFR-2 and VEGFR-3. In the thesis, these VEGF receptors will be

discussed in more detail. Similar to VEGF-C in structure is VEGF-D. Lungs, the cardiac, the colon, the small intestine, and human tissues all have high levels of VEGF-D mRNA. In tumours, VEGF-D induces local lymph node growth and tumour cell dissemination (Zhou *et al.,* 2021). This thesis concentrated on VEGF-A, which affects endothelial cells and is crucial for both pathological and physiological angiogenesis.

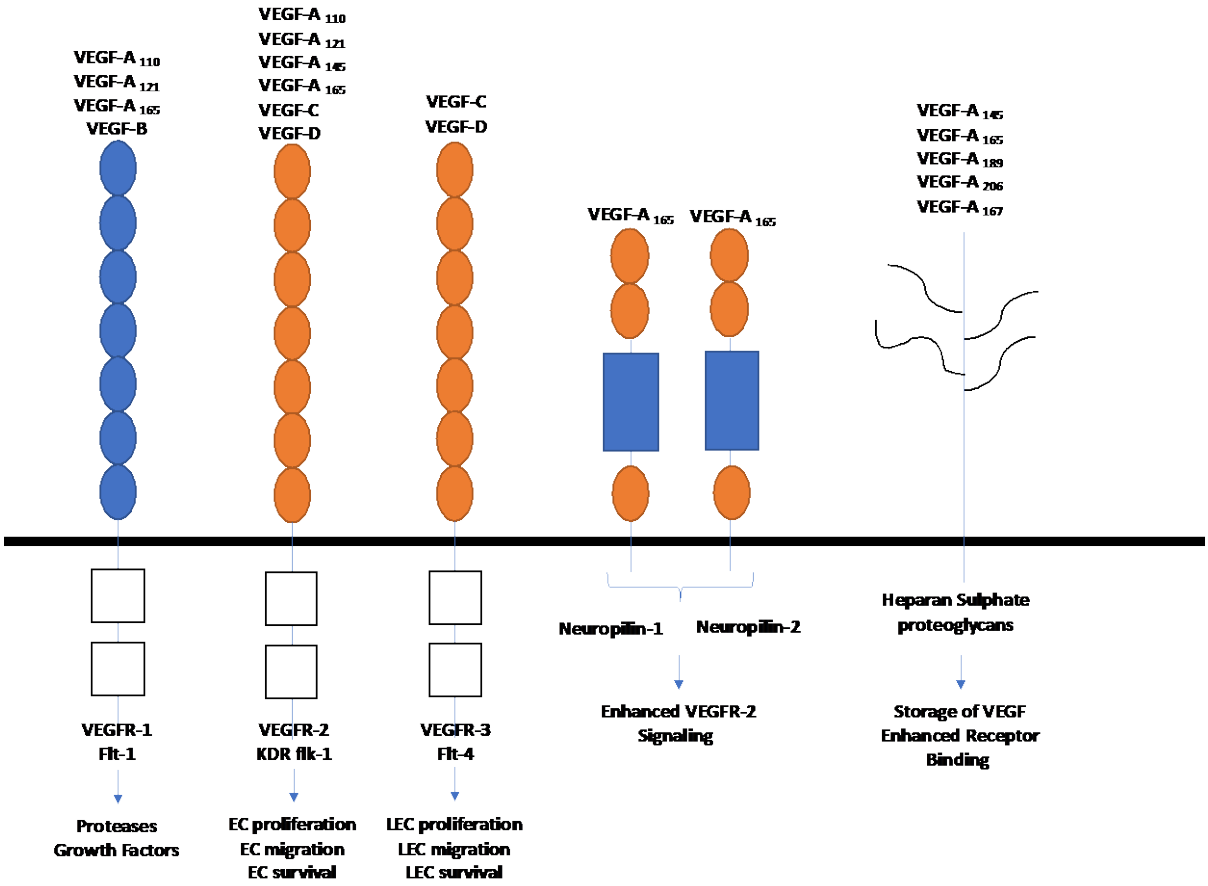

Figure 5: An example of VEGF family members shown interacting with respective VEGF receptors (created using biorender.com). The multiple VEGF-A and VEGF-B isoforms activate growth factors and proteases once they bind to VEGFR-1. VEGF-A, -C, and -D can regulate the migration, survival, and proliferation of endothelial cells by binding to VEGFR-2, while VEGF-C and VEGF-D regulate the proliferation, migration, and survival of lymphogenic endothelial cells. The neuropilin 1 and 2 interactions of VEGF-A165 enhance VEGFR-2 signalling. The storage of VEGF is increased, and receptor binding is enhanced by various VEGF-A isoforms.

1.2.1a VEGF-A

Numerous cells, tissues, and organs, including the liver, stomach mucosa, heart, cardiac myocytes, adrenal cortex, renal glomeruli, and lung, produce VEGF-A. VEGF-A is the most well-known and effective VEGF family member and angiogenesis inducer. VEGF-A is a vascular permeability factor (VPF) because it mediates inflammation and vascular permeability when VEGFR-1 and VEGFR-2 are together (Claesson and Welsh 2019). Physiological angiogenesis, often known as the process of tissue revascularisation, to generate blood vessels, involves a cascade of several signals. VEGF-A, which is crucial for angiogenesis and endothelial cell activities, is primarily used in this process. Diseases that are ischemic and inflamed cause pathological angiogenesis. Clinical investigations that assessed VEGF-A levels revealed a correlation between mid-term left ventricular ejection fraction (LVEF) and microvascular occlusion (MVO) after ST segment elevation myocardial infarction (STEMI). The use of this VEGF-A as a possible prognostic biomarker and indicator of MVO in STEMI patients has been suggested (Garcia *et al.,* 2019). The VEGF-A gene is a human protein that has 8 exons and 7 introns. It is found on chromosome 6p21.3. Figure 6 below illustrates how alternate VEGF mRNA splicing results in different lengths for human structural isoforms. Exon 6-7, which comprises heparin sulphate proteoglycan (HSPG) and heparin affinity areas, is where the distinctions between the isoforms' biological features occur. Exon 1–5 of all isoforms contain the identical sections (Itatani *et al.,* 2018). It has been revealed that the VEGF-A gene's splicing produces the angiogenic (VEGFxxx) and anti-angiogenic (VEGFxxxb) isoforms (Harris *et al.,* 2012). In contrast to VEGFxxxa isoforms, anti-angiogenic VEGFxxxb isoforms have an obscure mechanism that decreases VEGFR-2 activation (Ganta *et al.,* 2017). It has been determined that VEGF-A165 isoforms are the primary regulators of both physiological and pathological angiogenesis (Arcondeguy *et al.,* 2013). Endothelial cells, angioblasts, and pericytes are the principal expression cells in the cardiovascular systems. When there is inflammation and hypoxia, blood cells for example activated T cells, dendritic cells, monocytes, platelets, and neutrophils produce VEGF-A

(Melincovici *et al.,* 2018). Other cells, including tumour cells, retinal pigment epithelial cells, terminal chondrocytes, keratinocytes, and hypertrophic chondrocytes, also produce VEGF-A (Claesson and Welsh 2019).

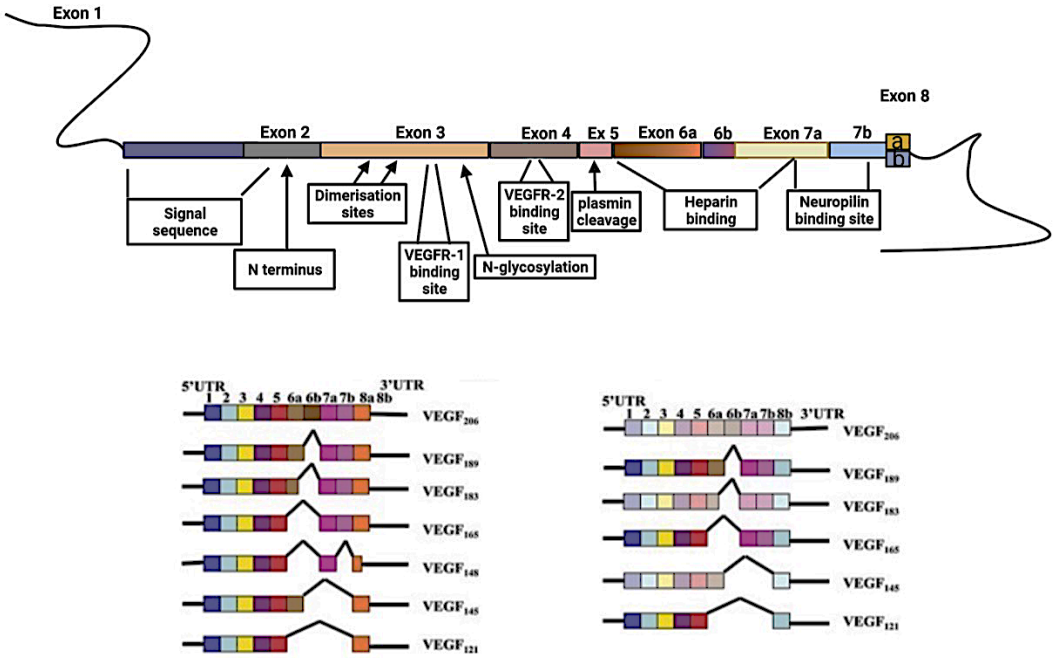

Figure 6: illustration of Exon structure of splice variants in VEGF-A isoforms (created using biorender.com)**.** The 8 exons that make up VEGF-A are coded for by a gene that has many distinctive structural properties. The human VEGF-A isoforms VEGF-A121, VEGF-A145, VEGF-A148, VEGF-A165, VEGF-A183, VEGF-A189, and VEGF-A206 are all created from a single pre-mRNA species by alternative splicing, with VEGF-A165 acting as the predominant form (Cross *et al*., 2003).

1.2.1b Role of VEGF-A

Hypoxia inducible factors (HIFs) regulate angiogenesis by promoting the overexpression of a number of pro-angiogenic factors, such as VEGF, in response to hypoxia. The integrity of the vascular function of the endothelium is restored in favour of higher VEGF-A, which also increases vascular permeability and promotes the vascular endothelial cells proliferation. As a result, the wounded myocardium will be protected, and hypoxia and ischemia will be

balanced out by the elevated VEGF-A (Ferrara, 2004). Additional VEGF-A upregulation mechanisms have been shown by several studies, such as the activation of the transcription coactivator PGC-1 in response to low oxygen and nutrition levels. PGC1, a crucial regulator of mitochondrial processes, aided angiogenesis by increasing VEGF expression. PGC-1 further activated the orphan nuclear receptor ERR-α to regulate an angiogenesis pathway without the participation of HIFs (Arany *et al.,* 2008). The TNFα/ NF-κB/ HIF/ VEGF signalling cascade in endothelial cells is activated in response to hypoxia, activating HIFs through an autocrine cycle, upregulating VEGF, and enhancing angiogenesis by the dependent mechanism of NF-κB (Jin *et al.,* 2019).

1.2.1c VEGF receptors

As was previously noted, there are three VEGF receptors: VEGFR-1, VEGFR-2, and VEGFR-3. Inflammatory cells, monocytes, macrophages, vascular smooth muscle cells, and other cells may also express VEGFR, a specific kind of cell receptor that is mostly present in endothelial cells. In addition to regulating angiogenesis, VEGFRs also control lymphangiogenesis and vasculogenesis (Lohela *et al.,* 2009). However, structurally, seven immunoglobulin-like domains, one transmembrane spanning region, and a split tyrosine-kinase domain make up the VEGFRs' cytoplasmic component. The receptors have varied kinase activity and different ligand binding capabilities (Takahashi and Shibuya, 2005). The epidermal growth factor receptor (EGFR), hepatocyte growth factor receptor (HGFR), and platelet-derived growth factor receptor (PDGFR) are examples of tyrosine kinase receptors that function similarly to VEGFRs (Olsson *et al.,* 2006). A docking site for signalling is created when a ligand binds with the corresponding receptor, forcing it to dimerise. Additionally, the activation of the tyrosine kinase domain results in the autophosphorylation of the receptor (Stuttfeld and Ballmer-Hofer, 2009).

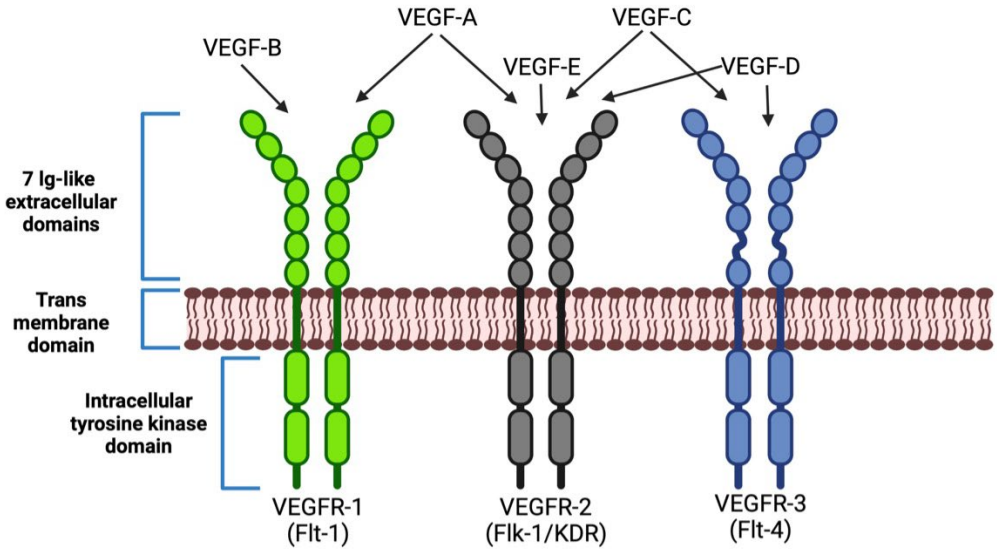

Figure 7: An example showing the three distinct VEGF receptors and their ligands (Created using biorender.com**).** VEGFs may interact with a number of VEGFRs, or VEGF receptors, which are members of the receptor tyrosine kinase superfamily. VEGFR-1 may interact with VEGF-A and VEGF-B. VEGFR-2 interacts with VEGF-A, -C, -D, and -E, in contrast to VEGFR-3, which may bind VEGF-C and VEGF-D. Fetal liver kinase 1 (Flk-1), a mouse subtype, is identified by VEGFR-2, fms-like tyrosine kinase 1 (Flt-1), and kinase insert domain (KDR).

1.2.1c (i) VEGFR-1

VEGFR-1 is a glycoprotein of the receptor tyrosine kinase family (RTKs) that has a size range of 180-185 kDa. It binds with VEGF-B and PlGF in addition to VEGF-A (Takahashi and Shibuya, 2005). VEGFR-1 has a lower affinity for VEGF-A and a kinase activity that is 10 times lower than that of VEGFR-2. VEGFR-1 is mainly expressed in endothelial cells, although it is also found in inflammatory cells, bone marrow-derived hematopoietic progenitor, vascular smooth muscle, myocardial infarction (MI), monocyte/macrophage, and cardiac fibroblast cells (Shibuya, 2006). Three domains make up VEGFR-1: the intracellular, extracellular, and transmembrane domains (Koch and Claesson-Welsh, 2012). According to what has already

been said, VEGFR-2 demonstrates a higher affinity for VEGF-A compared to VEGFR-1, yet under some circumstances, VEGFR-1's low kinase activity limits angiogenesis. By "seizing" VEGF-A during the embryonic stage, VEGFR-1 inhibits angiogenesis (Shibuya, 2006).

1.2.1c (ii) VEGFR-2

Another RTK, VEGFR-2 is a glycoprotein with a length of between 210 and 230 kDa (Park *et al.,* 2018). Other names for it include kinase-insert domain receptor (KDR). Known as foetal liver kinase-1 (FLK-1), the 1367 amino acid long mouse VEGFR-2 shares 83% of its sequence with the human KDR. Each of the three variants weighs 180, 200, or 220 kD in terms of molecular weight (Wang et al., 2020). Hematopoietic cells, neurons, and cancer cells all have low levels of VEGFR-2 expression (Luck *et al.,* 2019). Vascular permeability, angiogenesis, and inflammation are all controlled when VEGF-A binds to VEGFR-2. VEGFR-2 and VEGFR-1 both have three domains. VEGF-A binding to VEGFR-2 when activated, it is essential for migration, proliferation, vascular growth, and endothelial survival. Once VEGF-A attaches to the extracellular domain of VEGFR-2, as a consequence, signalling pathways are activated and tyrosine residues are autophosphorylated. This drive the endothelial cells to proliferate. When it comes to activation and signalling of VEGFR-2, the carboxyl terminus domain (CTD) is crucial. There are two autophosphorylation sites in the VEGFR-2 CTD: Try1175 (Y1175) and Try1214 (Y1214). The activation phosphorylates the Y1175 and Y1214 once VEGF-A binds to VEGFR-2. This makes it possible for the VEGF-activated VEGFR-2 to attach to a number of signalling molecules, which are covered in more detail later on in this thesis (Wang et al., 2020). When VEGF-A and VEGFR-2 work together, certain intracellular signalling pathways are activated, which in turn sets off particular cellular processes necessary for angiogenesis (Long *et al.,* 2020). The role of VEGF-A and VEGFR-2 as a crucial regulator of both pathological and physiological angiogenesis will be discussed in further depth in the next chapter.

1.2.1d VEGFR-2 mediated cellular signalling

The formation and maintenance of organ-specific vascular networks, the physiological function of many tissues, and the pathology of illnesses including cancer and heart disease all depend on the activity of the VEGF/VEGFR-2 signalling pathway. In order to promote vascular endothelial cell migration, proliferation, permeability, VEGF directly activates VEGFR-2 by binding to several molecules, including PLC, PI3K, adapter protein NCK by the phosphorylated Try1214 site (pY1214), and adapter proteins SHB and SCK by the phosphorylated Try1175 site (pY1175). This portion of the thesis examines how VEGFR-2 mediates different Endothelial cell survival, proliferation, migration, and increased vascular permeability were all influenced by VEGF-stimulated cellular signal transduction. interaction of VEGF-A to VEGFR-2 and activation of intracellular signalling cascades are shown in the figure below (Holmes et al., 2007).

1.2.1d (i) VEGFR-2 regulating survival of endothelial cells

For the growth of blood vessels and the survival of endothelial cells, VEGFR-2 is a crucial factor. VEGFR-2 activates the TSAd-Src-PI3K-PKB/AKT signalling pathway, which is primarily in charge of regulating endothelial cell survival. VEGF-A controls the survival of HUVECs by activating PI3K after activating VEGFR-2. PI3K is activated by VEGFR-2, which subsequently catalyses the synthesis of PIP3 from PIP2 and phosphorylates and activates the PKB/Akt pathway (Wang et al., 2020). Akt directly phosphorylates the apoptosis proteins caspase 9 and Bcl-2 associated death promoter (BAD). To ensure cell survival, this phosphorylation prevents their apoptotic activity (Wang et al., 2020).

1.2.1d (ii) VEGFR-2 mediating the proliferation of endothelial cells

Endothelial cell proliferation during angiogenesis is critically dependent on VEGFR-2. When VEGF-A attaches to VEGFR-2 on the cell membrane, it transmits extracellular signals to the cytoplasm and activates a range of downstream signalling pathways to govern the proliferation of endothelial cells. VEGFR-2 triggers the PLC-PKC-Raf-MEK-MAPK signalling pathway, which promotes DNA synthesis and promotes the proliferation of endothelial cells. Additionally, it sends VEGF signal to the nucleus. This is accomplished by the Y1175 C-terminal of VEGFR-2 interacting to and activating phospholipase C-γ (PLCγ), This in turn promotes the PLC's catalytic activity by phosphorylating it. The active PLC hydrolyses phosphatidylinositol 4, 5-bisphosphate (PIP2) to produce diacylglycerol (DAG) and inositol 1, 4, 5-trisphosphate (IP3). PKC is physiologically activated by DAG, and as a consequence, IP3 is able to increase the intracellular Ca2+ level. VEGF-activated VEGFR-2 mediates the activation and nuclear translocation of the PKC-Raf-MEK-ERK signalling cascade to bind to transcription factors that regulate gene expression in response to environmental cues. This makes it possible for VEGFR-2 to take part in the growth of endothelial cells (Holmes et al., 2007).

1.2.1d (iii) VEGFR-2 mediating the migration of endothelial cells

Migration of endothelial cells is important for angiogenesis, as stated in this thesis. Endothelial cell migration is regulated by a number of signalling pathways that communicate with VEGFR-2. VEGFR-2 controls cell motility through the Y1214 and Y1175 phosphorylation sites on its CTD as well as the activation of NCK, SHB, and PI3K-mediated pathways. VEGF-induced cell migration can be controlled by the adaptor protein SHB's Src homology domain-2 (SH2) by binding to the phosphorylated pY1175 Tyr1175 site at the CTD of VEGFR-2. The downregulation of SHB expression blocks PI3K activation, migration, and VEGF/VEGFR-2-mediated reorganisation of the cell scaffold. The NCK/ Src-p21/ Cdc42-SAPK2/ p38-MAPK

pathway, which is driven by VEGFR-2, participates in the remodelling of actin by phosphorylating Tyr1214 (pY1214) at the C-terminus domain of VEGFR-2 (Wang et al., 2020).

1.2.1d (iv) VEGFR-2 enhances vascular permeability

The factor for vascular permeability Nitric oxide (NO), which is produced by endothelial nitric oxide synthase (eNOS) when VEGF-A is signalled and activated, alters the blood vessels' permeability (Holmes et al., 2007). The release of NO generated by VEGF depends on the phosphorylation of the pY801 Try801 residue of VEGFR-2, and the pY801 activates eNOS through the PKC-PI3K/Akt pathway. Vascular endothelial cells produce more NO when they are exposed to VEGFR-2. VEGFR-2-mediated signals that promote eNOS binding to its molecular chaperone heat shock protein 90 may increase endothelial cell NO release (Hsp90) (Duval et al., 2007).

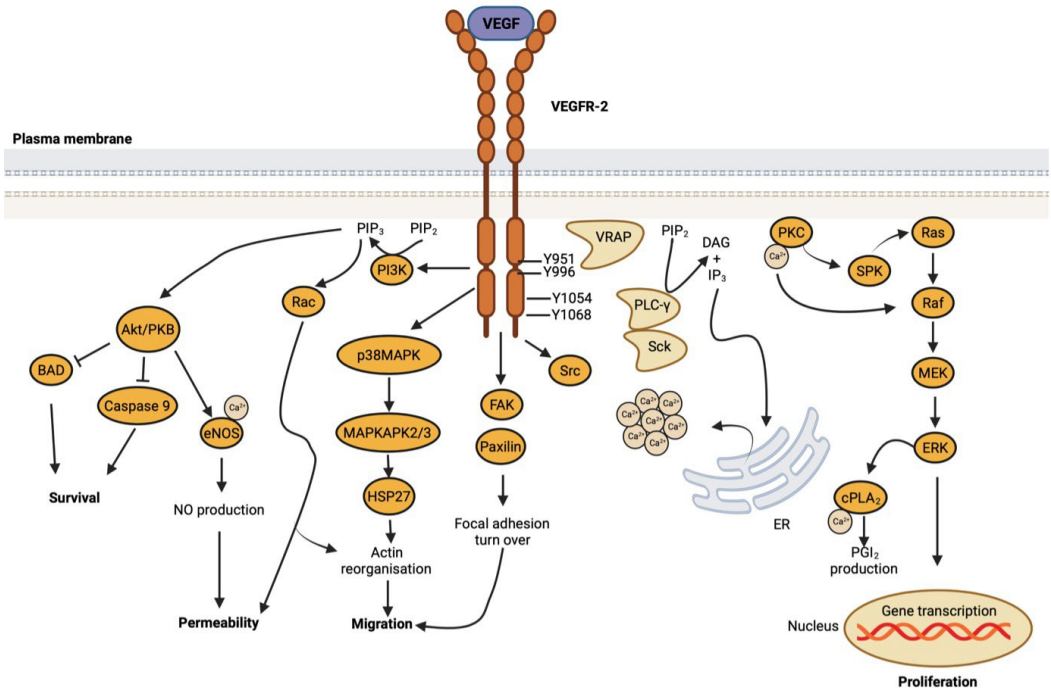

Figure 8: Illustration of VEGF-A binding to VEGFR-2 and activating intracellular signalling pathways (Created using Biorender.com).

1.2.2 Anti-angiogenesis therapy

1.2.2a inhibitors of VEGF-VEGFR

VEGF-A, one of the most significant angiogenic mediators, was originally identified in 1989 (Keck *et al.,* 1989). Independent teams investigated the mechanics of angiogenesis to show how VEGF-A contributes to angiogenesis (Leung *et al.,* 1989; Guyot and Pagès, 2015). Four years later, N. Ferrara's team discovered the first monoclonal antibody that directly inhibited VEGF-A, and it was utilised to treat retinal diseases, particularly wet age-related macular degeneration (Kim *et al.,* 1993). These antibodies were used to measure the growth of experimental models, which resulted in the inhibition of rhabdomyosarcoma, colorectal, glioma, and prostate cancer growth (Asano *et al.,* 1995; Warren *et al.,* 1995; Borgström et al., 1998). The development of anti-VEGF-A antibodies was prompted by these positive anti-tumor effects. One of the most crucial therapies for treating patients with diseases like eye problems, solid tumours, immunological disorders, and haematological malignancies uses monoclonal antibodies that target VEGF and VEGFRs (Andreakos *et al.,* 2002; Martin *et al.,* 2011; Wang and Jia, 2016). More than 40 therapeutic monoclonal antibodies have been approved by the US Food and Drug Administration (FDA), and more are being tested in clinical trials (Ecker *et al.,* 2015). A selection of these monoclonal antibodies will be discussed in this thesis.

1.2.2a (i) Bevacizumab (Avastin®)

Bevacizumab, the first monoclonal antibody to target VEGF and VEGFRs, is a humanised recombinant immunoglobin G (IgG) antibody (Presta *et al.,* 1997) and it was accepted by the FDA as a treatment for metastatic colorectal tumours in 2004 (Hurwitz *et al.,* 2004). Targeting VEGF-A, bevacizumab prevents endothelial cell attachment of VEGF-A to its receptor VEGFR2. As a result, this inhibits signalling pathways necessary for tumour angiogenesis and endothelial cell growth (Shih and Lindley, 2006). Bevacizumab has a half-life of 17 to 21 days

(Ferrara *et al.,* 2004). With remarkable specificity, it binds to all VEGF-A isoforms and prevents them from binding to their appropriate receptors and VEGF-mediated angiogenic signalling pathways (Shih and Lindley, 2006). Bevacizumab has been widely used since 2008 to treat a variety of malignancies, including metastatic renal cell carcinoma, glioblastoma, epithelial ovarian cancer, and breast cancer (Cohen *et al.,* 2009; Planchard, 2011; Rinne *et al.,* 2013). Bevacizumab does, however, cause some side effects, such as proteinuria, slowed wound healing, and severe hypertension (Shih and Lindley, 2006; Hurwitz *et al.,* 2004). The absence of nitric oxide produced by endothelial nitric oxide synthase (eNOS) in hypertension is caused by VEGF blockade, which also affects eNOS activation (Kamba and McDonald, 2007). Another factor contributing to the significant adverse effect is bevacizumab's prolonged half-life (Pieramici and Rabena, 2008).

1.2.2a (ii) Aflibercept (Zaltrap®)

VEGFR1 and VEGFR2 extracellular domains are joined with the Fc region of human IgG in aflibercept (Oman, 2014). This Fc fusion protein acts as a VEGF trap, preventing VEGF-A, VEGF-B, and PIGF activity while reducing tumour angiogenesis. In 2012, the US FDA approved the drug aflibercept for the treatment of people with metastatic colorectal cancer who had previously undergone an early- or advanced-stage oxaliplatin-based therapy (Andre and Chibaudel, 2013). These VEGF traps enable for improved tissue penetration because they are smaller than other inhibitors (Pieramici and Rabena, 2008). It binds to PIGF-1 and PIGF-2 in addition to all VEGF isoforms (Chen *et al.,* 2012). The primary cause of blindness in the elderly is wet age-related macular degeneration, and in 2011 the US FDA authorised Aflibercept (Eylea) for the treatment of this condition (Sarwar *et al.,* 2016).

1.2.2a (iii) Tanibirumab

Tanibirumab is a different human monoclonal antibody that binds selectively to VEGFR-2 and prevents the binding of VEGF-A, VEGF-C, and VEGF-D. In 2013, a phase I experiment including Tanibirumab was conducted in individuals with solid tumours (Lee *et al.,* 2017).

1.2.2a (iv) Ramucirumab (Cyramza ®)

Similar to Bevacizumab, which the FDA approved in 2006, Ramucirumab is a humanised monoclonal antibody fragment (Fab) that exclusively targets VEGFR2 and prevents the connection between VEGF and VEGFR as well as the start of intracellular signalling (Kourlas and Abrams, 2007). The affinity of binding to VEGF is the primary distinction between Ramucirumab and Bevacizumab, with Ramucirumab having a roughly 20-fold higher affinity. In addition, it has improved tissue penetration due to its smaller size compared to bevacizumab (Pieramici and Rabena, 2008). Additionally, in 2014, the US FDA approved ramucirumab for the treatment of advanced gastric or gastro-oesophageal cancer, metastatic non-small cell lung carcinoma, and adenocarcinoma (Poole and Vaidya 2014; Arrieta *et al.,* 2017). For advanced or metastatic urothelial carcinoma, phase III trials are currently being conducted for liver and breast cancer (Zhu *et al.,* 2015; Mackey *et al.,* 2015).

1.2.2b Inhibitors of VEGFRs

It was necessary to use alternative methods to inhibit angiogenesis. Small ATP mimics were created for this function because VEGFRs had tyrosine kinase domains, which were studied to decrease the activity of tyrosine kinase receptors implicated in angiogenesis (Qin *et al.,* 2019). These small molecule inhibitors bind specifically to the ATP binding site found in the cytosolic portion of the receptors, blocking ATP binding and signalling pathway activation (Gotink and Verheul, 2010). The first small molecule inhibitor of VEGFR2 tyrosine kinase,

sorafenib, received clinical approval in 2005. More VEGFR2 kinase inhibitors, like sunitinib, cabozantinib, nintedanib, and pazopanib, were created and discovered as a result of scientific communities' motivation. The majority of these inhibitors attach to the ATP-binding pocket of VEGFR2 kinase (Hartmann *et al.,* 2009). Due to the nature of these highly conserved pockets found in protein kinases, VEGFR2 small molecule kinase inhibitor exerts a high affinity for other tyrosine kinases like EGFR, RAF, and PDGF. This leads to side effects like anorexia and fatigue in addition to hypertension, bleeding, and haemorrhage when VEGFR inhibition is used (Fujita *et al.,* 2017). Patients with solid tumours have exhibited limited responses to these medications that target the VEGF/VEGFR signalling pathway, and some patients have demonstrated resistance to these medications because other pro-angiogenic factors such FGF are active in these patients (Itatani *et al.,* 2017; Zirlik and Duyster, 2018).

1.3 Notch signalling pathway

How do the tip cells migrate in relation to regulating the specification of endothelial tip and stalk cells? What regulates the proliferation and quantity of stalk cells? How do tip cells communicate with one another while new connections are formed? All of these procedures call for the influence of an environmental signal, which ought to be directed by a well-organized team. Numerous pathways, including Angiopoietin/TIE2, Wnt, Notch, FGF, S1P/Edg1, cell matrix/integrin signalling, and others, control the angiogenic response. The notch signalling pathway, which is largely conserved in all vertebrate species and has a variety of activities, including cell proliferation, patterning, and cell differentiation, has become increasingly obvious over the past few years. Four transmembrane receptors (Notch 1-4) and five canonical transmembrane ligands make up this pathway in mammals (Jagged 1,2, delta like ligand 1, 3, and 4). The canonical and non-canonical notch signalling pathways are the two types of notch signalling. When a notch receptor interacts with a notch ligand, the canonical notch signalling cascade is triggered, which starts the proteolytic cleavage of the receptor by enzymes such disintegrin metalloproteinase domain-containing protein 10 (ADAM10) and the

γ-secretase (Aquila et al., 2019). Because of this contact, the notch receptor intracellular domain (NICD), which translocates to the nucleus and serves as a transcriptional co-activator for the immunoglobulin kappa J region, is liberated from the cell membrane (RBPJ). In both healthy and malignant situations, the association between NICD and RBPJ activates notch target genes to control migration, proliferation, differentiation, and cell fate choice. Furthermore, via regulating the expression of a number of target genes, notch signalling affects crucial physiological processes (Kangsamaksin *et al.,* 2014). Non-canonical ligands may not require notch receptor cleavage to activate the non-canonical notch signalling pathway, which excludes the involvement of the RBPJ and suggests contact with alternative signalling pathways that are upstream of the NICD-RBPJ complex (Andersson *et al.,* 2011).

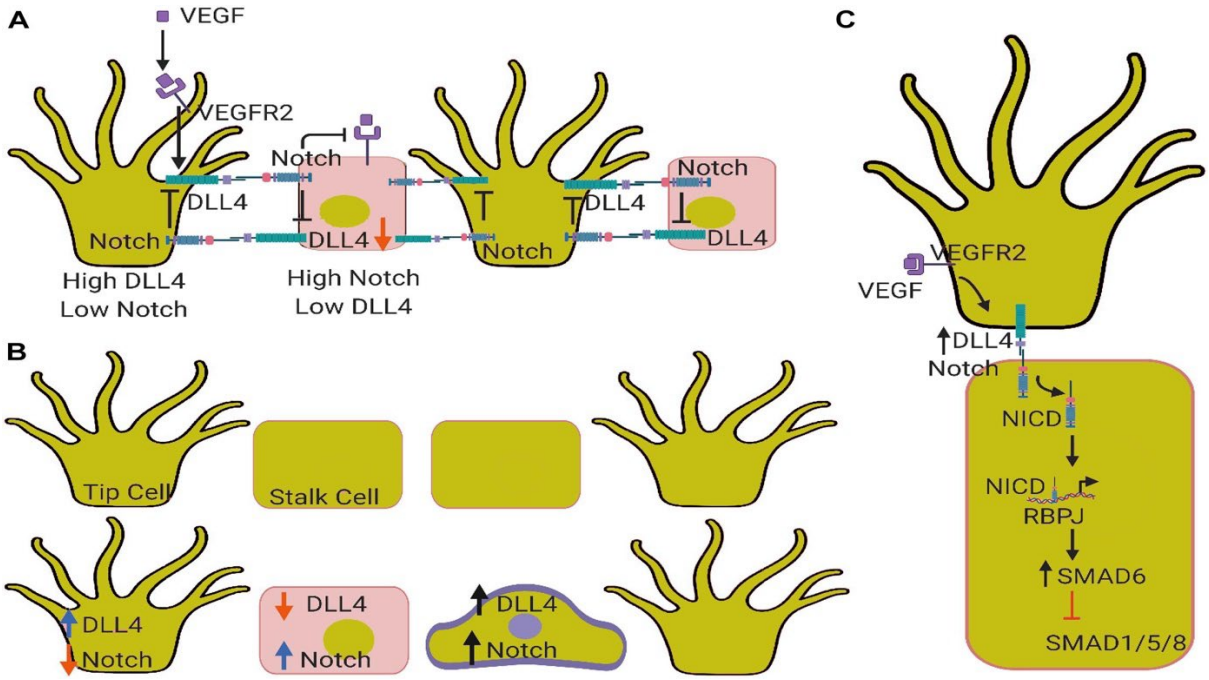

Figure 9: Schematic models of Notch signalling in vascular endothelial cell (EC) differentiation (created using biorender.com). (A) In endothelial tip cells, VEGF signalling induces DLL4 expression, which activates Notch1 signalling. In endothelial stalk cells, activation of Notch signalling via DLL4 suppresses differentiation toward a tip cell phenotype. (B) Graphic representation of lateral inhibition, where tip cells are separated exactly by one stalk cell. DLL4 of one cell binds to the Notch receptor of the adjacent cell, and Notch inhibits

DLL4 expression and the VEGFR2 signalling within the same cell. (C) Mathematic model of Notch signalling in asymmetric patterning. Where two tip cells might be separated by a few stalk cells, which could be determined by Jag. It is also possible that an intermediary tip cell may express similar DLL4 and Notch expression. Both theories involve a third EC state.

1.3.1 Notch signalling in endothelial cells and angiogenesis

An important part of angiogenesis is sprouting angiogenesis, as discussed in chapter 1.1.1b. Through interactions with the notch ligands and other signalling pathways, including VEGF signalling, the notch signalling pathway regulates this important mechanism. Delta like ligand 4 (*DLL4*) is an important notch ligand that promotes angiogenesis. Jagged1 (Jag1), a rival notch ligand, competes with *DLL4* to inhibit angiogenesis (Taslimi and Das, 2018; Naito *et al.,* 2020). Studies conducted in vitro have identified Jag1 as a powerful pro-angiogenic regulator that inhibits *DLL4*-mediated notch signalling in angiogenesis (Benedito *et al.,* 2009).

1.3.2 Notch signalling in endothelial differentiation and fate determination

In the vasculature, the development of stalk/tip cells and the control of cell destiny are both significantly influenced by notch signalling (Mack and Iruela-Arispe, 2018). By synchronising tip vs. stalk phenotypes, notch signalling is crucial for a sprout's development. Coordinating this is the expression of *DLL4* in the tip cell, which activates *Notch1* in the stalk cell. In order to maintain vascular endothelial cells, produce sprouts, and create endothelial cell heterogeneity, the link between VEGF and notch signalling is crucial (Blanco and Gerhardt, 2012). Loss of vascular hierarchy occurs from tip cells' inability to create stable complex connections and organise tubes as a result of Notch inactivation during the early stages of angiogenesis (Mack and Iruela-Arispe, 2018). Notch signalling is responsible for controlling excessive sprouting angiogenesis. The induction of tip cells is suppressed by a process known as lateral inhibition after *DLL4*-Notch activation. VEGF enhances the expression of *DLL4* in

tip cells during lateral inhibition, which activates notch in neighbouring cells. The two endothelial cell states and a third state were discovered using a new mathematical model of the notch-jagged signalling (tip or stalk) (Boareto *et al.,* 2015). Depending on which ligand is dominant, neighbouring cells might have similar or opposing fates because to the unique hybrid state's tip and stalk cell features. For instance, Jagged-mediated signalling causes cells to maintain the same fate while Delta-mediated signalling causes neighbouring cells to have the opposite fate.

Notch signalling in response to other pathways, such as BMP and SMAD1/5/8 signalling, causes the development of vascular branches (Mack and Iruela-Arispe, 2018). The expression patterns of Notch-*DLL4*, VEGF, and BMP between cells determine vessel widening and the development of new sprouts (Mack and Iruela-Arispe, 2018).

Beyond the selection of endothelial tip cells, notch signalling is crucial for cell proliferation, which enables a sprout to increase in length and diameter (Phng and Gerhardt, 2009). Again, this suppression of endothelial cell proliferation and cell-to-cell junction stability is caused by the *DLL4* and notch receptor interaction, which suggests that *DLL4* is essential for angiogenesis and vascular development (Lobov and Mikhailova, 2018).

1.4 Extracellular matrix and cell adhesion molecules

All aspects of vascular biology depend on the extracellular matrix (ECM). For instance, endothelial cells create a basement matrix rich in laminin to support cells and preserve stability. When angiogenesis first begins, proteinases and membrane-type matrix metalloproteinases (MT-MMPs) destroy the basement membrane. As angiogenesis progresses, the ECM supports signalling processes such endothelial cell migration, proliferation, survival, and invasion. When there is no cell-to-cell interaction, ECM acts as a scaffold for organisation. The ECM regulates the endothelial cell cytoskeleton to carry out complex processes like vascular morphogenesis, which enables proliferating endothelial cells

to form into multicellular tubes with functional lumens. These processes are carried out with the help of specific integrin-dependent signal transduction pathways. Because of this, the ECM and the chemicals connected to it enable ECM remodelling and degradation to regulate tube formation, maturation, and neovascular stability (Davis and Senger, 2005). macromolecules such as fibrous proteins and proteoglycans (PGs) make up the ECM. One of the key ECM proteins that is crucial for the early phases of angiogenesis is collagen. For vessels to form and endothelial cells to survive, a variety of collagens must be produced and deposited (Lamalice, 2007). PGs cover the extracellular and interstitial space in tissues and serve a variety of purposes, including chemical cell signalling, binding, and force resistance (Franca *et al.,* 2018).

Cell adhesion molecules are required for the migration of endothelial cells, which is essential for angiogenesis, the sprouting of new blood vessels from the preexisting vasculature. The extracellular matrix and cell adhesion molecules (ECM CAM) enable endothelial cell proliferation and survival, which significantly depend on cell-surface integrins. In particular, the activation of the mitogen-activated protein kinase (MAPK) signal transduction pathway is necessary for endothelial cell proliferation and angiogenesis (Davis and Senger, 2005).

1.5 Cell migration

Angiogenesis is significantly influenced by the endothelial cell migration. The progression of endothelial cell migration is enabled by the regulation of the motile process by three mechanisms: chemotactic, haptotactic, and mechanotactic stimuli. The activation of many signalling pathways enables cytoskeletal remodelling. This enables endothelial cells to undergo a range of actions, including expanding, contracting, and throwing their rears forward as they move forward (Lamalice *et al.,* 2007). During angiogenesis, the three processes are crucial for tip cell migration. Cells can move in the direction of a gradient of soluble chemical compounds thanks to the chemotaxis process of migration, this is stimulated by growth

hormones such as basic fibroblast growth factor (bFGF) and VEGF. Cells can move toward a gradient of immobilised ligands through haptotaxis. When activated in response to integrins binding to ECM components, this process facilitates increased migration of endothelial cells. Due to their position at the inner face of blood arteries, endothelial cells may experience shear stress, which influences migratory paths. This shear stress initiates mechanotaxis mechanisms, which regulate migration in a number of ways, such as adhesion to the matrix, extension at the edge, and release of adhesion at the rear (Lamalice *et al.,* 2007).

1.6 Cell cycle

Cell growth and proliferation, DNA damage repair and control, tissue hyperplasia in response to injury, and diseases like cancer all depend on the intricate process known as the cell cycle. Key regulatory proteins in the cell cycle guide cells through a predetermined order of events (Schafer, 1998). The cell cycle is carefully regulated and impressively preserved throughout genome duplication. The GO/G1 phase, also known as gap 1, S phase, during which DNA is synthesised, G2 (gap 2), and M phase (mitosis) are the four stages of the cell cycle. Key checkpoints for proper cell division include effective replication in the S phase and successful chromosomal aggregation into daughter cells, among others (Thu *et al.,* 2018). The G1 and G2 phases are important regulatory checkpoints, and between the G1 and S phases, there are restriction points that either allow passage into the S phase or force cells into the G0 phase, which stops the cell cycle. The cell cycle is regulated by cyclins and cyclin dependent kinases (CDKs), a family of serine/threonine kinases. In the various cell cycle phases, CDKs are activated, stabilised, and phosphorylated via complexes that they form with particular cyclins (Malumbres, 2014). By phosphorylating target genes like the tumour suppressor protein retinoblastoma (Rb), the cyclins/CDKs complex controls cell cycle progression. The activation of the cyclins and CDKs complex, which is initially stimulated by mitogenic signals, is inhibited by the activation of cell cycle checkpoints in response to DNA damage (Otto and Sicinski 2017). In response to extracellular and intracellular signals, CDKs control cell division

by forming a heterodimer complex with cyclins to act as the regulatory subunits. With the 20 CDKs and 29 cyclins found in human cells, they either directly regulate cell cycle transition and cell division, or they facilitate gene transcription (Ding *et al.,* 2020). *CDK4* and *CDK6* control the cell cycle's transition from the G0/G1 phase to the S phase. D-type cyclins include cyclin D1, cyclin D2, and cyclin D3 promote and positively regulate CDK4/6 activity. The CDK4/6 activity is adversely regulated by the INK4 family (Ding *et al.,* 2020). Cell cycle regulation by *CDK1* has been linked to the development of tumours. According to Gao et al. (2019), *CDK1* disruption prevents angiogenesis by causing cell cycle arrest and death. The results suggested that abnormal retinal angiogenesis involved an overexpression of *CDK1*. Short interfering (si)RNA sequences targeting *CDK1* inhibited HUVECs cell migration, proliferation, and tube formation. Cyclin A1, cyclin D1, and cyclin E1 expression levels were dropped when *CDK1* was silenced. Considering this, *CDK1* may provide a novel therapeutic target for retinal angiogenesis. However, more research is needed to determine *CDK1*'s function in pathological angiogenesis (Gao *et al.,* 2019).

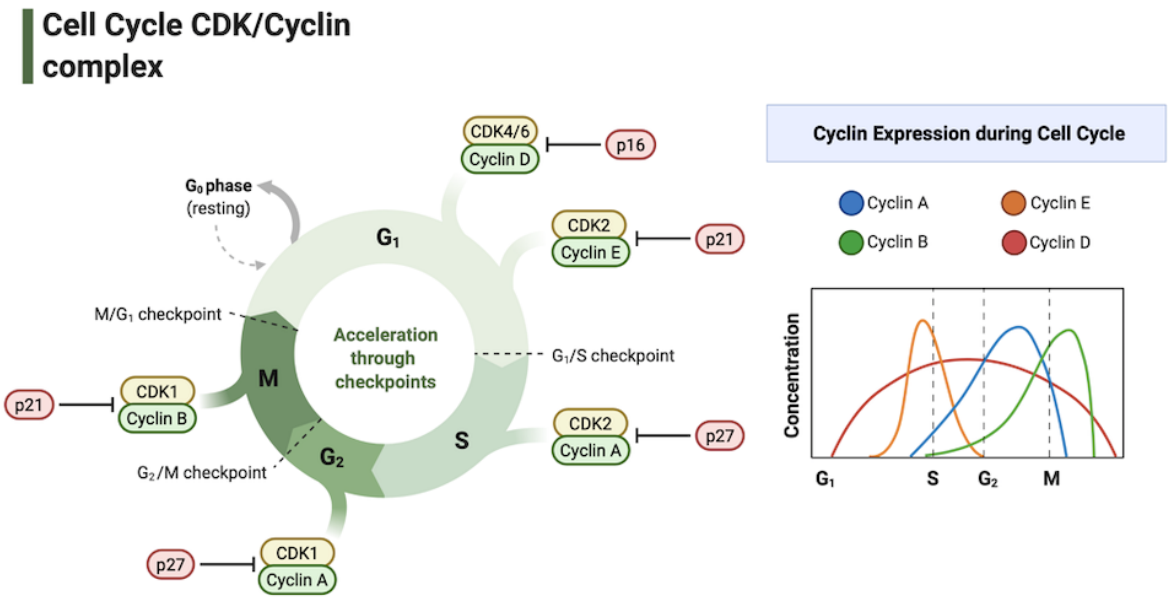

Figure 10: A diagram showing the CDK and cyclin complex at several cell-cycle stages (created using biorender.com). The four stages of the cell cycle are mitosis (M), gap 1 (G1),

DNA synthesis (S), and gap 2 (G2). The majority of non-dividing cells leave the cell cycle and enter a quiescent state (G0 phase), yet they can also re-join the cell cycle again with the right stimuli. Once a cell has passed the G1/S phase restriction points, it is committed to starting the cell cycle. The actions of cyclin-CDK complexes control the progression of every phase of the cell cycle.

1.7 MicroRNAs (miRNAs)

1.7.1a history of miRNAs

The first miRNA, lin-4, was discovered in Caenorhabditis elegans by the Ambros and Ruvkun groups in 1993 (Wightman et al., 1993; Lee et al., 1993). Years after Horvitz's lab first showed how the lin-4 gene controls the timing of C. elegans larval development (Horvitz and Sulston, 1980), The same team found that the wildtype of a lin-4 mutation was a lin-14 suppressor mutation in a null-lin-4 line, which produced the opposite phenotype from that of a gene named lin-14, in 1987. Lin-4 was identified by the Ambros and Ruvkun groups to be a tiny non-coding RNA and not a protein-coding RNA (Lee et al., 2004). The study teams found that the 3' untranslated region (3'UTR) of lin-14 had a complementary sequence with lin-4, suggesting that lin-4 controlled lin-14 at the post-transcriptional level. Lin-14 was downregulated post-transcriptionally via this region (O'brien et al., 2018). After this discovery, additional miRNAs were discovered in a variety of animals, and it was shown that they were mainly conserved across various species (De Rie et al., 2017).

MiRNAs, also known as small non-coding RNA molecules, are estimated to be 22 nucleotides long. Prior to being cleaved into precursor miRNAs (Pre-miRNAs) and mature miRNAs, miRNAs are firstly synthesised from DNA sequences (Hayes *et al.,* 2014; Wang *et al.,* 2016; Huang, 2017). Targeting the 3'UTR of mRNA in order to degrade mRNA or suppress protein translation is one of miRNA's primary roles. However, additional research has demonstrated that miRNAs interact with other areas such the 5'UTR, coding sequences, and gene promoters

(Broughton *et al.,* 2016). miRNAs play important roles in a wide range of biological functions and are essential for the development of numerous models, including mammals and many others (Fu *et al.,* 2013). Numerous human disorders, including cancer, liver disease, and cardiovascular conditions, have been demonstrated in studies to be brought on by the abnormal expression of miRNAs. However, it has been suggested that miRNAs may be useful as possible biomarkers for a number of disorders. In a particular disease, some miRNAs are raised while others are lowered, resulting in a distinctive miRNA pattern that could be used as a biological therapeutic target or biomarker. For instance, overexpressed miRNAs are frequently referred to as oncogenes in the context of cancer. On the other hand, certain miRNAs express themselves at extremely low levels in specific malignant cells and typically stop the growth of tumours. These miRNA subgroups are referred to as tumour suppressor miRNAs (Walayat et al., 2019).

1.7.1b miRNA therapies

At least two techniques are required to target miRNA expression for disease prevention and possibly therapy (Walayat et al., 2019). The use of oligonucleotides or virus-based constructs is the first technique to either directly decrease the expression of a disease-associated signature miRNA or to directly replace the loss of expression of the miRNA. The second method uses medications to target miRNA transcription and processing in order to change how they are expressed. To prevent miRNA expression, one can employ antisense oligonucleotides, miRNA-mask, miRNA sponges, and small RNA inhibitors. By employing synthetic miRNA (miRNA mimics) or by putting the miRNA gene into viral constructs like adenoviruses, it is possible to restore downregulated miRNA expression. To stop the transcriptional transitions from DNA transcript to pri-miRNA and pre-miRNA, small-molecule miRNA inhibitors may be used. Antisense oligonucleotides may be used to degrade mature miRNA or change it into a duplex form at the mature miRNA level. By complementarily attaching to the target mRNA's 3' UTR region, miRNA masks may compete with endogenous

miRNAs for binding to the particular target at the functional level. By exploiting complementary mRNA binding sites to bind target miRNA with miRNA sponges, target miRNA expression levels may be reduced (Walayat et al., 2019).

1.7.1c Biogenesis of miRNAs

MiRNAs are produced via a process called biogenesis. MiRNA biogenesis happens quickly. According to Drosophila study, which shows that miRNAs have one of the quickest rates of transcript synthesis, at least 40% of mature miRNAs are produced in only 5 minutes (Reichholf et al., 2019). Similar to protein-coding genes, miRNAs may have separate transcriptional regulatory units, but the fact that they are also present within host gene introns shows that transcription may potentially be co-regulated. In contrast to their host gene, several intronic miRNAs contain distinct transcriptional start sites, making them subject to different regulatory sequences and/or promoters (Bartel, 2004). There are two distinct routes that make up miRNA biogenesis: canonical pathways and non-canonical pathways as shown in Figure 11.

1.7.1c (i) Canonical pathway of miRNAs

The most common technique for processing miRNAs is the canonical pathway. To start miRNA production, the genome's primary miRNA transcripts (pri-miRNAs) are first processed post- or co-transcriptionally. RNA polymerase II performs the majority of canonical pri-miRNA transcription. The RNase III enzyme *DROSHA* cleaves pri-miRNAs, which form a hairpin structure in the nucleus, producing premature miRNAs (pre-miRNAs). Chromosome 8 of the DiGeorge syndrome (DGCR8) has a complex including *DROSHA* and RNA-binding protein (RBP). DROSHA cleavage depends on the hairpin shape and the distance between the pri-miRNA stem's single-stranded RNA basal segments and double-stranded RNA junction (Stavast and Erkeland, 2019). Pre-miRNAs are transported from the nucleus to the cytoplasm by an exportin 5 (XPO5)/RanGTP complex, where they are subsequently processed by the

RNase III endonuclease *Dicer* (Okada *et al.,* 2009). Cutting the terminal loop and producing a mature miRNA duplex is what the dicer enzyme does (Zhang *et al.,* 2004). The name of the mature miRNA form is determined by the orientation of the miRNA strand. The 3p strand starts at the 3' end of the pre-miRNA hairpin, whereas the 5p strand starts at the 5' end. Both strands of the miRNA duplex may be loaded in an ATP-dependent manner into the Argonaute (AGO) family of proteins (AGO1-4 in humans) (Yoda *et al.,* 2010). It is possible for both 3p and 5p strands to be incorporated into AGO or primarily one or the other because the amount of each loaded into AGO mostly depends on the cell environment or cell type (Meijer *et al.,* 2014). The selection of 3p or 5p strands for incorporation into AGO is based on the miRNA duplex's 5' end's thermodynamic stability (Khvorova *et al.,* 2003). The guide strand is the one that is favoured to be put into AGO and has the lowest 5' stability. According to the level of complementarity, the passenger strand—also known as the unloaded strand—is hypothesised to be unwound from the guide strand through a variety of mechanisms. In another phase, miRNA duplexes with central mismatches or miRNA that is not loaded with AGO2 are unravelled before being degraded. AGO2 cleaves the passenger strands of miRNA that have no mismatch, and the passenger strand is then degraded by cellular machinery (Ha and Kim, 2014).

1.7.1c (ii) Non-Canonical pathways

The way non-canonical routes utilise various combinations of canonical pathway proteins like Dicer, Drosha, AGO2, and exportin 5 is the primary distinction between them and canonical pathways. The independent *Drosha*/DGCR8 and *Dicer* pathways are two examples of independent pathways that make up the non-canonical miRNA biogenesis. When they are created through the Drosha/DGCR8 independent pathways, pre-miRNAs resemble Dicer substrates. Pre-miRNAs that are formed from introns during mRNA splicing are examples of these, as are pre-miRNAs that are 7-methylguanosine (m7G) capped (Ruby *et al.,* 2007; Babiarz *et al.,* 2008). Without the aid of Drosha for cleavage, these nascent RNAs are

exported to the cytoplasm directly through exportin 1. The significant bias of the m7G cap toward the 3p stand hinders the incorporation of the 5p strand into AGO (Xie *et al.,* 2013). Drosha, on the other hand, uses endogenous short hairpin RNA (shRNA) to process dicer independent miRNAs (Yang *et al.,* 2010). Because these pre-miRNAs are too short to serve as Dicer substrates, AGO2 helps them complete their mutation in the cytoplasm (Yang et al., 2010). This causes AGO2 to load the complete pre-miRNA, which in turn causes the 3p strand to be cut in a manner that is dependent on AGO2. Consequently, the 5p mutation's 3'=5' cutting is complete (Cheloufi *et al.,* 2010).

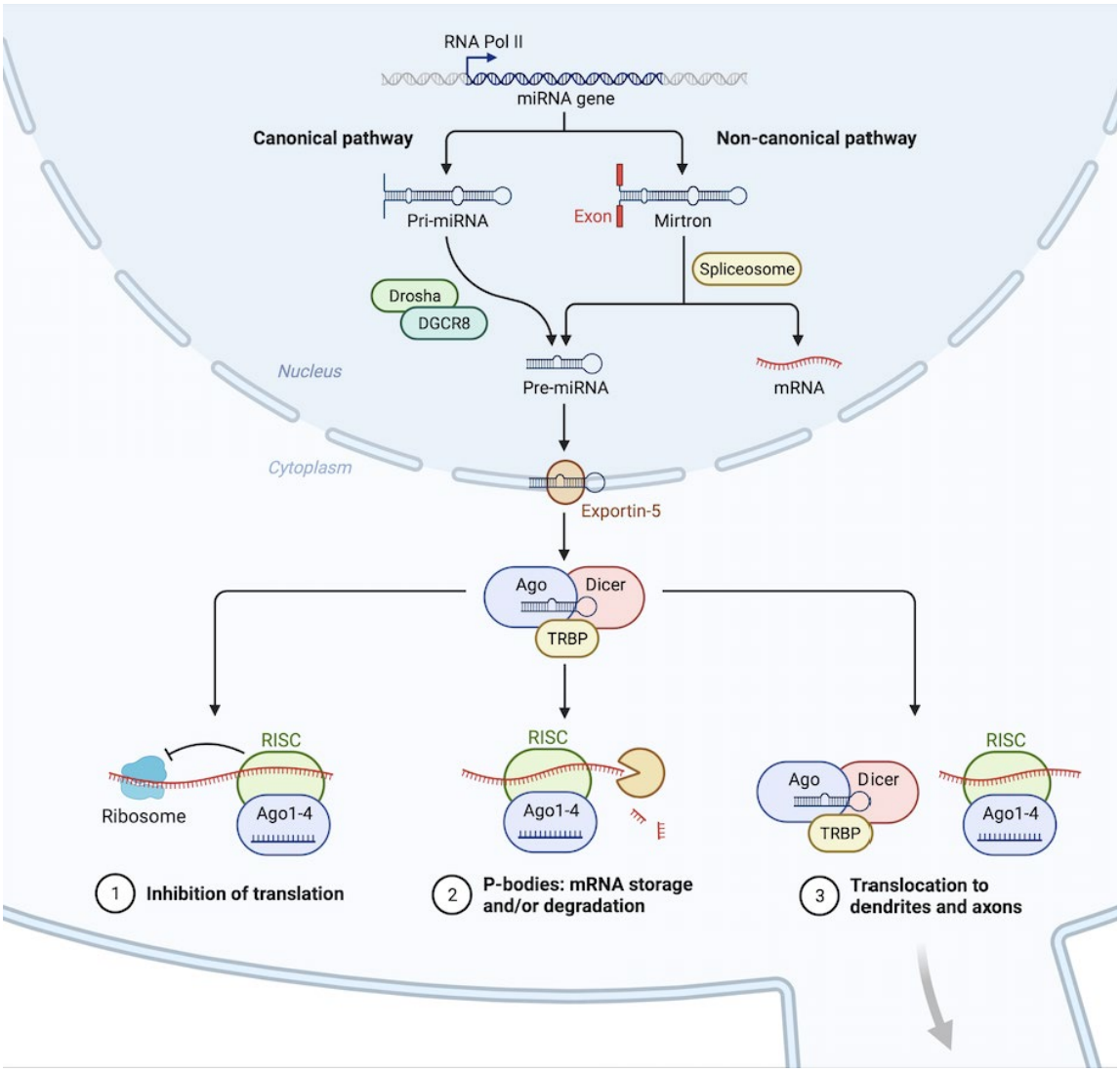

Figure 11: MicroRNA biogenesis and mechanism of action (Created using Biorender.com). To start the biogenesis process, RNA Polymerase II (POL II) or POL III first transcribes the miRNA genes. The primary (pri)-miRNAs are then processed by the DROSHA/DiGeorge syndrome critical region 8 (DGCR8). The produced pre-miRNAs are then exported to the cytoplasm by exportin-5 (XPO-5). Spliceosomes debranched the intron lariat and splice out miRtrons to produce pre-miRNAs. After being exported, DICER/trans-activation-responsive RNA binding protein (TRBP) cleaves pre-miRNAs. The component 3 promoter of the RNA-induced silencing complex (C3PO) complex then breaks down the passenger strand. The RNA-induced silencing complex (RISC), which is in charge of translational repression and subsequently degrading transcripts, has the guide strand as one of its parts.

1.7.1d miRNAs expression and regulation in endothelial cells

A study by Poliseno *et al.,* 2006 on miRNA profiling was performed in endothelial cells using human umbilical vein endothelial cells (HUVEC) and discovered 15 highly expressed miRNAs. The expression of these miRNAs' target genes, which included the angiogenesis-modulating factor receptors, was inhibited (Poliseno *et al.,* 2006). Additional 28 miRNAs were discovered in endothelial cells under typical circumstances (Caporali and Emanueli, 2011). Real-time PCR has also been used to identify the expression of miRNAs in endothelial cells. For instance, miR-126, miR-23a, and miR-24 are expressed in living microvascular endothelial cells (Larsson *et al.,* 2009). The number of miRNAs implicated in angiogenesis may be underestimated because diverse endothelial cell sources and analysis platforms were used. Further research is needed to determine how endothelial cells respond to stress and whether they originate from diseased organisms. For instance, endothelial cells express the miRNA miR-503 in response to ischemia and diabetes (Caporali *et al.,* 2011). More research has revealed that small RNA sequencing (next generation sequencing, or small RNA-seq) can be used to identify an extensive list of endothelial miRNAs that either positively or negatively

regulate endothelial cell functions, including angiogenesis. As an example, small RNA sequencing analysis on miRNAs expressed by endothelial cells under hypoxia (Voellenkle *et al.,* 2010). There is a bidirectional relationship between miRNAs and angiogenesis, according to the evidence from the literature about miRNA expression and activity in endothelial cells, which shows there are two types of endothelial miRNAs: Key angiogenesis pathways are targeted by miRNA, and miRNAs that do express themselves can be affected by stimuli that promote or inhibit angiogenesis (Caporali and Emanueli, 2010).

1.7.1e miRNAs target genes involved in angiogenesis

"Angio-miRNAs" (Angio-miRs), also known as miRNA, are widely found in endothelial cells, where they activate recognised actions via binding to angiogenesis target genes (Wang and Olson, 2009). Angio-miRs must be identified through further research, but some angio-miRs are well known, such as the miR-23/27, miR-126, miR-221/222, and miR-17-92 cluster. MiR-126, a negative regulator of VEGF signalling that targets *PIK3R2* and *SPRED1*, is crucial for maintaining vascular integrity during angiogenesis (Fish et al., 2008). Klf2a, a zinc finger-containing transcription factor, mediates the decrease of miR-126 by blood flow, which determines the activation of VEGF signalling in the endothelium (Nicoli *et al.,* 2010). response of angiogenesis to a stem cell factor (SCF). A particular miRNA found in HUVECs, miR-221, is involved in the control of angiogenesis. MiR-221 modifies the expression of c-kit, the SCF receptor that is essential for the migration of endothelial progenitor cells. According to a 2006 study by Li et al., high glucose levels, which simulate hyperglycaemia, promote the production of miR-221 but decrease the expression of c-kit in HUVECs, impairing endothelial cell motility. By exposing HUVECs to the antisense miR-221 (AMO-221) during treatment with high glucose, the expression of miR-221 and the c-kit protein was recovered. High glucose exposure's inhibitory effect on HUVECs transmigration was eliminated by the AMO-221 therapy. Thus, demonstrating that miR-221 is increased in HUVECS under hyperglycaemic circumstances, which inhibits c-kit and impairs HUVEC motility (Li et al., 2009). Studies have

revealed that overexpression of miR-23 and miR-27 increase angiogenesis by targeting genes with anti-angiogenic properties, such as *Sprouty2* and *Sema6A*. A complicated role for the miR-17-92 cluster in angiogenesis. The cluster's pro-angiogenic activity was detected in miR-17-5p, miR-18a, and miR-19a (Suarez *et al.,* 2008). While miR-17-5p has been found to affect endothelial cell proliferation and migration by targeting tissue inhibitor of metalloproteinase 1 (*TIMP1*), studies have shown that miR-18a and 19a target proteins containing thrombospondin type 1 repeats (*TSR*) (Otsuka *et al.,* 2008).

1.8 cardiac miRNAs

1.8.1 miR-1 and miR-133a

Cardiac miRNAs, which include miR-1, miR-133a, miR208a/b, and miR-499, are tissue-specific. These miRNAs are highly expressed in the myocardium and are crucial for the formation of the heart and the progression of some cardiovascular conditions, including myocardial infarction (MI), in both human patients and animal models. The primary global cause of morbidity and mortality is MI. MiRNAs are critical in cardiovascular disorders, according to mounting data. One of the most prevalent miRNAs in the heart, whether in the initial pathophysiology of MI or during cardiac remodelling, is miR-133a. studies have shown that MiR-133a may be a diagnostic biomarker for acute MI since it is down-regulated in the infarcted area and the border zone of the heart in both MI patients and laboratory animals (Boštjančič et al., 2018). Important MI markers include cardiac troponin T (cTnT) and creatine phosphokinase (CK), although research has shown that miR-133a levels rise quickly after the onset of chest pain even when cTnT or CK levels are not increased. Exosomes contain higher concentrations of circulating miR-133a, which suggests that the live myocardium may be its source (Kuwabara et al., 2011).

Two genes, *MIR-1-1* and *MIR-1-2*, respectively, encode miR-1-1 and miR-1-2. Three genes, *MIR-133A1, MIR-133A2*, and *MIR-133B*, respectively, code for miR-133a-1, miR-133a-2, and

miR-133b (Ohanian *et al.,* 2013). While miR-133a-1 and miR-133a-2 mature sequences are identical, miR-133b mature sequences differ at the 3' end by a single nucleotide. Typically, miR-1 and miR-133a are expressed from the same chromosomal locus; for instance, chromosome 20 contains both *MIR-1-2* and *MIR-133A1*, while chromosome 18 contains MIR-1-1 and MIR-133A2. After cardiac hypertrophy, miR-1 exhibits high expression levels, which alter in the opposite manner during myocardial infarction (MI) (Yang *et al.,* 2008). MiR-133a is linked to cancers like breast cancer and hepatocellular carcinoma in addition to heart disease and development (Ji *et al.,* 2016). MiR-1 and miR-133a promote heart function, cardio-genesis, and pathology. The primary regulators of the early stages of cardio-genesis are miR-1 and miR-133a, which regulate the commitment of embryonic stem cells and mesodermal precursors to the lineage of cardiac-specific muscle cells. By modulating both automaticity and cardiac conductance, miR-1 and miR-133a also control all stages of the cardiac action potential in the heart. Since the deletion of both miR-133a genes may result in abnormal heart smooth muscle gene expression, atypical apoptosis, and incorrect proliferation patterns, miR-133a is particularly important for heart development. MiR-133a is expressed at extremely low levels in endothelial cells under normal circumstances, but in pathological circumstances, miR-133a expression in the endothelium has been substantially linked to cardiovascular disease (Xiao *et al.,* 2019). The molecular and physiological processes by which miR-133a is down regulated in endothelial cells by high expression are largely unclear, despite the fact that aberrant expression of miR-133a causes endothelial dysfunction. Due to this, the abnormal expression of miR-133a in endothelial cells and its impact on angiogenesis were investigated (Xiao *et al.,* 2019).

1.8.1a Pathological role of miR-133a during angiogenesis

Recent research has demonstrated that miRNAs are critical players in major signalling pathways that either promote or decrease angiogenic processes by working with specific angiogenic components. According to studies, angiogenesis in PAD is impaired after hindlimb ischemia due to the increase of miR-133a, which also causes endothelial cells to produce less nitric oxide (NO) (Chen *et al.,* 2018). MiR-133a inhibits angiogenesis in HUVECs by targeting FGFR1 and VEGFR2, which has an impact on cell survival, migration, and proliferation (Soufi-Zomorrod *et al.,* 2016). Fluorescence in situ hybridization was used to compare the carotid arteries of normal rats and rats that had been given streptozotocin (STZ) to imitate diabetes in Peng et al (2016) publication. Because miR-133a is a muscle-specific miRNA, the findings indicated that it was expressed in alpha smooth muscle cell actin in healthy rats. However, in normal rats, endothelial cells did not express miR-133a. MiR-133a was shown to be expressed in endothelial cells in diabetic rats, proving that in addition to being found in smooth muscle cells, miR-133a is also expressed in endothelial cells in pathological circumstances (Peng *et al.,* 2016). Human miR-133a matures during biogenesis by unwinding into two strands that are each about 22 nucleotides long. These mature strands are known as miR-133a-3p and miR-133a-5p. Recent research suggests that increasing miR-133a expression, which is connected to restricting angiogenesis, greatly repaired injured endothelium (Soufi-Zomorrod et al., 2016) and (Chen et al., 2018). However, a recent investigation by Zhu et al., 2021 has shown that miR-133a has a distinct function as a pro-angiogenic regulator of endothelial cells (Zhu *et al.,* 2021). In the trials, exosome transplantation—a potential cell-free therapeutic approach to treat patients with ailments such ischemic heart disease—was used. In rat models, macrophage migration inhibitory factor (MIF)-modified exosomes from umbilical cord MSCs (ucMSCs) are more effective cardioprotective agents. In order to examine the cellular protection mechanisms in H9C2 cardiomyocytes and HUVECs under serum deprivation (H/SD), hypoxia, and infarcted hearts in rats, exosomes from ucMSCs (MSC-Exo), ucMSCs engineered with MIF (MIF-Exo), and ucMSCs with MIF downregulated (siMIF-Exo) were used

in the studies. When compared to MSC-Exo and siMIF-Exo, the results demonstrated that in vitro MIF-Exo dramatically increased migration, proliferation, and angiogenesis in HUVECs. Exosomal miRNA sequencing and qRT-PCR results showed considerably higher expression of miR-133a-3p in MIF-Exo. MiR-133a-3p mimics increased AKT phosphorylation in HUVECs, indicating a beneficial role for this miRNA in cardioprotection. Furthermore, MIF-Exo and miR-133a incubation reduced the biological effects of HUVECs (Zhu *et al.,* 2021). Given the differences reported on the role of miR-133a in endothelial cell angiogenesis this study focused on analysing the effect of miR-133a overexpression in angiogenesis.

1.9 Summary of literature studies, aims and objectives

To summaries the literature studies, angiogenesis is a neovascular process required to form new blood vessels from pre-existing ones. It is tightly regulated by maintaining a balance of both positive and negative regulatory pathways. Pro-angiogenic and anti-angiogenic factors maintain the physiological balance between inhibitory and stimulatory signals, which work alongside with the growth of blood vessels. Several pro-angiogenic factors promote angiogenesis, however the most abundant and important factor is VEGF-A, a potent cytokine, which regulates both physiological and pathological angiogenesis. This work mainly focuses on sprouting angiogenesis (SA) and studying the key angiogenic pathways and genes which regulate this process. In summary, the notch signalling pathway plays a key role in the formation of the tip cell and stalk cells. Key regulators of cell motility allow the tip cell to migrate, while key regulators of the cell cycle allow the stalk cells to proliferate. The initial phase of SA involves the degradation of the ECM, which involves key regulators of ECM-CAM.

As mentioned in the literature, emerging evidence have suggested that microRNAs play a key role as regulators of angiogenesis. miR-133a is a cardiac microRNA, which is expressed essentially in cardiomyocytes and skeletal muscle cells. It is expressed at very low levels in endothelial cells under physiological conditions, however studies have shown under

pathological conditions, elevated miR-133a expression strongly enhanced diseased endothelium. Previous studies on the effect of aberrant expression of miR-133a on endothelial cell angiogenesis have yielded conflicting results (Soufi-Zomorrod *et al.,* 2016, Chen *et al.,* 2018, and Zhu *et al.,* 2021) therefore this thesis aimed to clarify these discrepancies. Furthermore, this work also aimed to analyse the effect of aberrant expression of individual miR-133a strands (-3p or -5p) on angiogenesis, and to characterise their corresponding angiogenic target genes in resting/VEGF-stimulated endothelial cells.

To achieve these aims, the following objectives were established for this work:

1) To analyse the effect of aberrant expression of human miRNA mimics miR-133a-3p, miR-133a-5p, or a negative control mimic (miR-NC) on angiogenesis of primary human endothelial cells HUVEC using Matrigel tubular morphogenesis assays.
2) To determine how transfection of miR-133a-3p, miR-133a-5p, or negative control mimic in primary endothelial cells (HUVECs) affects endothelial cell proliferation, migration, and cell cycle. Analysis of proliferation, migration and cell cycle phases of the transfected cells will be determined by MTT or cell count assays, “wound healing migration assays” and cell-cycle flow cytometry analysis, respectively.
3) To identify specific or common target genes regulated by miR-133a-3p and miR-133a-5p in endothelial cells. Target genes involved in the pro-angiogenic cellular processes analysed in objective 2 will be identified by PCR-based screening of gene arrays containing oligonucleotides to detect the expression of genes related to notch signalling, cell cycle, extracellular matrix, and cell adhesion molecules. Upregulation or downregulation of identified target genes will be further validated Taqman RT-PCR.
4) Bioinformatic analysis of identified target genes for predicted cellular functions affected by miR-133a-3p will be performed to link the target genes to enriched biological functions, when endothelial cells overexpress miR-133a-3p (performed by

our collaborator Dr Manuel Gomez, Bioinformatic Unit, Centro Nacional de Investigaciones Cardiovasculares (CNIC), Madrid, Spain).

5) Search for potential binding sites for miR-133a-3p or -5p in the RNA of the identified target genes by bioinformatic analysis of their sequences using miRNA data bases miRWalk, TargetScan and miRDB.
6) The 3'UTR of the RNA of the selected genes which show potential binding sites for miR-133a-3p or -5p will be selected for cloning and analysis of identified potential binding using luciferase-based reporter vectors.

CHAPTER 2
METHOD AND MATERIALS

2 Method and materials

2.1. Tissue culture

Under aseptic circumstances, tissue culture was carried out using a class II microbiological safety cabinet (BioMAT 2, CAS, UK). The cabinet was sterilised with 1% Trigene (Sigma-Aldrich, UK) and 70% ethanol to reduce the possibility of cell contamination (Sigma-Aldrich, UK). Before beginning any tissue culture research, all solutions were warmed to room temperature.

To sustain and increase the number of cells, passages of the cultured cells were performed often. This procedure entailed aspirating the culture flask's media, then washing the cells in 1x phosphate buffered saline (PBS 1x). The cells were detached after the PBS 1x was aspirated and 0.25% trypsin-EDTA solution was added. A fresh complete medium was added to neutralise the trypsin after cells were inspected under a microscope to see if successful detachment had taken place. After being transferred into a sterile universal tube, the whole contents of the flask were centrifuged for five minutes at 1200 RPM. The pellet was re-suspended in new media, transferred to tissue culture flasks of the necessary size, and the supernatant was discarded. After that, cells were incubated at 37°C and 5% CO2.

2.1.1 Thawing cells

From the liquid nitrogen storage tank or the -80 freezer, a cryovial containing cells in a 10% solution of dimethyl sulfoxide (DMSO) and fetal bovine serum (FBS) was taken out. At 37°C, they thawed. To avoid cell damage, the cell solution was diluted 1:10 in sterile universal tubes filled with tissue culture media. The tubes were then centrifuged at 1200 RPM for 5 minutes. After discarding the supernatant, the cell pellet was re-suspended in new tissue culture media and put into tissue culture flasks of the appropriate size. Then, cells were grown at 37°C and 5% CO2.

2.1.2 Freezing cells

Following the method shown in chapter 2.1, the cell suspension in the flask which was trypsinised and neutralised by adding complete media was transferred to a sterile universal tube and centrifuged at 1200 RPM for 5 minutes. The supernatant was discarded, and the pellet was re-suspended in 1ml of freezing solution (10% DMSO, 90% FBS), and transferred to a labelled cryovial (Nalgene cryoware^{TM} Labware, Roskilde, Denmark) and stored at -80°C or liquid nitrogen, until further use.

2.1.3 Human Umbilical Vein Endothelial Cells (HUVECs)

Endothelial cell growth medium (ECGM), obtained from PromoCell, was used to cultivate HUVECs in tissue culture flasks that had already been coated with 0.1% gelatin. HUVECs were procured from TCS Cellworks. ECGM-supplement mix (Promocell, UK) containing 0.4% endothelial cell growth supplement, 2% FBS, 0.1 ng/ml epidermal growth factor (recombinant human), 90 g/ml heparin, 1 ng/ml basic fibroblast growth factor (recombinant human), and 1 g/ml hydrocortisone was added to 1% penicillin/streptomycin/amphoter. Between passages 4 and 8, HUVECs were employed, as after passage 8, the RNA of HUVECs reduces due to the age of the cells, which effect the further experiments mentioned in this thesis, such as transfection, RNA isolation, Complementary DNA (cDNA) synthesis, and real time PCR.

2.1.4 Human Dermal Fibroblast adult cells (HDFa)

HDFa purchased from TCS Cellworks were cultivated in T75 tissue culture flasks pre-coated with 0.1% gelatine and supplemented with the following nutrients in Dulbecco's Modified Eagle medium (DMEM) from Sigma-Aldrich in the UK: Penicillin/streptomycin/amphotericin B (1%), 1.73 mM L-glutamine, and 10% FBS (Sigma-Aldrich, UK). Following, DMEM "complete" shall be referred to as DMEM with additional supplements. The organotypic co-culture experiment

was performed using HDFa for the tubular morphogenesis analysis as mentioned in chapter 2.9.

2.1.5 Human Embryonic Kidney 293A cells (HEK293A)

HEK293A cells purchased from PromoCell were defrosted in tissue culture flasks pre-coated with 0.1% gelatine in DMEM "complete," and passaging was carried out in T175 tissue culture flasks without pre-coating with gelatine.

2.1.6 Cell cultures maintenance

Under a microscope, the cells were frequently checked for any changes to the cell population or growing media. Every 24 to 48 hours or whenever a pH decrease was detected (noted by a change in the medium's colour), the medium was replaced. The cells were cultured at 37 °C and 5% CO2 until they were more than 80% confluent.

2.1.7 Counting cells

The number of cells in a cell suspension were determined by adding 10 µl of mixed cell suspension to a haemocytometer and cells were counted under the microscope. Using the grids on the haemocytometer, the number of cells in 1ml of the suspension was calculated by multiplying by the number of cells in the haemocytometer x 10^4.

2.2 Transfecting HUVEC cells with miR-133a-3p, miR-133a-5p and miR-NC mimics

Primary HUVEC were transfected with microRNA mimics for human miR-133a-3p (NBS Biologicals, ref: MCH01280), mi-133a-5p (NBS Biologicals, ref: MCH01281) or a scramble negative control mimic (miR-NC) (NBS Biologicals, ref: MCH00000) as following. The day

before transfection HUVEC were seeded in 6-well tissue culture plates at a density of 3 x 10^5 cells/well. The following morning the cells were washed three times with PBS 1x to eliminate any traces of serum and antibiotics and were incubated in OPTIMEM (Gibco) free of serum and antibiotics for 1 hour at 37°C and 5% CO_2. Lipofectamine/miRNA mimic complexes were prepared by mixing 5 µl of Lipofectamine 2000 (1 mg/ml) (Invitrogen) and 100 pmol of microRNA mimics in a final volume of 500 µl. The Lipofectamine/mimics solution was incubated for 1 hour in the dark for complexes to form, and then it was carefully added dropwise to a 6 well-plate containing cells that were incubated in 5 ml of OPTIMEM as described above. The cells and transfection complexes were incubated at 37°C and 5% CO_2 for 6 hours. After 6 hours, the OPTIMEM containing the transfection solution was removed and replaced by 5 ml of complete ECGM. Cells were further incubated for 3 days at 37°C and 5% CO_2 and then used for experiments.

2.3 Cell stimulation

Complete ECGM was extracted for cell stimulation, and cells were then washed twice with PBS 1x. Each well received 5 ml of ECGM serum-free after the PBS had been aspirated. The wells were then incubated at 37°C and 5% CO2 for three hours. HUVECs were stimulated with vascular endothelial growth factor (VEGF) (Peprotech) at a final concentration of 50 ng/ml and incubated for various amounts of time after three hours of serum deprivation. Basic fibroblast growth factor (bFGF) (Peprotech) was used to activate HUVECs for the organotypic experiments outlined in section 2.10 at a final concentration of 25 ng/ml.

2.4 Cell lysis, RNA isolation and purification

For RNA isolation the culture medium was discarded, and the cells were washed with PBS 1x. The PBS 1x was discarded and any excess PBS was removed. Cells were lysed in 300 µl

of “RL lysing buffer” from a “Total RNA purification Kit” (Norgen, Canada). The lysate was stored at -80°C or processed immediately for RNA isolation.

To remove genomic DNA, the lysate was passed through a genomic DNA spin column (gDNA) provided in the kit, by centrifugation at 13,000 RPM for 1 minute. The column (containing the genomic DNA) was discarded and the flow through was mixed by vortex for 10 seconds with 200 µl of 100% (absolute) ethanol. This solution was passed through “RNA spin columns” by centrifugation at 13,000 RPM for 1 minute. The flow through was discarded and the column retaining the RNA was washed twice with 400 µl of wash solution by centrifugation at maximal speed for 1 minutes. To completely remove any traces of ethanol from the column, this was centrifuged at 13,000 RPM for 1 minute. RNA spin columns were placed inside new collection tubes, and 40 µl of “RNA elution buffer” were added to the columns that were incubated for 1 minutes at room temperature. RNA was eluted by centrifugation at 2000 RPM for 2 minutes and again at 13,000 RPM for 1 minute to ensure all RNA is extracted. The purified RNA flow through was transferred to labelled sterile eppendorfs.

2.5 RNA quantification

The nanodrop 2000 spectrophotometer (Thermo Scientific, UK) was used to determine accurate RNA concentration. The machine was blanked with 1.5 µl of elution solution. RNA concentration of each sample was measured by loading 1.5 µl of the sample to the machine. The RNA samples purity was determined at 40 ng/µl. The purity of each sample was determined by calculating the ratio of absorbance at 260nm and 280nm.

2.6 Complementary DNA (cDNA) synthesis

Using a "High-capacity cDNA reverse transcription kit" (Applied Biosystems, UK), RNA was retrotranscribed into cDNA. In nuclease-free water, 500 ng of total RNA were diluted to a final

volume of 10 µl. A reverse transcription (RT) master mix was prepared as shown in Table 2 using the components provided in the kit. 10 µl of RT master mix were added to the 10 µl of total RNA solution (50 ng/µl) samples, followed by a brief 10 second centrifuge. Before putting the tubes in a PTC-200 Peltier thermal cycler set for 25°C for 10 minutes, 37°C for 120 minutes, 85°C for 5 minutes, and 4°C until collection, they were placed on ice. After the retro-transcription was complete, samples were diluted with 80 µl of nuclease-free water and either stored at -20°C for long-term storage or put on ice for immediate use.

Table 2: Preparation of RT master mix using the components of a "High-capacity cDNA reverse transcription kit"

Component	Volume (µl)/reaction
10x RT Buffer	2.0 µl
25x dNTP mix	0.8µl
10x RT random primers	2.0 µl
MultiScribe reverse transcriptase	1.0 µl
Rnase inhibitor	1.0 µl
Nuclease free H20	3.2µl
Total per reaction	**10 µl**

2.7 Quantitative Real time PCR (qRT-PCR)

In a final volume of 10 µl, 2.8 µl of cDNA reaction (5 ng/µl), 0.5 µl of the appropriate TaqMan Gene Expression Assay (Applied Biosystems), and 5 µl of TaqMan™ Universal Master Mix II with UNG (2x) (Applied Biosystems) were combined to create TaqMan qPCR reactions in 96-

well MicroAmp® optical 96 well reaction plates. Table 3 lists the TaqMan gene expression assays that were utilised in this investigation.

Table 3: A reference of all 25 Taqman genes used in this research, with *HPRT-1* (housekeeping) gene used for normalisation.

Genes	Taqman probe ID
MSN	**Hs00741306**
PLAUR	**Hs00958880**
CD44	**Hs01075864**
ID1	**Hs03676575**
CCNE1	**Hs01026536**
CCND1	**Hs00765553**
DLL4	**Hs00184092**
HEY1	**Hs05047713**
JAG2	**Hs00171432**
NOTCH4	**Hs00965889**
NRARP	**Hs04183811**
HES4	**Hs00368353**
TIMP3	**Hs01026536**
ITGA6	**Hs01041011**
ADAMTS1	**Hs00199608**
THBS1	**Hs00962908**
SPARC	**Hs00234160**
CDK1	**Hs00938777**
CCNA2	**Hs00996788**
CCNB1	**Hs01030099**
MCM2	**Hs01091564**
MCM4	**Hs00907398**
CCND3	**Hs01017690**
CCNG1	**Hs00171112**
RCAN1.4	**Hs01120957**
HPRT-1	**Hs99999909**

After applying an optical clear seal, the plate was centrifuged for one minute at 900 RPM and 4°C. A Quant studio 6 Flex PCR equipment was used to carry out the PCR amplification (Applied Biosystems) according to the following conditions: a 10-minute first phase of 95 °C enzyme activation, followed by 40 cycles of 95 °C denaturation, 15 second annealing, and 1 minute of 60 °C extension. The Ct value in each sample was normalised according to the Ct value of the housekeeping gene *HPRT-1* and analysis was performed using the comparative $2^{-\Delta\Delta Ct}$ method.

2.8 SYBr green RT-PCR

In a 6 well plate, 3 x 10^5 HUVECs were transfected with miR-NC or miR-133a-3p. VEGF was applied to the cells for an hour, or they were left untreated. A master mix reaction was created by combining 100 µl of the relevant cDNA with 1350 µl of RT2 SYBR Green ROX master mix (Qiagen) and 1248 µl nuclease free water after RNA extraction and cDNA synthesis as previously reported. The 25 µl of this solution were added to each well of a RT^2 profiler PCR array kit (Qiagen). Gene arrays contain primers to detect 84 genes related to human Notch Signalling Pathway (Kit Ref PAHS-059Y) or cell cycle (Kit Ref PAHS-020Z). The plate was centrifuged at 900 RPM, 4°C for 1 minute. The plate was placed in a Quant studio 6 Flex PCR system (Applied Biosystems), the amplification was set to initial enzyme activation step at 95°C for 10 minutes, followed by 40 cycles of denaturation at 95°C for 15 seconds, and annealing and extension at 60°C for 1 minute. After PCR amplification, the Ct values after 3 independent experiments were analysed using the "Gene global analysing centre" (Qiagen) (https://geneglobe.qiagen.com/us/analyze). Human Extracellular Matrix & Cell Adhesion Molecules Kit (Ref PAHS-013Z) experiment was performed the same way as mentioned above, only that cells were stimulated with VEGF for 4 hours instead of 1 hour. An overview is shown in the figure below.

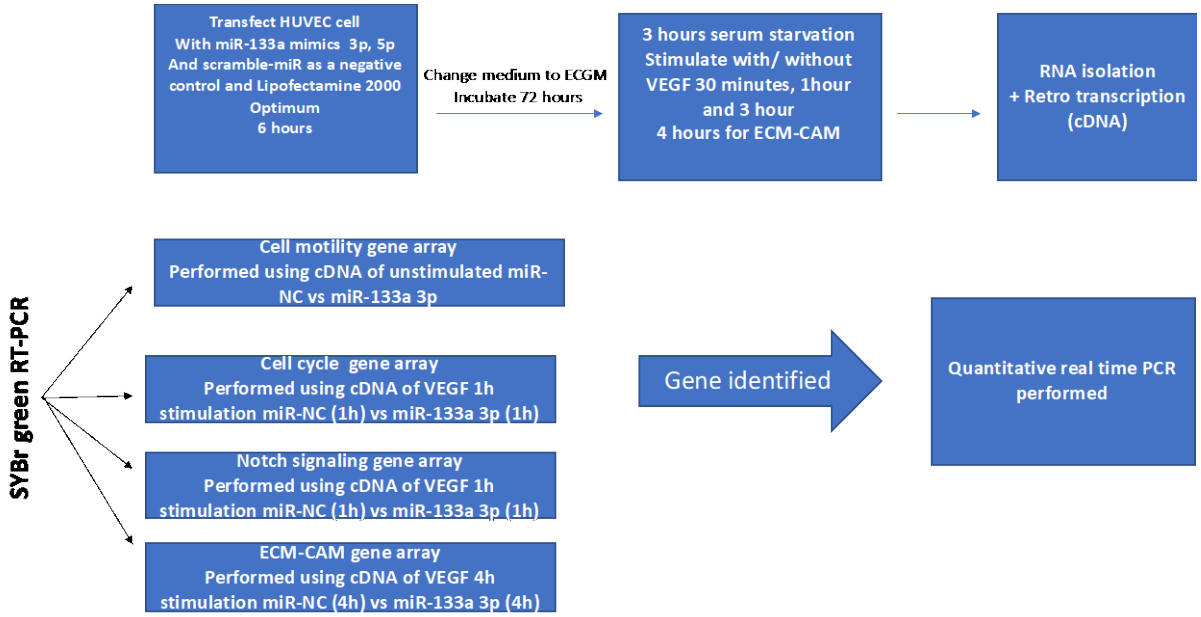

Figure 12: Identification of genes differentially expressed in human endothelial cells by ectopic expression of mimics for miR-133a or a scramble negative control. Overview of gene array screening using RT^2 profiler PCR array kit (Qiagen) containing genes related to cell cycle, Notch signalling, and extracellular matrix-cell adhesion molecules, using cDNA from HUVEC transfected with miR-133a-3p or miR-NC and stimulated with VEGF as indicated. Differential expression of identified genes by specific miR-133a strands (3p or 5p) was further analysed in a new set of transfections by performing qPCR using specific "TaqMan Gene Assays".

2.8.1 SYBr green RT-PCR analysis

After 3 independent experiments the Ct values were exported to "Gene global analysing centre" (Qiagen) (https://geneglobe.qiagen.com/us/analyze). The Ct values were analysed, and the software produced a table (tables shown in appendix), showing the upregulated and downregulated genes, which were highlighted in red and green, respectively. The table showed the following: average ΔCt (AVG ΔCt), 2^- ΔCt (fold induction), fold change and p-value. Genes showing values of AVG ΔCt ≥10 indicated high number of amplification cycles required in the PCR analysis and were not considered in further experiments to improve

accuracy and reproducibility of data. The software also produced the volcano plots, and the genes that had Log2(miR-133a-3p/miR-NC) values more 1 and -Log10(p-value) P values less than 0.05 were chosen as upregulated (red), and those that had values less than 1 and -Log10(p-value) P values less than 0.05 were chosen as downregulated (green). Therefore, for arrays performed on those pathways mentioned above, 25 genes which met the criteria in the volcano plots and tables were further analysed by Taqman RT-PCR.

2.9 Organotypic co-culture

3 x 10^4 Human dermal fibroblast adult (HDFa) cells were put on a 12-well plate that had already been treated with 0.1% gelatine. On 6-well plates, 3 x 10^5 HUVEC cells were also plated at the same time. At 5% CO2 and 37°C, the plates were incubated. The HUVECs were incubated for a further 48 hours after being infected for 24 hours with an adenovirus that expressed human miR-133a (Ad-miR-133a) or a control virus (Ad-miR-control) at a MOI of 200.The adenovirus Ad-miR-133a used in this study was purchased from abm (reference mh0169). This was a precursor miR-133a expressing GFP, for easier observation of the adenovirus using the EVOS microscope. As this was a precursor miR-133a, it expresses mature miR-133a-3p and -5p strands. Ad-miR-NC also purchased from abm (reference m009) was used as a negative control. This is a blank vector producing viruses that do not expresses any miR. Before studies were performed in this study, primary stocks received from the company were amplified and titrated in HEK293-A cells and aliquots of tertiary stock were stored. The amplification and titration of Ad-miR-133a from primary to tertiary stock was performed previously by Kurusamy, S (Kurusamy 2017). The tertiary stocks of Ad-miR-133a or Ad-miR-control, with the titration concentration and the MOI of 200 were used in this study to infect HUVECs.

Infected HUVEC were detached, and 3 x 10^4 cells were plated on top of the HDFa in 1 ml of “Angiogenesis seeding medium”. “Angiogenesis seeding medium” was prepared by adding 25

ml of “angiogenesis seeding supplement” (Cellworks, Ref KC1013) and 0.5 ml of “Gentamycin/Amphotericin B antibiotic supplement 1000x concentrated” (Cellworks, Ref KC1019) to 500 ml of “Angiogenesis Basal Medium” (Cellworks, Ref KC1012). After incubation for 24 hours the medium was replaced with 1 ml of “Angiogenesis Growth Medium” and cells incubated for 13 consecutive days with medium replacement every other day. “Angiogenesis Growth Medium” was prepared by adding 10 ml of “Growth supplement” (Cellworks, Ref KC1014) and 0.5 ml of “Gentamycin/Amphotericin B antibiotic supplement 1000x concentrated” (Cellworks, Ref KC1019) to 500 ml of “Angiogenesis Basal Medium” (Cellworks, Ref KC1012).

When indicated basic Fibroblast Growth Factor (bFGF) (25 ng/ml) were added to the cells. After 13 days post inoculation, tubular structures were visualised by staining endothelial cells using a “CD31 tubule staining kit” (Cellworks, kit Ref ZHA-1225) according to the manufacturer’s recommendation. Briefly, the growth medium was aspirated, and the cells washed with 0.5 ml PBS 1x. Cells were fixed in 0.5 ml of ice-cold ethanol 70% by incubation at room temperature for 30 minutes. Fixed cells were carefully washed three times with 0.5 ml/well of wash/blocking buffer (1% BSA in PBS). Cells were then incubated in 0.5 ml/well of a 1:200 dilution of mouse anti-human CD31 monoclonal antibody (0.1 mg/ml) (Cellworks, Ref KC1004) in wash/blocking buffer at 37°C for 1 hour. Unbound antibody was removed by washing with wash/blocking buffer three times, 5 minutes/each. Then samples were incubated for 1 hour with 0.5 ml/well of a 1:250 dilution of secondary antibody goat anti-mouse IgG1-Alkaline Phosphatase conjugate (1 mg/ml) (Cellworks, Ref KC1005) in blocking buffer. The secondary antibody solution was removed, and the wells were washed with 0.5 ml of dH_2O following the same procedure for washing off the primary antibody. To stain tubes, samples were staining by incubation in 0.5 ml/well of AP substrate at room temperature until tubules development showed a dark purple colour (usually 3-10 minutes). AP substrate solution was prepared by dissolving two tables of 5-bromo-4-chloro-3-indolyl phosphate/p-nitroblue tetrazolium chloride (BCIP/NBT) (Cellworks, Ref KC1010) in 20 ml of dH_2O. Substrate solution

was filtered using a disposable syringe through a 0.2 µm filter disc to eliminate aggregates. The staining was monitored to not exceed 20 minutes. The wells were then washed carefully once with 0.5 ml dH_2O. The dH_2O was removed and the plate was left to air dry. Images were taken on an EVOS microscope at 4x magnification. Number of junctions were quantified using the image J software with the macro's plugin angiogenesis analyser (Carpentier *et al.,* 2020).

2.10 Matrigel tube formation assay

Using the same procedure as chapter 2.2, miR-NC, miR-133a-3p, or miR-133a-5p were transfected into HUVEC cells (3 x 10^5 cells/well). In order to enable the Matrigel to harden, a 96-well culture plate was covered with Geltrex™ Matrix (low growth factors) (Invitrogen) and incubated at 37°C and 5% CO2 for 30 minutes. The transfected HUVEC cells were detached and 2 x 10^4 cells/well were plated on top of the Geltrex in ECGM serum free + 1% FBS containing VEGF 50 ng/ml when indicated. The plate was incubated at 37°C, 5% CO_2 for 24 hours and images were recorded using a Nikon DSFi1 digital camera coupled to a Nikon ECLIPSE TS100 microscope at 4x magnification. Tube formation was quantified using the image j software with the macro's plugin angiogenesis analyser (Carpentier *et al.,* 2020).

2.11 Wound healing cell migration assay

Using a "CytoselectTM 24-well wound healing test kit" (Cell Biolabs), cell migration studies were carried out on HUVEC cells (3 x 10^5 cells/well) transfected with miR-NC, miR-133a-3p, or miR-133a-5p (Cell Biolabs). The assay kit's 24 well cell culture plates with 0.1% gelatine were used to cultivate the transfected HUVECs after they had been removed and plated at a density of 7 x 10^4 cells per well. Gap inserts were utilised to create a 0.9 mm gap on the surface of the well the cells were in. For 24 hours, the plates were incubated at 37°C with 5% CO2 to promote cell adhesion. Gap producers were eliminated, and cells representing time zero (T=0) were stained using a 0.6% crystal violet/0.025% ammonium oxalate/5% ethyl

alcohol solution (Sigma-Aldrich, UK), which was incubated for 15 minutes at 37°C with 5% CO2. The excess dye was removed by washing the wells three times with PBS 1x, and the cells were then fixed for 10 minutes at room temperature using formalin solution (10% neutral buffer containing formaldehyde 4% w/v) (Sigma-Aldrich, UK). The fixed cells were washed twice with PBS 1x, and images were taken on a Nikon ECLIPSE TS100 microscope at 4x magnification, which was coupled to a NikonDSFi1 digital camera. Gap creators was removed from the plate containing cells corresponding to time 24 hours (T=24), and the medium was changed to ECGM supplemented with VEGF (50 ng/ml) and incubated at 37**°**C, 5% CO_2 for 24hours. After incubation, cells were stained, fixed and images captured as mentioned above. Cell migration was analysed using image j. The value of the non-migrated area at time 24 hours was subtracted from the original wound area at time 0 hours to compute the migrated area, which was then reported as a percentage of the initial wound area.

2.12 MTT assay

HUVEC endothelial cell growth was assessed using MTT assays. HUVEC that had been transfected as described with mimics of miR-NC, miR-133a-3p, or miR-133a-5p were planted on 96-well tissue culture plates at a density of 4 x 10^3 cells/well without the use of gelatine pre-coating. To help the cells adhere to the plates, they were incubated at 37°C and 5% CO2.The following day MTT assay was performed on the plates corresponding to day zero (T=0) by adding 50 µl/well of a 5 mg/ml solution of MTT (3-(4,5-dimethyllthylthiazol-2-yl)-2,5-diphenyl tetrazolium bromide) directly to the culture medium. The MTT solution is light sensitive, therefore, the plates were wrapped in aluminium foil and incubated at 37**°**C, 5% CO_2 for 4hours. After incubation, the medium containing the MTT solution was aspirated and 80 µl of DMSO and 20 µl of Sorensen's glycine buffer (0.1 M glycine-0.1 M NaCl equilibrated to pH=10.5) were added to the wells containing the cells. A Multiskan Ascent plate reader (Thermo Labsystems, UK) was used to measure the absorbance at 540 nm. In the remaining plates corresponding to 3 days (T=3), the medium was aspirated and ECGM supplemented

with VEGF (50 ng/ml) was added and plates were incubated at 37°C, 5% CO_2 for 3 days. After 3 days of incubation, MTT analysis was performed as mentioned above. By dividing the absorbance at 540 nm of samples from cells cultured for 3 days by the absorbance of samples from cells at time = 0, the proliferation rate was estimated.

2.13 Cell cycle

The stages of the cell cycle that are impacted when miR-NC or miR-133a-3p are transfected into HUVECs were examined using flow cytometry assays. HUVEC were transfected with miR-NC or miR-133a-3p as described in chapter 2.2. Transfected cells were trypsinised and neutralised with ECGM complete. Transfected cells were detached and centrifuged at 1500 RPM for 5 minutes. The pellets were resuspended in PBS 1x to remove excess media and centrifuged again at 1500 RPM for 5 minutes. Cells were then resuspended in 100μl of PBS 1x and 900μl of ice cold 70% ethanol for fixation. The cells were fixed overnight at 4°C. The following day, fixed cells were washed twice with PBS1x to remove excess ethanol and the pellets were resuspended in 300 μl of propidium iodide (50μg/ml PI with 100μg/ml RNAse A in PBS 1x). A BD FACSMelody™ cell sorter was used to perform flow cytometry on the tubes after they had been incubated at room temperature for 15 minutes and covered with foil. The proportion of cells in each cell cycle phase was then calculated.

2.14 Recombinant DNA technology

2.14.1 Luria broth and antibiotic agar plates preparation

Luria broth (LB) solution was made by combining 1 litre of deionized water with 25 grammes of Luria broth powder (Sigma Aldrich). 15 g of agar (Fluka Biochemika) was added per litre of Luria Broth solution to prepare LB-agar. The solutions were autoclaved at 121°C for 15 minutes. The autoclaved LB-agar was melted in a microwave and kept at 50°C until the

antibiotic was added to make antibiotic agar plates. In a sterile setting, 25 ml of LB-agar with 100 µg/ml of ampicillin was placed onto petri dishes, and the solution was allowed to set up overnight.

2.14.2 DNA agarose gel electrophoresis

Ultrapure Agarose, purchased from Invitrogen, UK, was used to prepare the different percentages of agarose gel depending on the size of the DNA fragments. DNA fragments which are approximately 800 bp or less, were analysed with a 2% agarose gel, whereas for DNA fragments greater than 1000 bp, a 0.7%- 1% gel was used. Ultrapure agarose was dissolved in tris acetate-EDTA buffer (TAE) 1x (Invitrogen). The solution was heated to dissolve the agarose and cooled slightly before adding Ethidium Bromide (EtBr) (0.3 µg/ml final concentration). The agarose gel was poured into a gel casting device and comb insert was placed. After the gel polymerised, 15 µl of the 1 Kb Plus DNA Ladder (Invitrogen) 50 ng/µl, was added first followed by DNA samples. The gel was run at 90V until the DNA fragment of interest could be quickly recognised and separated. Under UV light, DNA was seen using a SYNGENE DNA gel documentation system.

2.15 preparation of plasmid DNA

2.15.1 Mini prep

The colonies were collected from the agar plates using sterile loops and inoculated in universal tubes containing 10 ml of LB broth and ampicillin (100 µg/ml final concentration) and placed in a 37°C incubator with rotary shaking for 24 hours. The tubes were removed from the shaker, A cloudy solution indicated the presence of bacteria in the tubes. The mini prep plasmid preparation was performed using a “QIA prep ® Miniprep Kit” (QIAGEN). To collect the bacteria containing plasmid, 1 ml of grown bacterial culture was transferred to eppendorf tubes

and centrifuged at 4,000 RPM for 2 minutes. The supernatant was discarded, and this procedure was repeated 3 more times. After the final discard, the bacterial pellet was resuspended in 250 µl P1 buffer followed by 250 µl of P2 buffer. The suspension was mixed by inversion to form a thick mucus confirming lysing of bacteria. The suspension was neutralised using 350 µl of N3 buffer and was mixed by inversion for chromosomal DNA to form precipitates. Centrifugation was used to separate the precipitates for 5 minutes at 13,000 RPM. To further purify the plasmid, the supernatant was then added to the kit's supplied column. The column was centrifuged at 13,000 RPM for 1 minute. The flow through was discarded and the column containing the plasmid was washed by adding 750 µl of PE buffer (wash buffer) followed by centrifugation for 1 minute. The waste was discarded, and the column further spun to remove excess of PE buffer as it contains ethanol and should be completely removed before the elution step. Plasmid DNA was eluted by adding 50 µl of elution buffer to the column after it had been placed into a fresh collection tube. The columns were centrifuged at 13,000 RPM for 1 minute after being incubated at room temperature for 1 minute. The plasmid-containing flow-through was collected and kept at -20°C.

2.15.2 Maxiprep

The samples which contained the newly generated plasmid were selected for maxiprep. To achieve maximal bacterial growth, bacteria were inoculated into 400 ml of LB-antibiotic from a culture in the lag phase. As a general protocol, the day before inoculation, 1 ml of miniprep culture were inoculated in 9 ml of LB-ampicilin and incubated at 37°C in a rotary shaker incubator overnight. The following day the culture was diluted 1:10 in fresh LB-ampicillin medium in a new culture tube and incubated at 37°C in the rotary shaker till the evening. At the evening, the lag phase culture was inoculated into 400 ml of LB-antibiotic and incubated at 37°C in the rotary shaker overnight.

By centrifuging the cultures for 15 minutes at 4500 RPM, the bacteria were extracted from the growing cultures. The pellet was resuspended in buffer P1 from a plasmid maxi kit (Qiagen) after the supernatant was discarded.10 ml of P2 buffer was added and mixed by gently inversion to lyse the bacteria. 10ml of buffer P3 was added for neutralization and mixed by inversion until precipitates were observed. The suspension was centrifuged for 15 minutes at 4500 RPM to remove precipitates of cellular debris and chromosomal DNA. 10 ml of "Equilibration Buffer" were passed through the column to provide the right pH and moisture conditions to the columns before applying the solution containing the plasmid. Once all "Equilibration Buffer" completely passed through the column, 25 ml of the solution containing the plasmid was added to the columns. The solution passed through the column and the plasmid DNA was retained in the column. The column was washed twice with of 30 ml of "Wash buffer". Plasmid was eluted from the column by adding 15 ml of "Elution Buffer". Once the solution completely passed through the column, the plasmid was precipitated by adding 10.3 ml of isopropanol. Precipitated plasmid was collected by centrifugation at 9600 RPM for 1hour. The supernatant was discarded, and the pellet was resuspended in 300 µl nuclease free water. Plasmid concentration was measured using a nanodrop UV-Vis spectrophotometer (Thermo Scientific™). The plasmid concentration was obtained by measuring the absorbance at 260 nm. As reference, a solution of 50 ng/µl yielded 1 unit of absorbance at 260 nm. The maxiprep samples were then stored at 20°C for further experiments.

2.16 Cloning

2.16.1 Amplification of the 3' untranslated region of CD44 RNA by PCR

CD44 was one of the genes affected when HUVEC cells were transfected with miR-133a-3p and -5p. A bioinformatic prediction website called Target scan predicted that miR-133a-5p targets the 3'UTR of *CD44* RNA at position 3063 to 3070. Therefore, to demonstrate CD44 is a target of miR-133a, the 3'UTR of CD44 was cloned into the pmirGLO dual luciferase Vector (Promega).

cDNA generated from total RNA isolated from HUVEC was used as template. To generate this cDNA, 500 ng of HUVEC total RNA were retro-transcribed as described in section 2.6, except that oligo dT primer was used instead of random primers.

Amplification of the full-length sequence of *CD44* 3' UTR was not achieved due to the long length of the sequence. Therefore, the 3'UTR of *CD44* was split into several fragments and clone these fragments downstream of the luciferase gene in pmirGLO. To amplify different fragments of the 3' UTR of *CD44* gene (NCBI accession number NM_000610.4) oligo forward and reverse were included in PCR reactions using HUVEC cDNA as template as indicated in Table 4. *Sfi* master mix ready-to-use 2X (Invitrogen) solution containing Taq DNA polymerase with proof-reading activity, dNTPs, $MgCl_2$ and reaction buffers at optimal concentrations, were used for efficient PCR amplification of DNA templates.

Table 4: PCR master mix preparation

PCR set-up	X1
Template (HUVEC cDNA)	10 µl
Oligo forward (100 ng/µl)	1 µl
Oligo reverse (100 ng/µl)	1 µl
Nuclease free water	13 µl
Sfi master mix 2x	25 µl
Total	50 µl

Oligonucleotides to amplify different fragments were purchased from Sigma-Genosys, UK, and resuspended to a final working concentration of 100 ng/µl. Positions and sequences of the oligos used in this study are shown in Table 5

Table 5: positions and sequences of the oligos used in the study of the human *CD44* 3'UTR

Oligo names (ALA)	Position	sequences
ALA 314-315	2164 to 3947	Oligo 314 forward CTCGAGCCTCAGCTAAGACTGGGTCCTTTG Oligo 315 reverse CTCGAGCCCCAGGCACTTAACTCATCCTA
ALA 319-318	3911 to 5725	Oligo 319 forward CTCGAGATGCAGTTGCTATTTAGGATGAGT Oligo 318 reverse CTCGAGCCTTTAGTCTTTTAATGTTAGCCT
ALA 314-322	2164 to 3026	Oligo 314 forward CTCGAGCCTCAGCTAAGACTGGGTCCTTTG Oligo 322 reverse CTCGAGAACCCTGGGAAATGTCCTTAGCTG

ALA 323-315	3003 to 3947	Oligo 323 forward CTCGAGCAGCTAAGGACATTTCCCAGGGTT Oligo 315 reverse CTCGAGCCCCAGGCACTTAACTCATCCTA
ALA 319-325	3911 to 4809	Oligo 319 forward CTCGAGATGCAGTTGCTATTTAGGATGAGT Oligo 325 reverse CTCGAGAAATAACCTCCTGTCTCAGCCTC
ALA 324-318	4786 to 5725	Oligo 324 forward CTCGAGGAGGCTGAGACAGGAGGTTATTT Oligo 318 reverse CTCGAGCCTTTAGTCTTTTAATGTTAGCCT

Annealing temperature in PCR amplification conditions was set 3°C lower than the Tm of the oligos used in the PCR reaction. Tm for each oligonucleotide was calculated according to the formula:

Tm = (A+T) x 2 + (G+C) x 3

PCRs were performed in a PTC-200 Peltier thermal cycler according to the following conditions:

- Using the oligonucleotides (ALA314 and ALA315), the CD44 RNA 3'UTR fragment between nucleotides 2164 and 3947 was amplified 35 times in which each cycle consisted of 1 minute of 94°C denaturation, 1 minute of 55°C annealing, and 1 minute of 72°C extension. For a final extension phase, reactions were conducted for 10 minutes at 72°C.
- Using the oligonucleotides (ALA319 and ALA318), the CD44 RNA 3'UTR fragment between nucleotides 3911 and 5725 was amplified 35 times in which each cycle consisted of 1 minute of 94°C denaturation, 1 minute of 51°C annealing, and 1 minute of 72°C extension. For a final extension phase, reactions were conducted for 10 minutes at 72°C.
- To amplify the fragment of the CD44 RNA 3'UTR between nucleotides 2164 and 3026, oligonucleotides (ALA314 and ALA322) must first undergo a denaturation phase at 94°C for two minutes, followed by 35 cycles of 1 minute of denaturation at 94°C, 1

minute of annealing at 57°C, and 1 minute of extension at 72°C. For a final extension phase, reactions were conducted for 10 minutes at 72°C.

- Using the oligonucleotides (ALA323 and ALA315), the CD44 RNA 3'UTR fragment between nucleotides 3003 and 3947 was amplified 35 times in which each cycle consisted of 1 minute of 94°C denaturation, 1 minute of 55°C annealing, and 1 minute of 72°C extension. For a final extension phase, reactions were finished at 72°C for 10 minutes.
- Using the oligonucleotides (ALA319 and ALA325), the CD44 RNA 3'UTR fragment between nucleotides 3911 and 4809 was amplified 35 times in which each cycle consisted of a denaturation phase lasting 1 minute at 94°C, an annealing phase lasting 1 minute at 51°C, and an extension phase lasting 1 minute at 72°C. At 72°C for 10 minutes, reactions were finished for the last extension step.
- Using the oligonucleotides (ALA324 and ALA318), the CD44 RNA 3'UTR fragment between nucleotides 4786 and 5725 was amplified 35 times, with each cycle lasting 1 minute, followed by 1 minute at 51 degrees Celsius for annealing and 1 minute at 72 degrees Celsius for extension. For a final extension phase, reactions were finished at 72°C for 10 minutes.

2.16.2 DNA Precipitation

Amplified fragments were precipitated from the PCR reaction precipitation by adding 0.1 volumes of 3M sodium acetate and 2.5 volumes of absolute ethanol to the reaction tube. The solution was mixed by stirring and incubated at -20°C for at least 24 hours. Centrifugation was used to obtain precipitated DNA for 10 minutes at a speed of 13000 RPM. The DNA pellets were redissolved in water devoid of nucleases after the supernatant was discarded.

2.16.3 DNA digestion with restriction enzymes

DNA plasmids were digested with restriction enzymes (Promega), using the buffer recommended by the manufacturer (Promega), BSA, which has been acetylated, was combined with nuclease-free, ultra-pure distilled water to a final volume of 30 µl. 50% of the enzyme was introduced in the morning and the digesting process was incubated at 37°C until the evening in order to maximise the activity of the restriction enzyme. The samples were incubated at 37°C overnight after the remaining 50% of the enzyme was introduced in the evening. After DNA precipitation, PCR-amplified fragments were resuspended in 70 µl of nuclease-free water and digested with restriction enzymes and corresponding buffers, which are shown in table 6, although the final volume was 100 µl.

Table 6: enzymes and corresponding buffers for the fragments used in this study.

Plasmids	Digest for size	Corresponding Buffer	Digest for right orientation	Corresponding Buffer
2164 to 3947 (ALA 314-315)	*xhoI*	Buffer D	*xbaI*	buffer D
3911 to 5725 (ALA 319-318)	*xhoI*	Buffer D	*SalI + ScaI*	buffer D
2164 to 3026 (ALA 314-322)	*xhoI*	Buffer D	*ApaI*	buffer A
3003 to 3947 (ALA 323-315)	*xhoI*	Buffer D	*xbaI*	buffer D
3911 to 4809 (ALA 319-325)	*xhoI*	Buffer D	*xbaI*	buffer D
4786 to 5725 (ALA 324-318)	*xhoI*	Buffer D	*xbaI*	buffer D

2.16.4 DNA gel purification

Once plasmids of PCR products were digested, 6x loading dye was added to the digestion reaction to obtain a 1x final concentration of loading dye buffer. DNA fragments were separated by DNA gel electrophoresis, and the part of the gel containing the DNA fragment of interest was cut out and extracted from the gel using a “QIAquick® gel extraction kit” (Qiagen) according to the manufacturer’s instructions. Briefly, 600 µl of “QG Buffer” was added to a

tube containing the cut piece of gel and heated at 50°C for 10 minutes with 2 mins intervals of vortexing to allow the gel to dissolve. Once the gel completely dissolved in QG buffer, 200 µl of isopropanol was added and the mixture was mixed by in version. The solution was passed through a centrifugation column provided in the kit by centrifugation at 13,000 RPM for 1 minute. The DNA was retained by the column and the flow through was discarded. 500 µl of QG buffer was added again to the columns, and these centrifuged at 13,000 RPM for 1 minute, to ensure all impurities were removed. The flow through was discarded and 750 µl of “Buffer PE” (wash buffer containing ethanol) was added to the columns. The columns were centrifuged at 13,000 RPM for 1 minute. To guarantee that all of the wash buffer was removed, the flow through was discarded, and the columns underwent one more centrifugation. New collecting tubes were installed in their place of the old ones. The columns received 20 µl of "EB Elution buffer" before being centrifuged at 13,000 RPM for 1 minute after being incubated at room temperature for 1 minute. The purified DNA-containing elute was put into sterile, marked eppendorfs and kept at 4°C.

2.16.5 Preparation of pmiRGLO plasmid for cloning

15 µg of pmirGLO Dual-Luciferase Vector (Promega) were digested with *XhoI* as described. As this vector was going to be used in ligation reactions, digested pmirGLO plasmid was precipitated and 5’ ends dephosphorylated using Alkaline Phosphatase (AP)(Promega), in a solution containing their corresponding buffer that was incubated a 37°C water bath for 60 minutes. Digested and dephosphorylated plasmid was run through a 0.7% agarose gel and purified from the gel as described in chapter 2.16.4.

2.16.6 Ligation

The following was the setup for ligation reactions: In a final volume of 20 µl, combine 25 ng of vector, insert (1:3 molar ratio between the vector and insert utilised in the ligation process),

nuclease-free water, ligase buffer 1X (New England Biolabs), and *T4 DNA Ligase* (2x106 U/ml). Samples were incubated in a PTC-200 Peltier thermal cycler for the whole night at 15°C.

2.16.7 Bacterial transformation

The ligation reaction was added to 200 µl of competent E.*coli* JM109 (transformation efficiency 10^8 cfu/µg) (Promega) and the mixture incubated ice for 30 minutes. The sample was then heat shocked at 42°C for 2 minutes and immediately cooled down by placing it back on ice. 300 µl of Luria Broth (LB) medium was added to the sample that was placed horizontally in a 37°C shaker for 1 hour to allow bacteria to produce ampicillin resistance. Bacteria were plated on LB agar plates with ampicillin (100 g/ml) after an hour, and they were then left to incubate overnight at 37 °C. The following morning ampicillin-resistant colonies (containing the plasmid) were collected and inoculated in universal tubes containing 10ml of LB broth ampicillin (100 µg/ml) and placed in a 37°C rotary shaker for 24 hours for further experiments.

2.16.8 Sequencing

To verify the accuracy of the PCR results, the plasmids produced in this work were sequenced at the Department of Vascular Biology and Inflammation, Centro Nacional de Investigaciones Cardiovasculares CNIC, Madrid, Spain. Sequencing of the plasmids confirmed the fidelity of the PCR amplification, successful recombination, and generation. To do this, plasmids were sent to the company “Eurofinsgenomics”, (http://eurofinsgenomics.eu) for sequencing by standard Sanger technology according to the manufacturer’s recommendation. Briefly, the plasmids were diluted to 200 ng/µl with Nuclease free water. 5 µl of plasmid solution was placed in an eppendorf tube and 5 µl of the appropriate forward or reverse primers (at a concentration of 5 pmol/µl) were added and mixed thoroughly. The sequences of the primers

used, were pmirGLO sequencing forward 5' AAGGACTGACCGGCAAGTTGGAC 3', pmirGLO sequencing reverse 5' TCTTATCATGTCTGCTCGAAGCG 3'. Sequencing reactions were performed by the company. Electropherogram of sequencing reactions were provided as .ab1 files. ab1 files containing sequences were visualised using software Chromas 2.5. sequences were stored in FASTA files, that were used to validate the fidelity of the sequences of the PCR amplified fragments by comparing them to published sequences using Blast software (http://blast.ncbi.nlm.nih.gov).

2.17 Luciferase reporter analysis

2.17.1 Co-transfection of miR-133a mimics and plasmids into HEK293 cells

HEK293-A cells were plated on 12-well tissue culture plates pre-coated with 0.1% gelatine at 2 x 10^5 cells/well. The following morning the cells were washed three times with PBS 1x to eliminate any traces of serum and antibiotics and were incubated in 1 ml of OPTIMEM (Gibco) free of serum and antibiotics for 1 hour at 37°C and 5% CO_2. Lipofectamine/plasmid complexes were prepared by mixing 1.6 µl of Lipofectamine 2000 (1 mg/ml) (Invitrogen) and 2 µg of plasmid together with 100 pmoles of the corresponding miRNA mimic in a final volume of 170 µl. The Lipofectamine/miRNA mimic/plasmid solution was incubated for 1 hour in the dark for complexes to form, and then it was carefully added dropwise to the 12-well plate containing HEK293 cells incubated in OPTIMEM as described above. The cells and transfection complexes were incubated at 37°C and 5% CO_2 for 24 hours. Then, the OPTIMEM containing the transfection solution was removed and replaced by 1 ml of complete DMEM. Cells were further incubated for 24 hours at 37°C and 5% CO_2 and then used to measure luciferase activity of the cells.

2.17.2 Dual Luciferase assay

A "Dual-Luciferase® Assay Kit" (Promega, UK) was used to evaluate the activities of Firefly and Renilla Luciferase in the transfected cells. The medium was removed from the plates 24 hours after transfection, and 400 µl of "Passive lysis buffer Reagent" 1X was used to lyse the cells (Promega, UK). The plates were incubated at room temperature for 5 minutes on a rocker. The next procedure involved measuring firefly and renilla luciferase of all the well. Firefly luciferase activity was measured by mixing 100 µl of “Firefly luciferase Substrate” (Promega, UK) and 5 µl of cell lysate. Relative Light Units (RLU) produced by Firefly Luciferase were measured for 30 seconds using a SIRIUS Luminometer V3.1 (Berthold detection systems, UK). Once firefly luciferase was measured, *Renilla* luciferase (*hRluc-neo*) was measured by adding in the same tube 100 µl of “Dual-Glo® Stop & Glo® Reagent” and measuring emitted RLUs for another 30 seconds. *Renilla* luciferase activity was used for normalisation of Firefly Luciferase activity between the different samples.

2.18 Bioinformatic analysis

The 25 genes selected from the gene arrays as mentioned in chapter 2.8.1, the 3'UTR sequences of the differentially expressed genes were analysed using bioinformatic methods using the databases miRWalk, Target-scan, and miRDB to see whether any putative sequence motifs that are complementary to the sequence for miR-133a-3p or -5p exist. The selection criteria involved look at which strand (-3p/-5p or both) target which position of the 3’UTR of the selected genes. The databases also gave a prediction score of the binding of the miR-133a strands to the position in the RNA of the selected genes. A table showing the selection criteria are shown in the appendix 4.

CHAPTER 3
RESULTS

3 Results

3.1 Aberrant expression of miR-133a attenuates VEGF- and bFGF- induced tubular morphogenesis of endothelial cells

Finding out how miR-133a's influence on endothelial cell tubular morphogenesis affected angiogenesis was the first step in investigating the effects of aberrant expression on angiogenesis. The first initial study involved primary endothelial cells (HUVEC) to be infected with adenovirus miR control (Ad-miR-NC) and adenovirus miR-133a (Ad-miR-133a) with a MOI of 200. Ad-miR-133a, is a precursor miR-133a, expressing both miR-133a-3p and miR-133a-5p therefore the first step involved looking at endothelial cell tubular morphogenesis when HUVECs overexpress a precursor miR-133a. then further study endothelial cell tubular morphogenesis affected angiogenesis expressing the two mature strands. The infected cells were stimulated with bFGF (25 ng/µl) or left unstimulated (control). The focus of this PhD research is mainly on VEGF, however another pro-angiogenic factor, basic fibroblast growth factor (bFGF) was also analysed for tubular morphogenesis, to see if aberrant expression of miR-133a attenuates bFGF-induced angiogenesis. Tubular morphogenesis was determined after 13 days by organotypic co-culture assay. Cell stimulation with pro-angiogenic stimuli bFGF strongly activated tube formation in endothelial cells infected with Ad-miR-NC (Fig 13). However, expression of miR-133a in cells infected with Ad-miR-133a significantly attenuated bFGF-induced angiogenesis (Fig13).

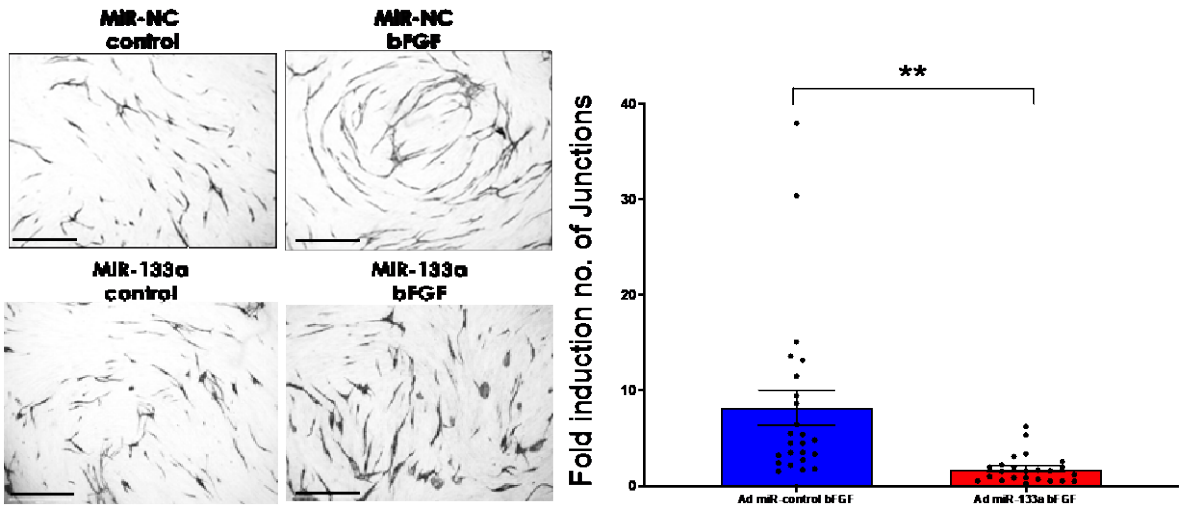

Figure 13. Tube formation in HUVEC cells infected with Ad-miR-NC vs Ad-miR-133a treated with pro-angiogenic stimuli bFGF (25 ng/µl). Representative microscopy fields of endothelial tube formation after staining with anti-CD31 antibody. Control, untreated cells. bFGF, cells treated with bFGF (25 ng/ml). MIR133a, cells infected with Ad-miR-133a. MIR-NC, cells infected with Ad-miR-NC. Scale bars, 1000 µm. Histograms show data as mean ± SEM, n = 8 **, *P* = 0.0012, for comparison of bFGF-induced tube formation in Ad-miR-133a vs Ad-miR-NC infected cells by unpaired t-test

The second study, miR-NC, miR-133a-3p, or miR-133a-5p mimics were transfected into primary endothelial cells (HUVEC), and Matrigel tubular tests were used to measure tube formation to demonstrate which mimic affected endothelial cell tubular morphogenesis. When compared to HUVECs transfected with the control miR-NC, miR-133a-3p substantially reduced tubular morphogenesis, as seen in Figure 14. While HUVECs transfected with miR-133a-3p demonstrated little response to VEGF stimulation, those transfected with miR-NC showed a significant increase in tube formation. When compared to the control group, overexpression of miR-133a-5p showed a reduction in tubular morphogenesis, despite the fact that the impact of the 5p strand was less potent than that of the 3p strand. VEGF stimulation in cells overexpressing miR-133a-5p still significantly increased tube formation. Overall, our findings imply that aberrant miR-133a-3p expression in HUVECs inhibited both basal and VEGF-induced tubular morphogenesis.

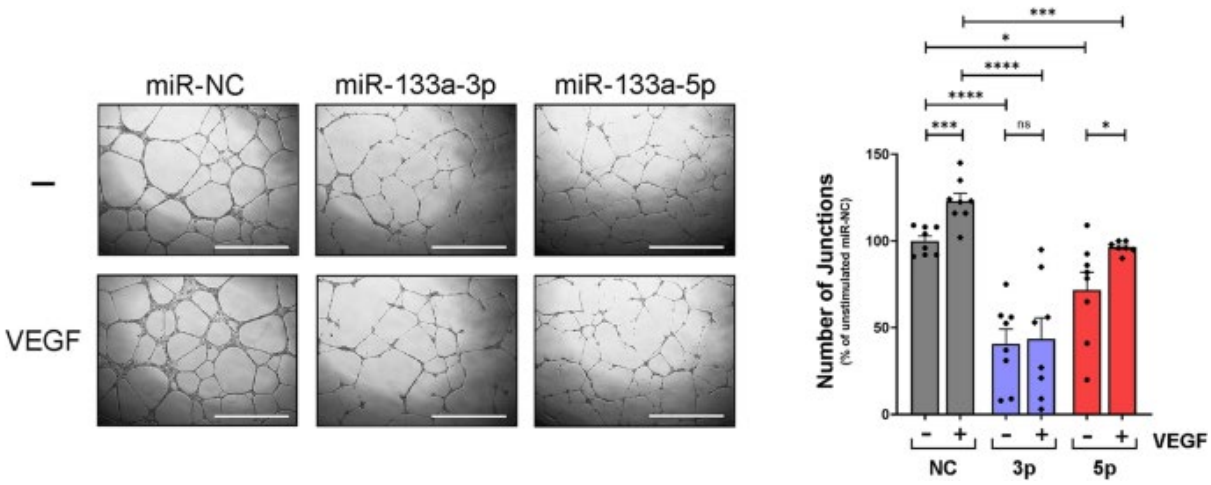

Figure 14. Ectopic expression of miR-133a-3p or miR-133a-5p inhibits HUVEC tubular morphogenesis. HUVEC transfected with miRNA "mimics" for miR-133a's -3p and -5p strands or the negative control miRNA (miR-NC). Cells were plated on Growth-Factor Reduced Matrigel (Geltrex) in ECGM media with 1% FBS at a cell density of 70,000 cells per well. Cells were either left untreated (-) or stimulated with VEGF at a final concentration of 50 ng/ml (+), as indicated. Images are typical experimental fields are shown in the histogram. Cells transfected with miR-NC, miR-133a-3p, and miR-133a-5p, respectively, are shown by the grey, blue, and red bars. ns = non-significant; *, P≤ 0.05; ***, P≤ 0.001; ****, P≤ 0.0001 (unpaired two-tailed Student's t-test when comparing the indicated groups); data are shown as mean ±SE, n = 7. Scale bars at 1000 μm.

The findings suggest that both strands of miRNA-133a may target various angiogenic cellular pathways, including notch signalling, cell cycle, extracellular matrix, and cell adhesion molecules. These findings demonstrate that both strands of miRNA-133a inhibit endothelial cell angiogenesis in different ways. These findings imply that miR-133a-3p controls endothelial cell angiogenesis negatively.

3.2 Notch signalling pathway

VEGF-induced sprouting angiogenesis is regulated by members of the Notch signalling system (De Smet et al.,2009). VEGF-induced endothelial cell tubular morphogenesis is strongly inhibited by miR-133a, as seen in Figure 14. Further studies looked at how miR-133a-3p affects the expression of key notch signalling genes because notch signalling is crucial for controlling the course of angiogenesis by controlling the production of tip and stalk cells. RNA was isolated from the transfected cells and used to screen an RT2 Profiler^{TM} PCR Array Human Notch Signalling Pathway Plus Kit (Ref PAHS-059Y, Qiagen), which contained 84 primers to detect the expression of a selection of Notch-related genes. HUVECs were transfected with mimics miR-NC as a control or miR-133a-3p. The kit's appendix 1 has a table listing the genes relevant to Notch signalling that are included. To conduct the tests, RNA was extracted from HUVEC that had been transfected with miR-NC or miR-133a-3p and stimulated for 1 hour with VEGF (50 ng/ml). Figure 15A displays the outcomes of three separate trials that were analysed using the Gene Globe Data Analysis Center (Qiagen). The red-hued genes are those that were chosen to be elevated. Downregulated genes are those highlighted in green. *Hey1, DLL4, Notch4, Jag2, Hes4* and *NRARP* expression significantly increased in VEGF-stimulated HUVECs when miR-133a-3p was expressed ectopically (figure 15A). A fresh transfection using mimics of miR-133a-3p, miR-133a-5p, and control miR-NC was performed in order to further corroborate these findings and to see whether the strand miR-133a-5p had any impact on the regulation of the genes impacted by miR-133a-3p. At various time intervals, the cells were stimulated with VEGF. HUVEC were either left unstimulated (0h) or stimulated with VEGF (50 ng/ml) for the specified times after being transfected with mimics for the miRNAs 133a-3p, 133a-5p, or negative control miR-NC (grey bars, blue bars, and red bars, respectively). With the help of qPCR TaqMan Gene Expression Assays tailored to each gene, RNA extracted from these samples was converted to cDNA and used to assess changes in gene expression. According to Figure 15B-G, ectopic expression of miR-133a-3p dramatically boosted the expression of *Hey1*, *DLL4, Notch4, Jag2, Hes4* and *NRARP* both at

rest and after VEGF stimulation. When miR-133a-5p was overexpressed, however, *DLL4* expression increased significantly, but only after VEGF stimulation. The other Notch signalling genes previously described had no impact on miR-133a-5p's ability to regulate their expression.

The *ID1* and *CD44* expression levels were downregulated by miR-133a-3p, as shown by the volcano plot (figure 15A). Taqman qPCR was used to confirm that abnormal expression of the miRNAs 133a-3p and 133a-5p strongly reduced the expression of these genes to the same degree (figure 15H-I).

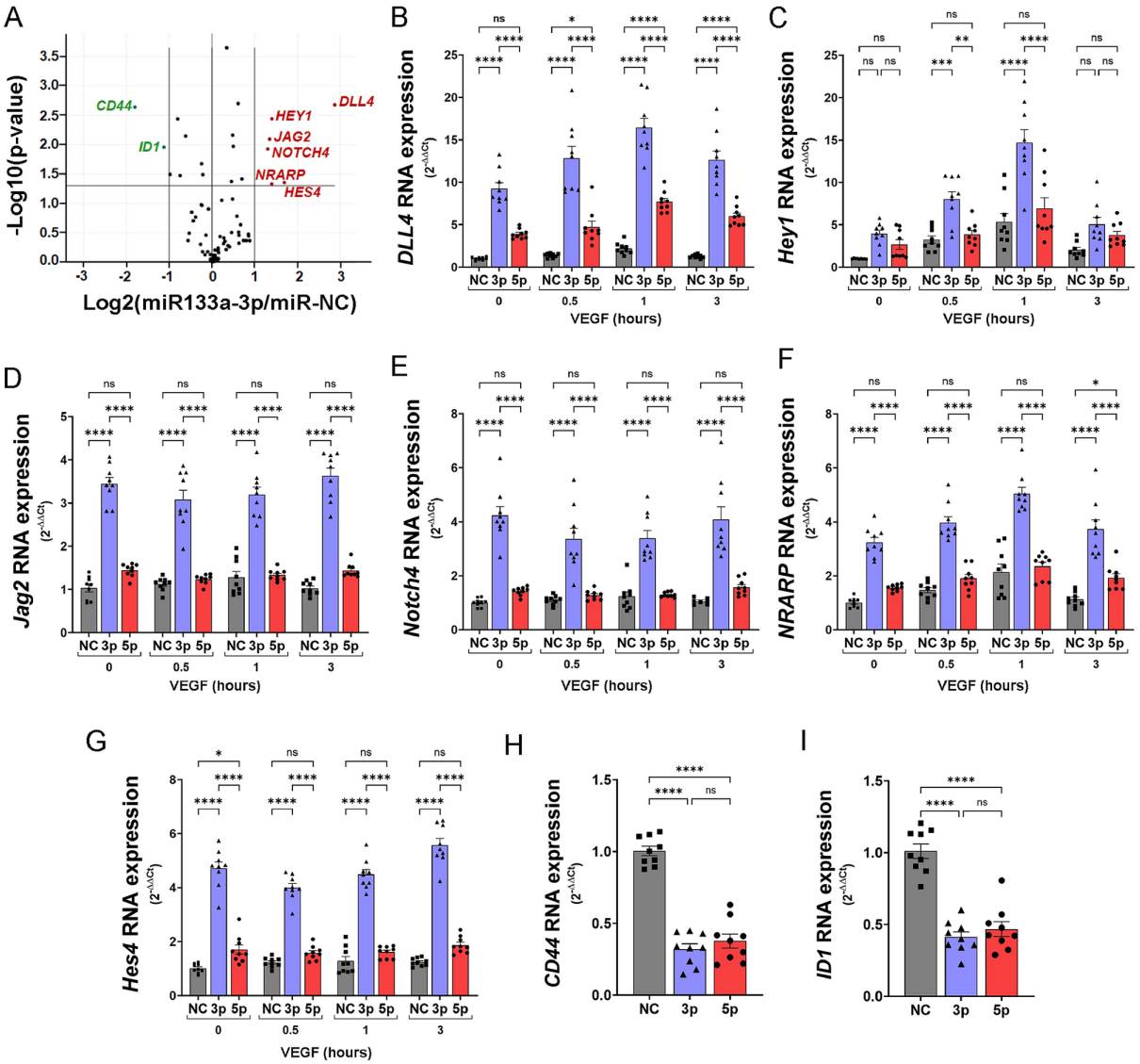

Figure 15. Aberrant expression of miR-133a in endothelial cells alters the expression of key genes of the Notch signalling pathway. Mimic miR-NC or mimics miR-133a-3p and miR-133a-5p were transfected into HUVECs. They were either kept unstimulated for 0 hours or stimulated with VEGF for the respective durations (50 ng/ml). After screening an RT2 ProfilerTM PCR Array Human Notch Signalling Pathway Plus Kit, a volcano plot in (A) demonstrating distinct gene expression in RNA obtained from HUVEC transfected with miR-NC or miR-133a-3p and stimulated with VEGF for 1 hour is shown (Ref PAHS-059Y, Qiagen). Three different trials were examined using the Gene Globe Data Analysis Center (Qiagen). Genes that had Log2(miR-133a-3p/miR-NC) values more than 1 and -Log10(p-value) P values less than 0.05 were chosen as upregulated (red), and those that had values less than 1 and -Log10(p-value) P values less than 0.05 were chosen as downregulated. (B-I) HUVEC transfected with miR-133a mimics that were either left unstimulated (0h) or stimulated with VEGF (50 ng/l) for the specified durations. The mimics used were negative control (NC, grey bars), miR-133a-3p (3p), and miR-133a-5p (5p). qPCR TaqMan Gene Expression Assays tailored to each gene were used to analyse changes in the gene expression of the genes visible in (A). Data are presented as mean ±SE, with a n of 9. The post hoc Tukey's comparison test was used to analyse statistical differences using either a two-way (B-G) or one-way (H-I) ANOVA. ns = non-significant; *, P≤ 0.05; **, P≤ 0.01; ***, P≤ 0.001; ****, P≤ 0.0001.

3.3 Endothelial cell proliferation and cell cycle

Endothelial cell proliferation in response to pro-angiogenic factors is important for the development of new blood vessels. To ascertain whether the expression of miR-133a in endothelial cells has a detrimental effect on endothelial cell proliferation, MTT assays were performed, which is a gold standard method to measure cell viability. HUVEC were transfected with mimics of miR-133a-3p or miR-133a-5p, and miR-NC. After three days of culture in endothelial cell growth media, the absorbance readings were used to determine the

proliferation rate, by taking the absorbance of MTT detected on day 3 and dividing by the absorbance on day 0. As shown in Figure 16A, the proliferation rate of miR-133a-3p and -5p were inhibited when compared to miR-NC, however it is evident that the 3p strand caused more inhibition. In order to more fully understand the decrease in endothelial cell proliferation rate shown in figure 16A, further studies were performed to assess whether aberrant miR-133a expression had any impact on the expression of crucial genes involved in the cell cycle. In order to accomplish this, RNA from HUVEC transfected with miR-NC or miR-133a-3p and stimulated with VEGF for 1 hour was utilised to screen a gene array including primers to find the expression of several genes related to cell cycle. The list of distinct cell cycle-related genes included in this kit is provided in Appendix 2. Red-hued genes were chosen because they were elevated. The genes highlighted in green were chosen to be downregulated. MiR-133a-3p, which encodes crucial cell cycle regulators, strongly downregulated the expression of cyclin A2 (*CCNA2*), cyclin-dependent kinase 1 (*CDK1*), and cyclin B1 (*CCNB1*) (Fig 16B). Mini-chromosome maintenance protein 4 (*MCM4*) and 4 (*MCM2*), which encode initiates of genome replication, show a substantial downregulation in expression as well (Fig 16B). The cyclin G1 (*CCNG1*) and D3 (*CCND3*) genes' expression was increased by the presence of miR-133a-3p (Fig 16B). A fresh transfection using the mimics miR-133a-3p, miR-133a-5p, and the control miR-NC was conducted to further validate these findings and assess if the regulation of these genes was affected by the miR-133a-5p strand. HUVEC that had been transfected with mimics for the miR-133a-5p (5p, red bars), miR-133a-3p (3p), or negative control miR-NC (grey bars) were either kept unstimulated for 0 hours or stimulated with VEGF (50 ng/ml) for the times specified. With the help of qPCR TaqMan Gene Expression Assays tailored to each gene, RNA extracted from these samples was converted to cDNA and used to assess changes in gene expression. The results obtained from the gene array, as indicated in the volcano plot in figure 16B, were validated by the Taqman qPCR (figure 16C-I). MiR-133a-3p was expressed ectopically, which resulted in a significant downregulation of the expression of *CDK1, CCNA2, CCNB1, MCM2, MCM4*, and an upregulation of *CCND3* and *CCNG1*. The presence of miR-133a-3p in all cases reduced baseline gene expression, as

shown in figure 16C-I. The miR-133a-dependent downregulation of these genes was still present following VEGF stimulation at various time intervals, proving that the downregulation of these genes was not dependent on VEGF stimulation. Additionally, miR-133a-5p-transfected HUVEC showed decreased expression of genes such as *CDK1, CCNA2, CCNB1, MCM2*, and *MCM4* that were suppressed by miR-133a-3p. However, the expression of *CCND3* and *CCNG1* was unaffected by the presence of miR-133a-5p, indicating that the -3p strand is specifically targeting both genes.

These findings demonstrate that miR-133a-3p affected the expression of important cell cycle regulators and initiators. Cyclins and MCM proteins are crucial for controlling how a cell enters the S phase of its cell cycle (Otto and Sicinski, 2017). HUVECs were transfected with miR-133a-3p or miR-NC, and the progression through the cell cycle of the transfected cells was examined by flow cytometry to determine whether phases of the cell cycle are impacted by ectopic expression of miR-133a. When compared to cells transfected with miR-NC, HUVEC transfected with miR-133a-3p showed a larger percentage of cells entering the G0/G1 phase (Fig 16J). In comparison to HUVEC transfected with miR-NC, a reduced proportion of cells expressing miR-133a-3p were seen entering the S and G2/M stages of the cell cycle (Fig 16J). These findings imply that miR-133a-3p influences cyclin and MCM protein production in ways that hinder a cell's ability to move through the cell cycle. These findings are consistent with the inhibition of HUVEC cell proliferation rate that followed miR-133a-3p transfection (Fig 16A).

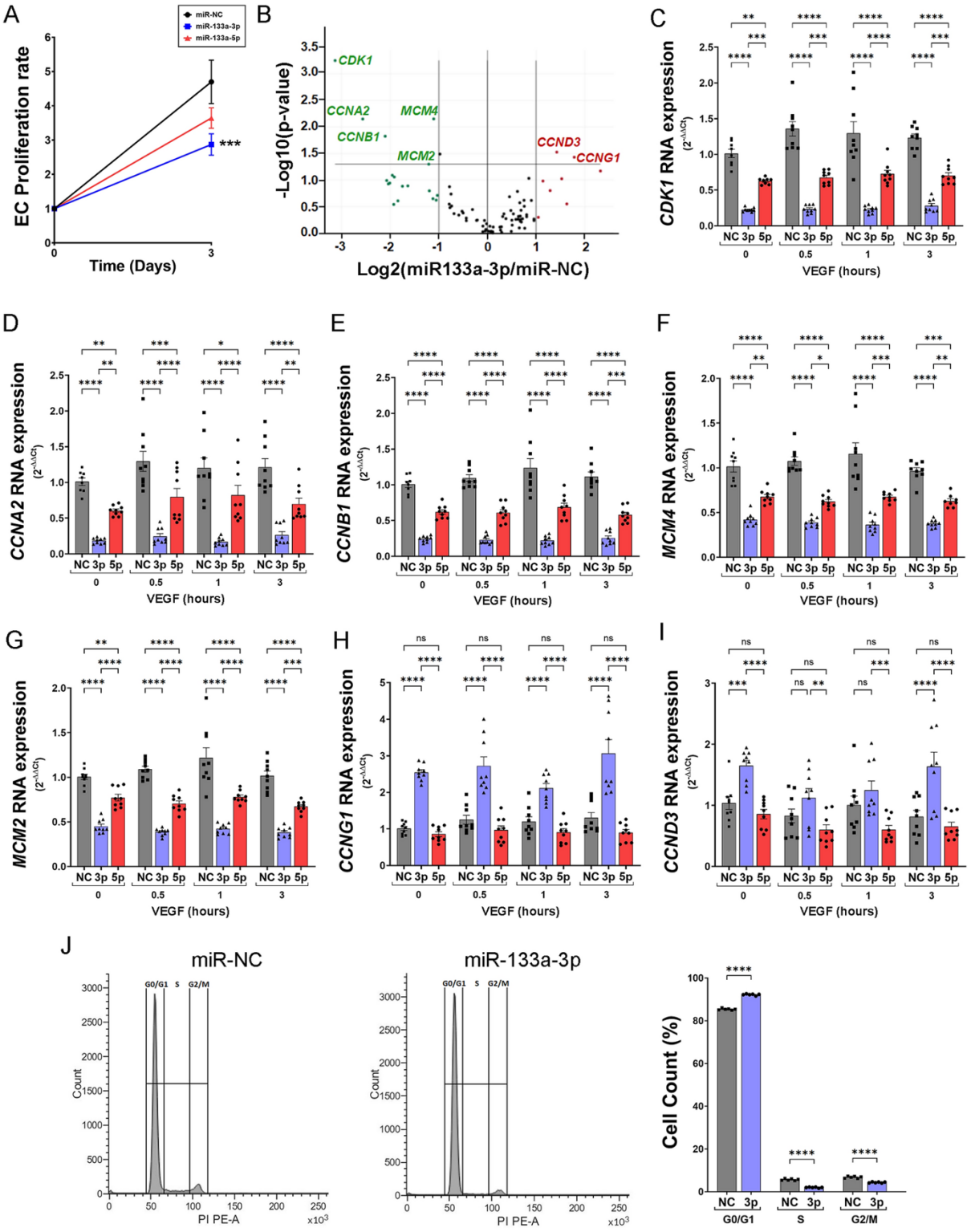

Figure 16: Aberrant expression of miR-133a, inhibits endothelial cell proliferation, alters the expression of cyclins and MCM proteins, and inhibits the entry of cells into S phase. Mimics of miR-133a-3p, miR-133a-5p, or miR-NC were transfected into HUVECs, which were then either left unstimulated or stimulated with VEGF (50 ng/ml) at various time points. (A)

Utilizing the MTT method, the proliferation rate of HUVEC transfected with miR-NC, miR-133a-3p, and miR-133a-5p was evaluated. To determine the proliferation rate, the absorbance of MTT detected on day 3 was divided by the absorbance on day 0. Data were analysed by two-way ANOVA with a post hoc Tukey's comparison test on miR-133a-3p vs. miR-NC at day 3 and are shown as mean ±SE, n = 8, and P ≤ 0.001. (B) Using an RT2 ProfilerTM PCR Array Human Cell Cycle Kit, RNA extracted from three separate trials of HUVEC transfected with miR-NC or miR-133a-3p and stimulated with VEGF for one hour was utilised to examine differential gene expression of genes encoding cell cycle regulators (Ref PAHS-020Z, Qiagen). Results from analysis using GeneGlobe Data Analysis Center are shown in the Vocano graphic (Qiagen). Genes (red) chosen as upregulated were those with a Log2(miR-133a-3p/miR-NC) > 1 and a -Log10(p-value) P≤ 0.05, whereas genes (green) chosen as downregulated were those with a Log2(miR-133a-3p/miR-NC) < 1 and a -Log10(p-value) P 0.05. (C-I) RNA recovered from HUVEC that had been transfected with the mimics miR-133a-3p (3p), miR-133a-5p (5p), and negative control (NC, grey bars), which had been either left unstimulated (0h) or stimulated with VEGF (50 ng/µl) for the specified durations. qPCR TaqMan Gene Expression Assays tailored to each gene's expression level were used to analyse changes in gene expression. Data are presented as mean ±SE, with a n = 9. Two-way ANOVA was used to analyse statistical differences using the post hoc Tukey's comparison test. *, P ≤ 0.05; **, P ≤ 0.01; ***, P ≤ 0.001; ****, P ≤ 0.0001. ns Indicates non-significant. (J) Using flow cytometry, miR-NC or miR-133a-3p mimic-transfected HUVECs were utilised to analyse the various cell cycle stages. The amount of DNA in the fraction of HUVEC at each stage of the cell cycle was measured using propidium iodide. Typical cell count/PI PE-A graphs are shown. Data are presented as mean ± SE, n = 6. ****, P ≤ 0.0001, which are examined utilising a two-way ANOVA and a post hoc Tukey's comparison test for the corresponding groups.

3.4 Endothelial cell motility

Endothelial cells move toward angiogenic stimuli like VEGF in large part due to sprouting angiogenesis. When there is a wound, the level of VEGF, one of the most powerful pro-angiogenic agents, increases in the skin, encouraging endothelial cell migration to seal the wound (Johnson and Wilgus 2014). In order to examine the impact of miR-133a-3p and miR-133a-5p overexpression on endothelial cell motility, wound healing migration tests were carried out. Figure 17A depicts endothelial cell migration in wound healing migration assays carried out with HUVECs transfected with miR-133a-3p, miR-133a-5p, and miR-NC at the beginning time 0h and after 24 hours of incubation. When compared to cells transfected with miR-NC, it was found that ectopic production of miR-133a-3p reduces endothelial cell motility after 24 hours (Fig 17A). When miR-133a-5p was transfected into endothelial cells, there was no discernible difference in the motility of the cells (Fig 17A). Some genes that miR-133a targets have been found to be crucial in controlling cell motility in earlier research. One of these genes, Moesin, produces a protein that is essential for tubular morphogenesis and endothelial cell movement (Wang Q, et al., 2016; Kinoshita T, et al., 2021). It's interesting to note that Moesin has been demonstrated to mediate endothelial cell tube formation and uPAR-dependent chemotaxis (Degryse B, et al., 2017). Therefore, HUVECs were transfected with miR-NC, miR-133a-3p, and miR-133a-5p and carried out Taqman qPCR experiments to confirm the influence of miRNA-133a on the expression of these genes. Figure 17B-C demonstrates that HUVEC transfected with both strands exhibit downregulated RNA expression of both genes, however the statistical significance of the alterations brought on by miR-133a-3p transfection was greater than when employing -5p.

Additionally, *RCAN1.4* expression was also looked at (Figure 18). A crucial role as a negative regulator of angiogenesis, *RCAN1.4* is a gene that is stimulated by VEGF in endothelial cells. As previously mentioned, HUVECs were transfected, and at various time points, they were stimulated with VEGF. When cells were transfected with miR-133a-3p, qPCR of RNA extracted from these cells revealed a substantial increase in RNA expression of *RCAN1.4* in

comparison to the control (Fig 18). However, miR-133a-5p-transfected cells showed no change (Fig 18).

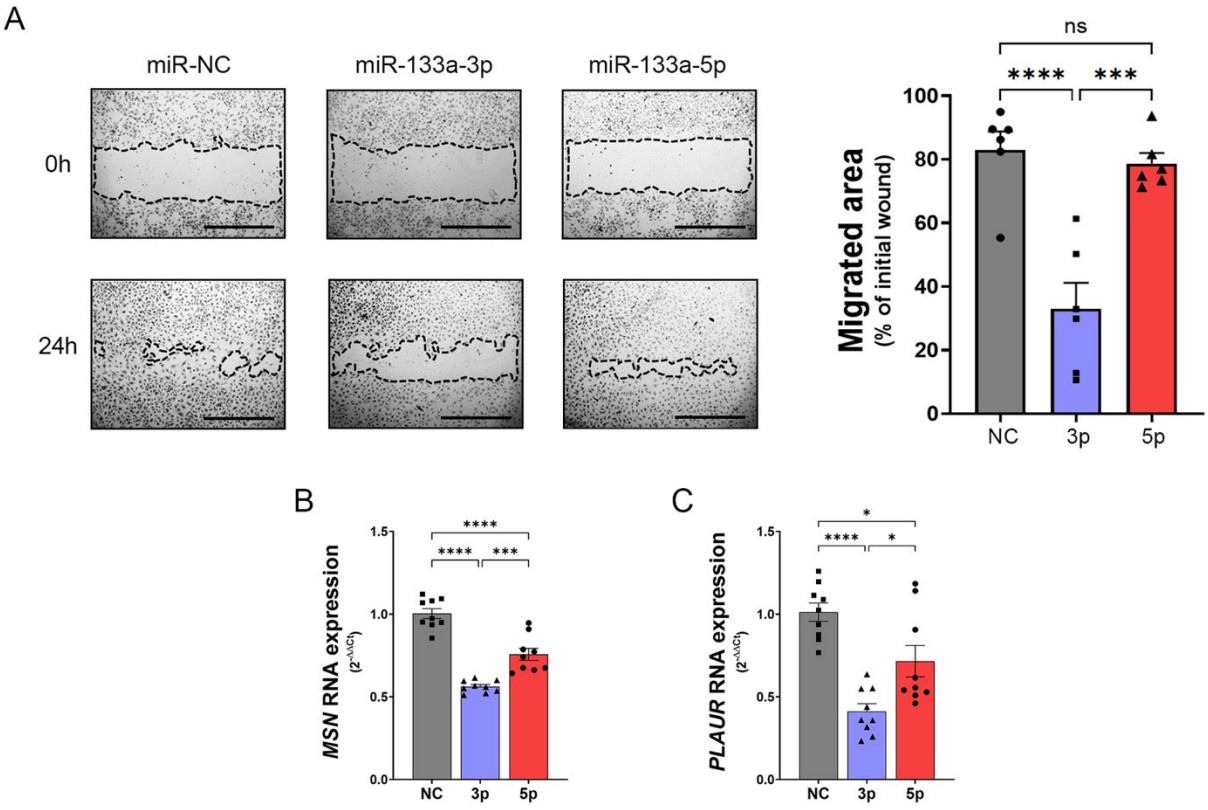

Figure 17. Ectopic expression of miR-133a-3p attenuates endothelial cell motility. (A) For the wound healing cell migration tests, HUVECs transfected with miR-NC, miR-133a-3p, or miR-133a-5p were employed. Images were obtained at 0h and again at 24h. The spots that had not moved were identified using Image J. In order to determine the migrated area, the non-migrated area value at time zero was subtracted, and the result was expressed as a percentage of the total area at time zero. 1000 g on the scales. Data are presented as mean SE, with a n of 6. By employing the post hoc Tukey's comparison test and a one-way ANOVA, statistical differences were examined. ***, P ≤ 0.001; ****, P ≤ 0.0001; ns = not significant. (B-C) TaqMan RT PCR was performed to determine the RNA expression of *MSN* and *PLAUR* from HUVEC transfected with the above miRs. Data are presented as mean ± SE, n = 9, with the following statistical significance levels for the indicated groups: *, P 0.05; ***, P 0.001; ****, P 0.0001. One-way ANOVA was used to analyse the data.

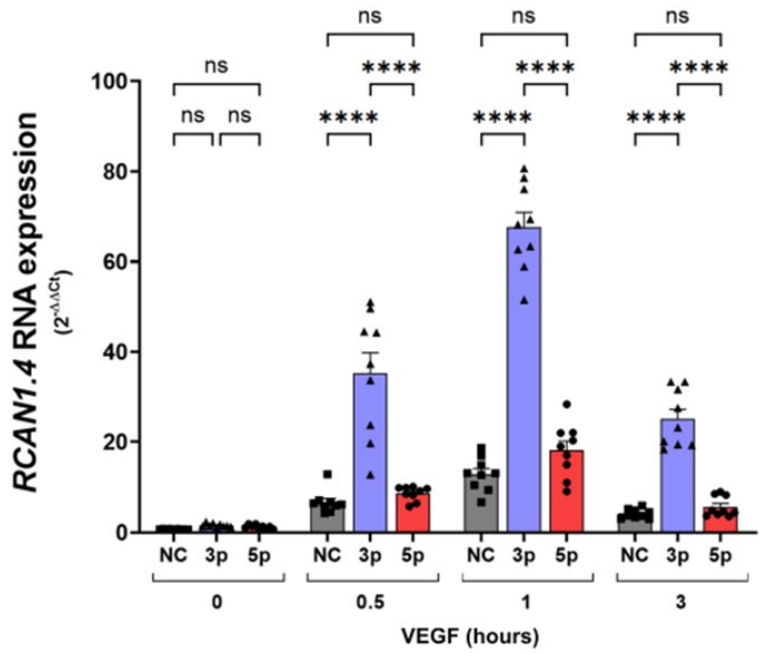

Figure 18. Gene expression of *RCAN1.4* in HUVEC expressing miR-133a-3p and -5p. VEGF was used to activate HUVEC for 30 minutes, an hour, and three hours after miR-133a-3p, miR-133a-5p, or negative control miR-NC (grey, blue, or red columns) transfection. *RCAN1.4*'s RNA level was markedly increased in cells that had miR-133a-3p transfected into them. The Ct values of the housekeeping gene *HPRT-1* were used to normalise the Ct values. Utilizing the comparative 2^−ΔΔCt miR-NC technique, data analysis was done (0h). ns= non-significant, ****, P ≤ 0.0001 two-way ANOVA with post hoc Tukey's comparison test for the indicated groups. Data are presented as mean ± SE, n=7.

3.5 Endothelial genes related to extracellular matrix and cell adhesion molecules (ECM-CAM)

Extracellular matrix (ECM) remodelling offers the body's cells and tissues structure and support. The ECM facilitates cell attachment and interaction with neighbouring cells. Endothelial cell migration and the development of new vascular sprouts in response to pro-angiogenic signals are not achievable without the remodelling of the ECM. In the region

around vascular branching, secreted proteases cause ECM remodelling. Endothelial cell migration, which is essential for angiogenesis, such as the emergence of new blood vessels from the vasculature already present, is mostly regulated by cell adhesion molecules (CAM) (Davis and Senger, 2005). HUVECs were transfected with miR-NC or miR-133a-3p mimics to see if abnormal miR-133a expression in endothelial cells affects the expression of important ECM-CAM-related genes. VEGF (50 ng/ml) was used to activate the transfected cells for 4 hours. The RNA extracted from these cells was used to screen a gene array that contains 84 primers encoding for extracellular matrix and cell adhesion molecules (RT2 ProfilerTM PCR Array Human Extracellular Matrix and Cell Adhesion Molecules Kit, Ref PAHS-013Z, Qiagen) (Qiagen). The appendix 3 includes a table that lists the genes that are part of this kit. Utilizing the Gene Globe Data Analysis Center (Qiagen), the outcomes of three separate trials were analysed, and the volcano plot is displayed in figure 19A. When a gene's Log2(miR-133a-3p/miR-NC) value was greater than 1 and -Log10(p-value) less than P 0.05, the gene was considered to be upregulated. Conversely, a gene was considered to be downregulated when its Log2(miR-133a-3p/miR-NC) value was lower than 1 and -Log10(p-value) P 0.05. Thrombospondin 1, *ITGA6*, *ADAMTS1* (ADAM metallopeptidase with thrombospondin type 1 motif 1), and *SPARC* (sequestered protein acidic and cysteine rich) were all expressed more strongly in HUVECs after miR-133a-3p transfection (Fig 19A). A fresh transfection using the mimics miR-133a-3p, miR-133a-5p, and the control miR-NC was conducted to further validate these findings and assess whether the strand miR-133a-5p had any impact on the regulation of these genes. The transfected cells were either treated with VEGF for 4 hours or left unstimulated for 0 hours (4h). Each individual gene's expression was measured using qPCR and TaqMan gene expression assays. Figure 19B-E demonstrates how miR-133a-3p transfection of HUVECs statistically increased the expression of *THBS1, ITGA6*, and *SPARC* in unstimulated cells. The expression of these genes was not significantly altered when transfected cells were stimulated with VEGF, indicating that the impact of miR-133a-3p expression was independent of VEGF. In HUVECs transfected with miR-133a-3p, *ADAMTS1* gene expression was also increased, but only after VEGF stimulation. None of these genes

were affected by miR-133a-5p transfection in HUVECs. Although the analysis of these data failed to reach statistical significance, the volcano plot in figure 19A demonstrated that the presence of miR-133a-3p in endothelial cells dramatically elevated the expression of *TIMP3*. TaqMan gene expression assays were employed in qPCR to further examine the impact of miR-133a on the expression of *TIMP3*. According to figure 20, as compared to the control group, miR-NC, transfection of HUVECs with miR-133a increased the expression of this gene both at a basal level and when stimulated with VEGF.

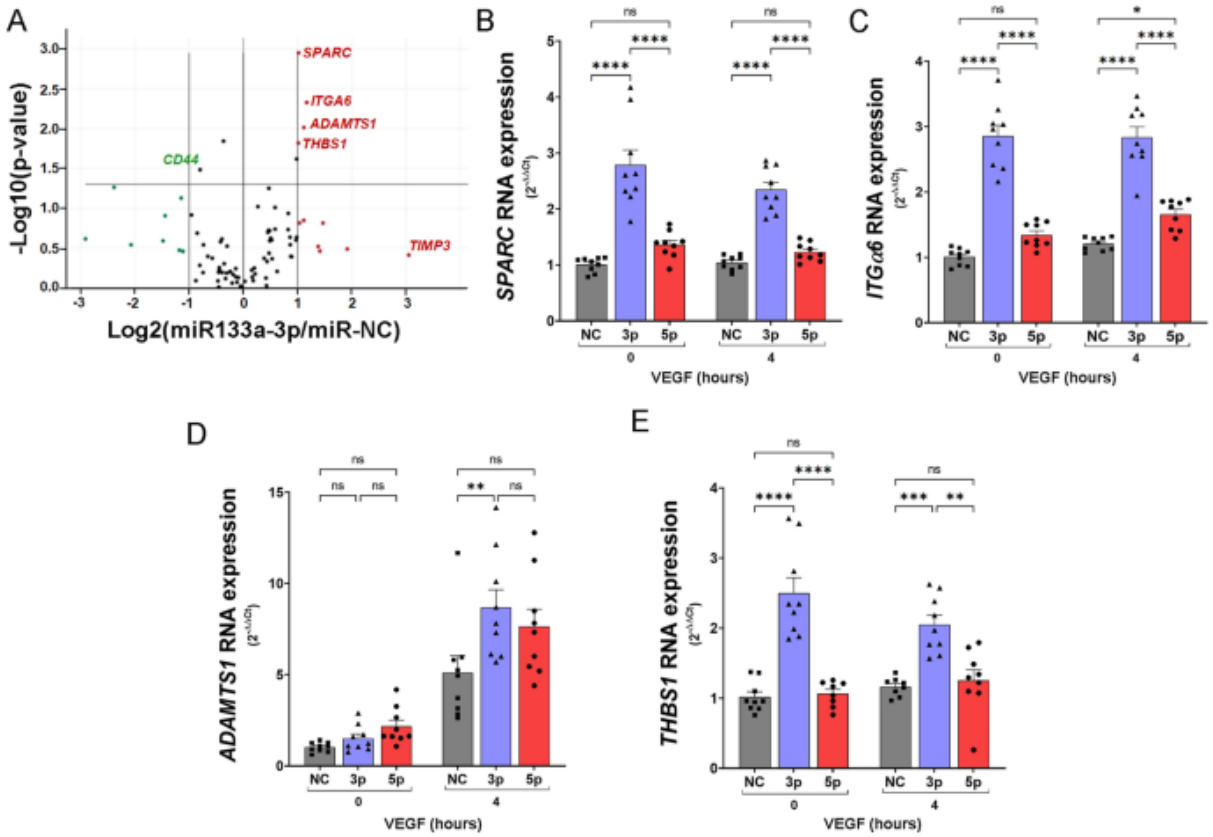

Figure 19. Aberrant expression of miR-133a-3p in endothelial cells alters the expression of key mediators of ECM remodelling. A) The RT2 ProfilerTM PCR Array Human Extracellular Matrix & Cell Adhesion Molecules Kit was tested using RNA extracted from HUVEC transfected with a negative control (miR-NC) or miR-133a-3p and stimulated with VEGF (50 ng/ml) for 4 hours (Ref PAHS-013Z, Qiagen). Utilizing the Gene Globe Analysis Centre, the Ct values from three different trials were analysed (Qiagen). The red genes (indicating upregulation) on the volcano plot are those with a Log2 (miR-133a-3p/miR-NC) > 1 and -Log10 (p-value) P ≤ 0.05. Downregulated genes were those with a Log2 (miR-133a-3p/miR-NC) 1 and -Log10 (p-value) P ≤ 0.05 (green). (B-E) RNA extracted from HUVEC transfected with mimics of miR-133a-3p, miR-133a-5p, or negative control miR-NC was stimulated with VEGF (50 ng/ml) for 4 hours or left unstimulated (0h). By using qPCR TaqMan gene expression tests for each individual gene, changes in gene expression were discovered. The findings are shown as mean ± SE, with n = 8. Two-way ANOVA was used to analyse the data for significant differences, followed by a post hoc Tukey's comparison test. *, P ≤ 0.05; **, P ≤ 0.01; ***, P ≤ 0.001; ****, P ≤ 0.0001. ns Indicates non-significant.

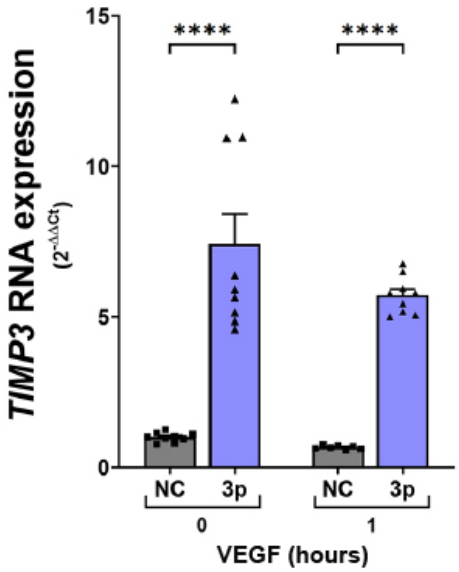

Figure 20. Gene expression of *TIMP3* in HUVEC expressing miR-133a-3p and -5p. HUVEC that had been transfected with miR-133a-3p, miR-133a-5p, or negative control miR-NC (grey columns, blue columns, or red columns) were either left unstimulated for 0 hours or were stimulated with VEGF for 1 hour. *TIMP3* RNA was markedly increased at both the basal and VEGF-stimulated levels in cells transfected with miR-133a-3p. The Ct values of the housekeeping gene *HPRT-1* were used to normalise the Ct values. Utilizing the comparative 2^−ΔΔCt miR-NC technique, data analysis was done (0h). ns= nonsignificant, ****, P≤ 0.0001 two-way ANOVA with post hoc Tukey's comparison test for the indicated groups. Data are presented as mean ± SE, n=7.

3.6 Ingenuity pathway analysis

Manuel J. Gómez worked on this component of the thesis in the Unidad de Bioinformática at the Centro Nacional de Investigaciones Cardiovasculares in Madrid. With his permission, the results are presented.

25 differentially expressed genes were discovered through the examination of gene arrays for Notch signalling, cell cycle, or ECM-CAM, together with aberrant expression of miR-133a-3p in endothelial cells. As mentioned in chapter 2.8.1, after performing the gene arrays the tables and volcano plots from the gene global analysis centre demonstrated the genes that had Log2(miR-133a-3p/miR-NC) values more 1 and -Log10(p-value) P values less than 0.05 were chosen as upregulated (red), and those that had values less than 1 and -Log10(p-value) P values less than 0.05 were chosen as downregulated (green). Therefore, for arrays performed on those pathways mentioned above, 25 genes which met the criteria in the volcano plots and tables were further analysed by Taqman RT-PCR. To highlight the impact of miR-133a-3p's aberrant expression on angiogenesis, the differential gene expression profiles for the 25 genes were examined. As was previously mentioned, when performing the various gene arrays, transfected cells were either stimulated with VEGF for 1 hour, as was the case with the notch signalling gene array or the cell cycle gene array, or they were stimulated with VEGF for 4 hours, as was the case with the ECM-CAM gene array. Only the data obtained from qPCR TaqMan gene expression tests utilising RNA extracted from HUVEC transfected with miR-NC or miR-133a-3p and either left unstimulated (0h) or stimulated with VEGF (50 ng/ml) for 1 hour were used for the ingenious pathway analysis. In relation to miR-NC 0h, Table 7a and 7b displayed the fold induction RNA levels for the genes with differential expression.

Table 7a: Differential gene expression of 25 angiogenic related genes in HUVEC expressing miR-NC or miR-133a-3p, unstimulated. HUVECs transfected with miR-133a-3p (blue columns) or the negative control miR-NC (grey columns), were left unstimulated for 0 hours. For each gene designated as miR-NC 0h, the fold induction RNA levels are shown in the rows. The housekeeping gene *HPRT-1* Ct values were used to normalise the Ct readings. The data were analysed using the comparative 2^−ΔΔCt approach; nd = non-determined.

GENES	NC 0H Fold induction									3P 0H Fold induction								
PLAUR	0.64	1.49	1.05	1.04	0.94	1.03	1.02	0.96	1.02	0.29	0.35	0.38	0.26	0.30	0.31	0.51	0.59	0.59
MSN	0.91	1.26	0.87	0.98	0.97	1.05	0.85	1.27	0.92	0.51	0.70	0.50	0.58	0.65	0.62	0.59	0.61	0.59
RCAN1.4	1.01	0.91	1.09	0.94	1.10	0.97	0.99	0.98	1.04	2.06	1.81	2.37	1.17	1.39	1.38	1.33	1.46	1.45
CD44	1.00	1.31	0.76	0.91	1.00	1.09	1.06	0.95	0.99	0.18	0.34	0.21	0.24	0.21	0.20	0.47	0.33	0.50
ID1	0.79	2.47	0.51	1.12	0.94	0.95	1.71	0.35	1.69	0.19	0.30	0.22	0.38	0.34	0.37	0.70	0.76	0.58
CCNE1	0.75	0.95	1.41	0.85	1.08	1.09	0.78	1.25	1.03	0.86	1.07	1.06	0.63	0.70	0.69	0.64	0.71	0.68
CCND1	0.80	0.99	1.25	0.92	1.07	1.01	0.80	1.24	1.01	0.95	1.14	1.29	0.83	0.91	0.73	0.59	0.79	0.83
DLL4	1.02	0.84	1.17	0.71	1.11	1.26	0.90	1.13	0.98	8.28	8.05	13.28	9.04	11.88	10.08	8.16	7.74	6.74
HEY1	0.97	1.09	0.95	1.00	0.97	1.03	1.04	1.01	0.95	4.65	4.59	5.04	3.46	3.76	3.97	2.67	1.47	5.81
JAG2	0.69	1.29	1.13	0.70	1.01	1.40	0.73	1.23	1.11	3.69	4.07	3.96	3.53	3.41	3.41	2.81	3.30	2.82
NOTCH4	0.79	1.20	1.06	0.79	1.03	1.22	0.73	1.23	1.11	3.72	4.01	4.02	4.35	6.35	4.92	2.81	3.30	2.82
NRARP	0.87	1.04	1.10	0.79	0.94	1.34	0.82	1.09	1.12	3.48	3.59	3.09	2.98	3.66	4.23	2.99	2.52	2.65
HES4	0.83	1.24	0.97	0.92	0.94	1.15	0.75	1.11	1.19	4.84	5.74	5.02	4.10	5.33	4.79	4.59	4.82	3.27
TIMP3	0.77	nd	1.30	1.03	0.94	1.04	1.05	0.97	0.98	7.23	9.49	8.00	6.80	6.83	6.24	4.33	4.29	4.51
ITGB2	1.13	1.87	0.47	1.40	0.84	0.85	1.07	0.91	1.03	4.19	6.07	4.01	3.37	3.39	3.05	2.70	2.21	2.31
ADAMTS1	0.99	1.41	0.72	1.07	1.06	0.88	0.91	1.28	0.86	0.70	1.02	0.85	0.34	0.28	0.33	0.66	0.49	0.73
THBS1	1.07	1.01	0.92	0.96	0.97	1.08	0.78	1.40	0.91	1.75	2.48	1.70	1.90	2.21	1.89	1.90	1.47	1.50
SPARC	0.86	0.98	1.19	0.74	1.19	1.13	0.80	1.07	1.17	2.79	2.64	3.45	2.76	2.67	2.65	2.25	2.34	2.25
CDK1	0.89	nd	1.13	0.85	0.98	1.20	0.76	1.08	1.22	0.22	0.26	0.22	0.19	0.19	0.22	0.22	0.23	0.28
CCNA2	0.89	nd	1.12	0.77	1.21	1.07	0.88	1.00	1.13	0.21	0.22	0.22	0.14	0.15	0.16	0.14	0.19	0.24
CCNB1	0.86	nd	1.16	0.83	1.04	1.16	0.95	1.01	1.05	0.27	0.30	0.25	0.18	0.22	0.23	0.20	0.26	0.28
MCM2	0.84	1.03	1.15	0.90	1.00	1.10	1.00	0.98	1.02	0.38	0.42	0.42	0.37	0.42	0.42	0.60	0.53	0.51
MCM4	0.80	1.07	1.17	0.80	1.11	1.13	0.85	0.89	1.32	0.43	0.47	0.40	0.35	0.43	0.38	0.35	0.40	0.58
CCND3	0.65	1.72	0.89	0.76	1.14	1.16	0.87	1.05	1.09	1.22	1.32	1.41	1.73	1.95	1.86	1.71	1.86	1.79
CCNG1	1.24	0.87	0.93	0.80	1.05	1.20	0.82	1.08	1.13	2.59	2.87	2.63	2.48	2.53	2.84	2.20	2.44	2.33

Table 7b: Differential gene expression of 25 angiogenic related genes in HUVEC expressing miR-NC or miR-133a-3p, stimulated with VEGF (50 ng/ml) for 1 hour. HUVECs transfected with miR-133a-3p (blue columns) or the negative control miR-NC (grey columns), were stimulated with VEGF (50 ng/ml) for 1 hour. The fold induction RNA levels are shown in the rows. The housekeeping gene *HPRT-1* Ct values were used to normalise the Ct readings. The data were analysed using the comparative 2^−ΔΔCt approach; nd = non determined.

GENES	NC 1H Fold induction									3P 1H Fold induction								
PLAUR	0.90	0.91	1.06	0.85	0.94	1.02	1.02	0.95	1.01	0.39	0.49	0.51	0.34	0.40	0.24	0.47	0.50	0.58
MSN	1.11	1.10	1.13	0.85	1.02	1.00	1.04	0.88	1.07	0.69	0.64	0.59	0.32	0.40	0.53	0.66	0.67	0.72
RCAN1.4	15.0	6.8	18.7	13.2	10.5	9.5	13.2	12.8	17.0	76.1	68.2	58.9	63.4	78.6	69.4	62.67	80.7	51.5
CD44	0.90	0.98	0.86	1.01	0.97	0.92	1.15	1.21	0.95	0.28	0.25	0.29	0.14	0.19	0.21	0.34	0.36	0.39
ID1	0.76	0.45	0.42	0.87	0.94	1.25	0.56	0.50	0.48	0.40	0.25	0.53	0.29	0.30	0.43	0.45	0.46	0.39
CCNE1	1.05	1.77	0.98	1.78	1.14	1.02	0.96	1.20	0.88	0.80	0.96	0.93	0.69	0.99	0.76	0.64	0.61	0.72
CCND1	1.11	1.84	0.99	nd	1.72	0.84	1.32	1.69	1.04	0.99	1.30	1.29	0.81	0.78	0.85	0.62	0.70	0.85
DLL4	1.76	1.95	1.96	1.30	2.69	1.74	2.45	3.58	2.40	14.6	17.9	15.9	11.7	21.5	21.2	14.4	14.1	16.6
HEY1	4.31	6.20	4.73	3.28	9.32	2.07	4.11	10.89	3.21	19.5	21.9	15.0	13.2	11.1	12.6	17.9	14.1	6.80
JAG2	1.01	1.76	0.91	1.12	1.96	0.87	0.96	1.66	1.30	3.48	3.23	3.36	3.58	3.02	4.18	2.72	2.48	2.69
NOTCH4	1.43	1.36	0.70	1.22	2.41	1.01	0.96	1.66	1.30	2.59	3.12	2.79	4.34	4.94	4.19	2.72	2.48	2.69
NRARP	1.17	2.25	1.18	1.60	3.31	1.30	2.35	3.39	2.73	4.40	4.58	4.80	4.85	5.02	6.68	5.03	4.47	5.59
HES4	0.91	1.62	0.88	1.19	2.18	0.91	1.18	1.85	0.84	4.97	4.03	4.60	4.18	4.57	5.60	4.48	3.77	4.18
TIMP3	0.65	0.58	0.67	0.77	0.81	0.89	0.70	0.65	0.70	8.99	6.74	7.35	5.11	6.58	8.26	4.76	4.59	4.72
ITGB2	1.10	0.99	0.72	1.17	1.09	1.01	0.80	0.83	0.80	6.29	4.45	5.96	2.49	4.30	3.57	3.14	2.39	3.41
ADAMTS1	3.37	3.05	5.27	1.60	1.40	1.44	3.06	3.15	3.24	9.64	8.71	8.31	1.93	2.15	2.61	6.14	4.75	5.91
THBS1	1.18	1.17	1.17	0.97	1.01	0.94	1.28	1.34	1.27	2.25	1.87	2.17	1.53	1.93	2.66	1.89	2.12	2.15
SPARC	1.15	1.00	1.07	0.88	1.41	0.65	1.09	1.57	1.35	2.21	2.18	2.40	2.08	1.78	2.27	2.24	2.56	2.21
CDK1	1.06	1.93	1.04	1.20	1.55	0.64	1.13	2.15	0.96	0.25	0.23	0.30	0.17	0.16	0.20	0.22	0.25	0.28
CCNA2	1.12	1.98	1.09	1.73	1.08	1.09	0.74	1.34	0.65	0.20	0.23	0.27	0.13	0.18	0.13	0.12	0.11	0.15
CCNB1	1.15	2.05	0.93	1.04	1.59	1.01	1.11	1.44	0.82	0.29	0.25	0.32	0.18	0.14	0.19	0.19	0.17	0.26
MCM2	1.01	1.49	0.99	1.05	1.46	0.78	1.14	1.89	1.16	0.36	0.37	0.44	0.49	0.43	0.50	0.36	0.39	0.47
MCM4	1.21	1.83	0.92	1.03	1.69	0.91	0.88	1.18	0.76	0.50	0.48	0.30	0.37	0.33	0.40	0.29	0.25	0.35
CCND3	0.73	1.15	0.64	1.24	1.98	1.05	0.69	1.01	0.55	1.00	1.03	1.09	1.73	1.76	2.02	0.86	0.85	0.90
CCNG1	1.23	1.98	1.07	0.99	1.58	0.97	0.74	1.38	0.87	2.49	2.51	2.62	1.71	2.31	2.10	1.89	1.60	1.81

The Ingenuity pathway analysis (IPA) software programme, one of the most sophisticated bioinformatic tools, analyses gene expression patterns using a built-in database based on scientific literature. IPA studies were carried out to further examine if the 25 genes mentioned above have an inhibitory influence on angiogenesis. According to the results in figure 21, "DNA replication," "Cell cycle, recombination, and repair," and "Cardiovascular system growth and function" were areas of cellular processes that were enhanced. The bar charts in figures 21A and 21C depicted decreased cellular activities such as "cell cycle progression," "branching of vasculature," "proliferation of endothelial cells," "tubulation of endothelial cells," "DNA replication," "entry into S phase," "synthesis of DNA," and "mitosis" as a result of the activated Z score prediction. Figures 21B and 21D use circular plots to link enriched biological functions to the corresponding differentially expressed genes. Either blue, which stands for repression, or red, which stands for activation, were displayed on the activation z-score scale. Upregulation is shown as red on the logFC scale, and downregulation is shown as blue.

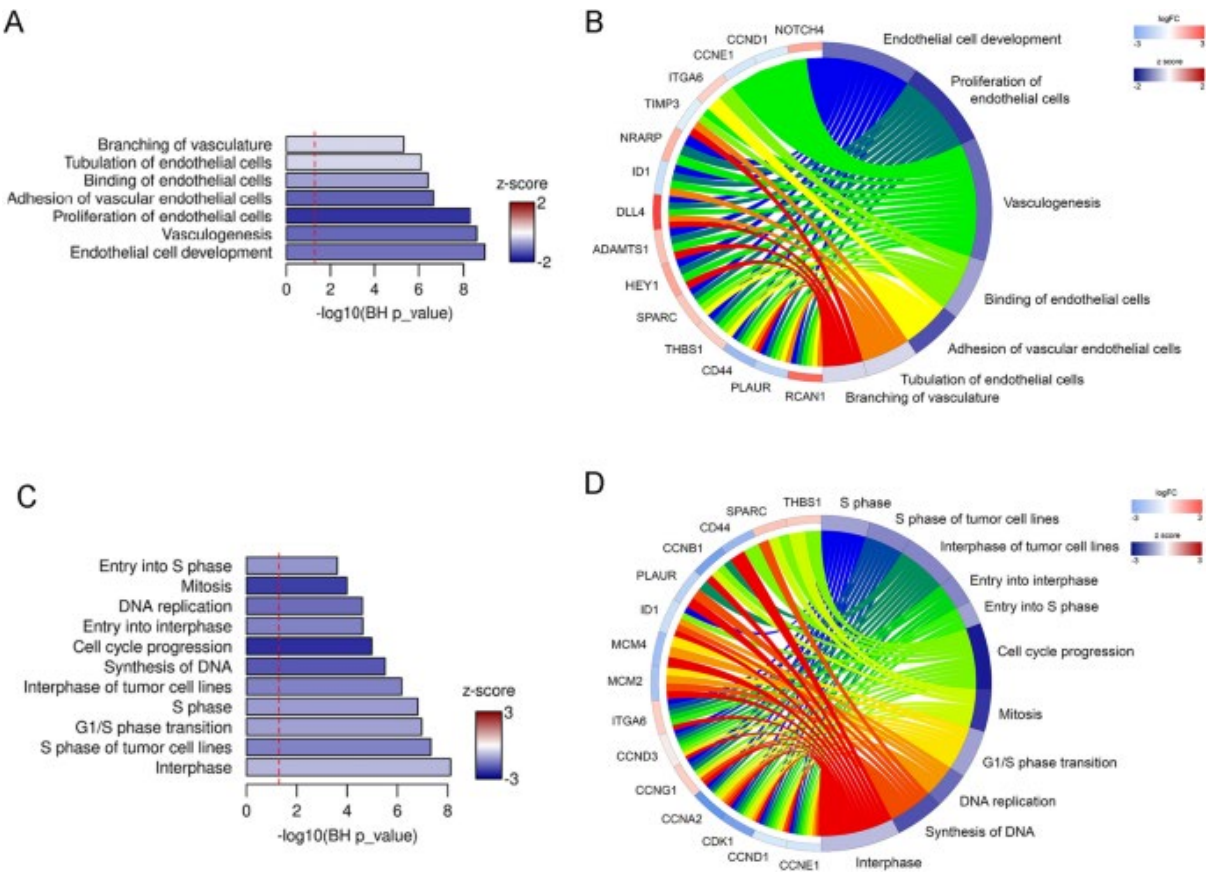

Figure 21. Ingenuity Pathway Analysis via Ingenuity Pathway of the genes with differential expression in endothelial cells that express ectopic miR-133a-3p. (A, C) Bar graphs illustrating enriched biological processes predicted by IPA under the categories of "Cell Cycle" and "DNA replication, recombination, and repair" (A) and "Cardiovascular system development and function" (C) (C). Bar lengths are given as a function of enrichment significance (-log10) (Benjamini-Hochberg adjusted P values). (B, D) Circular plots showing enhanced biological processes found in the categories "Cell Cycle," "DNA replication, recombination, and repair" (B) and "Cardiovascular system development and function" (D) (D). The corresponding differentially expressed genes are linked to enhanced biological functioning. Fold change, or FC. Blue denotes repression; red, activation on the activation z-score scale. Red indicates upregulation on the LogFC scale; blue indicates downregulation. The figure is given with Manuel Gomez's agreement. He works for CNIC in Madrid, Spain.

3.7 Bioinformatic analysis with miRNA data bases (target scan, miRWalk and miRDB)

Our findings demonstrate that miR-133a-3p or miR-133a-5p differentially regulate the expression of a set of 25 genes that code for angiogenesis regulators. It is hypothesised that the decrease in gene expression may be caused by miR-133a's direct binding to complementary regions in the targeted gene's sequence. In the study by Kinoshita et al. (2012), in silico analysis indicated the probable miR-133a-3p binding sites in the 3'UTR of *MSN*, which may help to explain the decline in RNA expression seen for this gene. The 3'UTR sequences of the differentially expressed genes were analysed using bioinformatic methods using the databases miRWalk, Target-scan, and miRDB to see whether any putative sequence motifs that are complementary to the sequence for miR-133a-3p or -5p exist. Except for *MSN*, none of the genes were predicted to have miR-133a-3p binding sites using Target-scan and miRDB, and only a small number were found in the miRWalk database, as shown in Table 8 below. In 2 out of the 3 databases examined, miR-133a-5p binding sites were predicted to be present in the *RCAN1.4, CD44, HEY1,* and *ADAMTS1* genes. Nevertheless,

none of the genes were generally anticipated by the three databases to have miR-133a binding sites. The table in the appendix 4 shows the predicted score of the differentiated genes which have miR-133a-3p or -5p binding sites. Both Target-scan and miRDB have shown a prediction score more than 90%, which explains the publication by Kinoshita et al. (2012), indicating the direct binding of miR-133a-3p to the 3'UTR of *MSN.* Which supports the decrease shown in RNA expression in this study. The purpose of cloning the 3'UTR of *CD44,* is because miR-133a-3p and -5p downregulate the RNA expression of *CD44* as shown in figure 15H. MiR-133a-5p was predicted to bind directly to the 3'UTR of *CD44* at positions 3063 to 3070 by both miRWalk and Target Scan. Taking in consideration that this is a predicted bioinformatic study, and also as shown in the table in the appendix 4, miRWalk showed a predicted score of 92% and Target scan a score of 21%. miR-133a-5p as mentioned above was predicted to be present in *RCAN1.4, HEY1* and *ADAMTS1*, however as shown in our result there was no statistical significant reduction in the RNA expression of these gene, when endothelial cells overexpress miR-133a-5p.

Table 8: Bioinformatic analysis of miR-133a predicted binding sites using miRWalk, TargetScan and miRDB databases on the 25 differentially expressed genes.

Genes	miR-133a-3p miRWalk	miR-133a-3p TargetScan	miR-133a-3p miRDB	miR-133a-5p miRWalk	miR - 133a-5p TargetScan	miR-133a-5p miRDB
PLAUR	YES	NO	NO	NO	NO	NO
MSN	NO	YES	YES	NO	NO	NO
RCAN1	YES	NO	NO	YES	YES	NO
CD44	YES	NO	NO	YES	YES	NO
ID1	NO	NO	NO	NO	NO	NO
CCNE1	YES	NO	NO	YES	NO	NO
CCND1	YES	NO	NO	NO	NO	NO
DLL4	YES	NO	NO	YES	NO	NO
HEY1	YES	NO	NO	YES	YES	NO
JAG2	YES	NO	NO	YES	NO	NO
NOTCH4	YES	NO	NO	YES	NO	NO
NRARP	NO	NO	NO	NO	NO	NO
HES4	YES	NO	NO	NO	YES	NO
TIMP3	YES	NO	NO	YES	NO	NO
ADAMTS1	YES	NO	NO	YES	YES	NO
ITGA6	NO	NO	NO	YES	NO	NO
THBS1	YES	NO	NO	YES	NO	NO
SPARC	YES	NO	NO	NO	NO	NO
CDK1	NO	NO	NO	NO	YES	NO
CCNA2	NO	NO	NO	NO	NO	NO
CCNB1	YES	NO	NO	NO	NO	NO
MCM2	NO	NO	NO	YES	NO	NO
MCM4	NO	NO	NO	NO	NO	NO
CCND3	YES	NO	NO	NO	YES	YES
CCNG1	NO	NO	NO	NO	NO	NO

3.8 Cloning of *CD44* 3'UTR

In HUVECs transfected with miR-133a-3p and -5p, *CD44* RNA expression was downregulated, according to studies of gene arrays including genes for Notch signalling or for ECM-CAM molecules (Fig 15A and 19A, respectively). Additionally, additional qPCR tests employing certain Taq Man gene assays confirmed that endothelial cells carrying miR-133a reduced *CD44* expression (Fig 15H). In order to find probable miR-133a binding sites in the 3'UTR of *CD44* RNA, a bioinformatic study was performed. MiR-133a-5p was predicted to bind directly to the 3'UTR of *CD44* at positions 3063 to 3070 by both miRWalk and Target Scan. Therefore, the 3'UTR was cloned in a luciferase-reporter plasmid, to investigate the possibility of miR-133a interacting with this sequence. The 3' UTR of *CD44* was cloned using the pmirGLO vector. By including miRNA target sites downstream of the firefly luciferase gene (luc2) into the multiple cloning site, this 7350 bp vector can be used to quantitatively assess miRNA activity (MSC). Following the steps outlined below, fragments of the *CD44* 3'UTR were amplified by PCR and cloned into pmirGLO.

3.8.1 PCR amplification of *CD44* 3' UTR fragments

The human *CD44* RNA corresponding to the 3' UTR was divided into numerous pieces due to the size of the *CD44* 3'UTR, which is 3567 bp, and was amplified by PCR using RNA extracted from HUVEC cells as a template. Retro-transcription of HUVEC RNA was carried out utilising oligo-dT (Promega) as a primer. The PCR procedures used the cDNA template. 250 ng of cDNA, 100 ng of targeted oligo sense(s), 100 ng of targeted oligo antisense(s), 25 µl of 2x platinum SuperFi PCR Master Mix (Invitrogen), and nuclease-free water were used in the PCR reactions.

To make future sub-cloning easier, the forward and reverse oligonucleotides employed in the PCR process have restriction sites for the nuclease XhoI.

The following fragments were generated:

1) A fragment (NCBI accession number NM 000610) that encompasses nucleotides 2164–3947 of the *CD44* mRNA and corresponds to the proximal region of the 3' UTR of *CD44*
2) A fragment of the *CD44* mRNA that corresponds to the distal region of the 3' UTR and spans the nucleotides 3911–5725 (NCBI accession number NM 000610)
3) The NCBI accession number NM 000610 designates a segment that corresponds to the 3' UTR of *CD44*'s proximal region and includes nucleotides 2164–3026 of the *CD44* mRNA.
4) The NCBI accession number NM 000610 designates a fragment that corresponds to the 3' UTR of *CD44*'s proximal region and spans nucleotides 3003–3947 of the *CD44* mRNA.

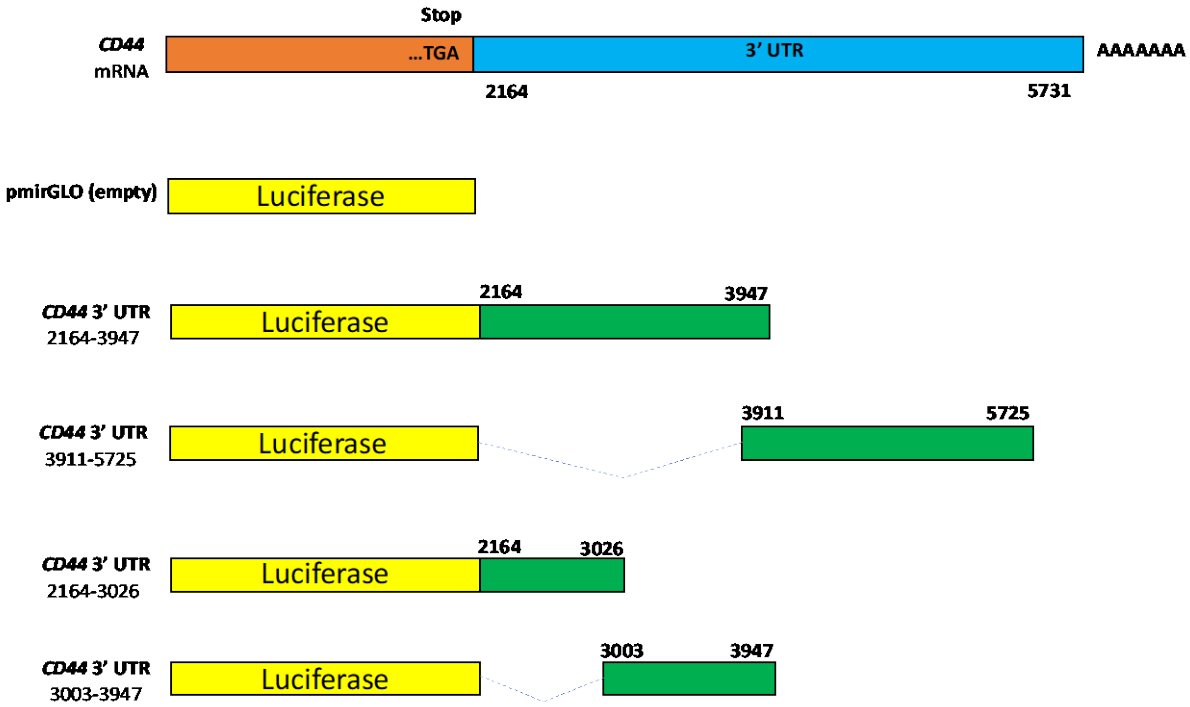

Figure 22: Schematic representation of the *CD44* RNA constructs with 3' UTR regions inserted downstream of the Luciferase gene. The orange bar is showing the coding region (CDS), the blue bar shows the 3'UTR region to be cloned. The yellow bars illustrate the luciferase gene (*luc2)*. After *luc2*, is the multiple cloning site (MCS), however in this schematic diagram, downstream of the *luc2*, the cloned fragments are inserted, which are shown in green bars

Cloning started using the fragments (2164-3947) and (3911-5725). The first fragment was then further divided into segments (2164-3026) and (3063-3070), which include the expected region where miR-133a-5p targets the 3' UTR of *CD44* (3003-3947). After ligation, bacterial transformation, and maxiprep of DNA, the portions of the 3' UTR were cloned in the pmirGLO vector downstream of the luciferase enzyme. The forward and reverse oligonucleotides employed in the PCR processes had restriction sites for the nuclease *Xhol*.

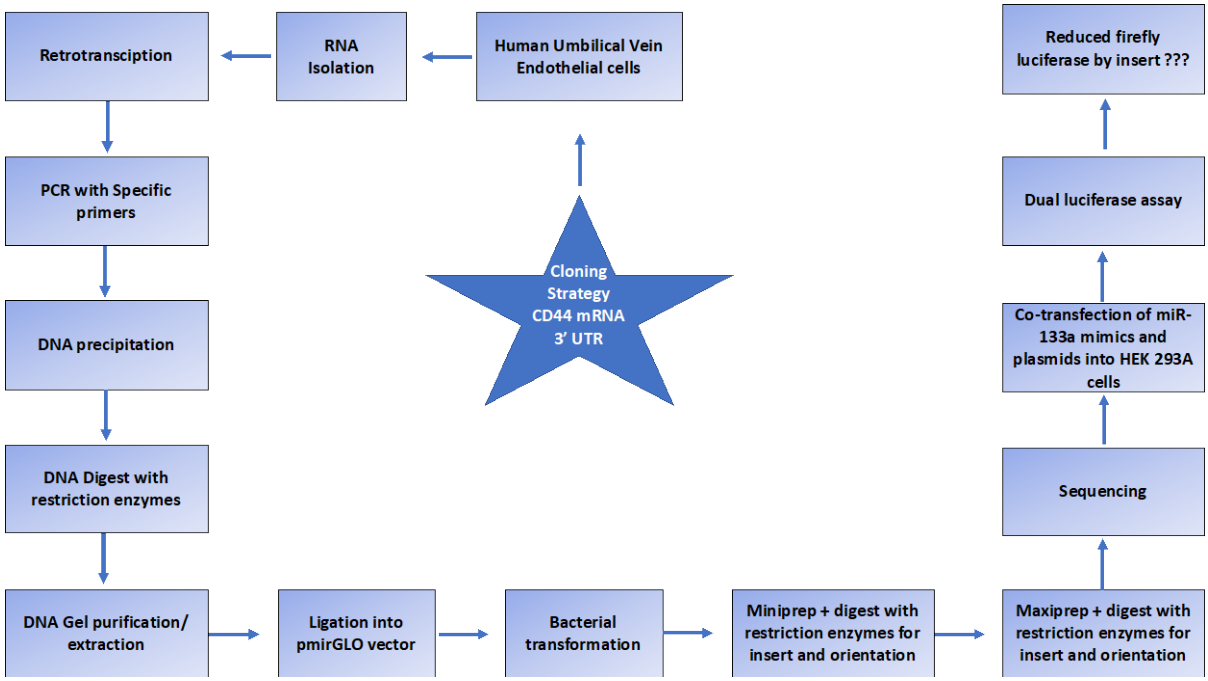

Figure 23: An illustration of the experimental procedures used to evaluate the impact of the created pmirGLO constructs incorporating parts of the *CD44* RNA 3' UTR is shown in a schematic flow diagram.

3.8.2 Preparation of pmirGLO dual luciferase vector

The Promega-created pmirGLO dual luciferase miRNA target expression vector may be used to impartially measure miRNA activity by including miRNA target sites downstream of the firefly luciferase gene luc2. The main reporter gene is firefly luciferase, and by adding miRNA binding sites or 3' UTR downstream of this gene, lower firefly luciferase expression signals the binding of miRNAs to the cloned miRNA target region. This vector also consists of *Renilla* luciferase (*hRluc-neo)*, which acts as a control gene for normalisation of transfection efficiency. A multiple cloning site (MCS) is located 3' of the firefly luciferase reporter gene *luc2*, which is where the 3' UTR of *CD44* mRNA is inserted. Just after the MCS, there is a SV40 late poly(A) signal sequence to provide efficient transcription termination and mRNA polyadenylation.

As shown in the schematic flow diagram (figure 23), after the fragments were precipitated and purified, the fragments had to be ligated to the pmirGLO vector. The pmirGLO dual luciferase vector was prepared by digestion with *XhoI,* to generate the corresponding sticky ends for insertion of the *CD44* 3' UTR region downstream of the luciferase gene. After digestion, the digested vector was precipitated, dephosphorylated, and purified by gel electrophoresis. The concentration of the resulting lineal vector was quantified by gel electrophoresis (Fig 24).

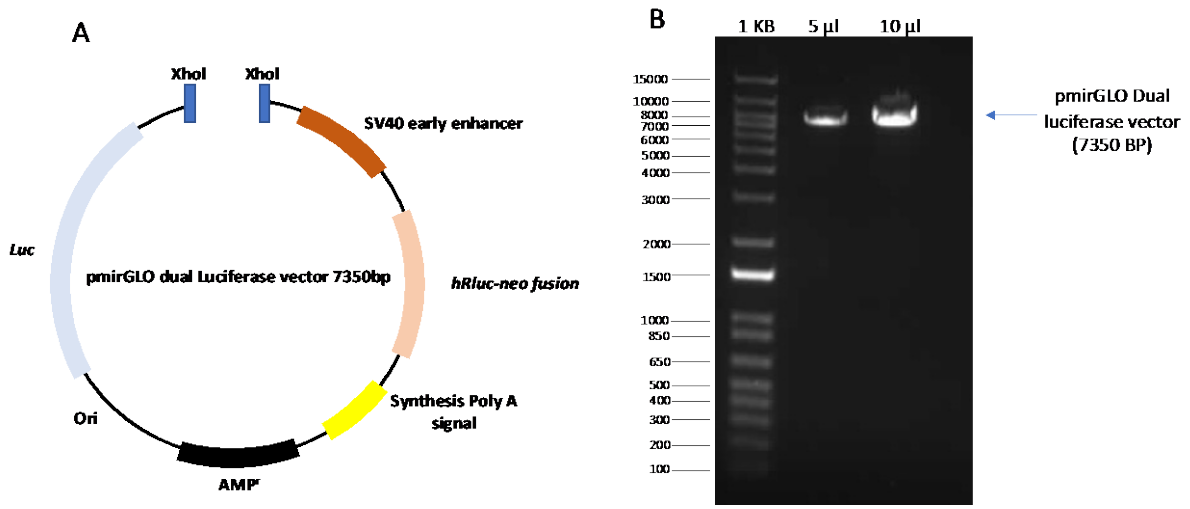

Figure 24: pmirGLO dual luciferase vector quantification. A) Schematic diagram of pmirGLO dual luciferase vector with *XhoI* restriction sites. Downstream of the *luc* gene is the MCS. For selectivity on media, the vector contains an ampicillin resistance gene (AMP^r). B) Agarose gel electrophoresis showing the 7350 bp pmirGLO dual luciferase vector digested with XhoI and dephosphorylated.

3.8.3 Generation of plasmid harbouring the region 2164-3947 of *CD44* 3' UTR mRNA

Two segments were cloned into the pmirGLO dual luciferase vector due to the size of the *CD44* 3' UTR. The first section that was copied covered the range from position 2164 to 3947. At positions 3063 to 3070 in this fragment, miR-133a-5p is predicted to target the 3' UTR of *CD44*. As shown in figure 25, this fragment with a size of 1.783 Kb was cloned into the

pmirGLO dual luciferase vector. Amplifying the relevant segment in a PCR reaction was the first step. The PCR reaction's precise size of the fragment, 1783 bp (3947-2164), was validated by agarose gel electrophoretic examination (Fig 25A). This amplified fragment was subsequently precipitated, Xhol-digested, and purified/extracted from an agarose gel at a 0.7% concentration. The extracted sample from the agarose gel was quantified to estimate the amount needed to ligate the fragment into the pmirGLO vector (Fig 25B). By adding 5 µl or 10 µl (half dilution procedure) to a 0.7% agarose gel along with 20 µl of a 1Kb plus ladder with known band size/concentration, the amount of DNA in the purified sample was measured. To determine the concentration of the purified fragment, the intensity of the 10 µl band was compared to the known band size/concentration of the 1Kb ladder (Fig 25B). The T4 DNA ligase kit (New England Biolabs) was used to set up the ligation process, which needed the pmirGLO vector digested with *Xhol* as illustrated in figure 24. The vector and insert concentrations were set up in a 1:3 molar ratio. The ligated design was used to transform JM109 capable E. coli cells, which were then plated onto ampicillin-containing LB-Agar plates for selection. Further inoculations of 9 ampicillin-resistant colonies in LB media were made in order to extract the plasmid DNA for miniprep analysis. The miniprep samples were digested with *Xhol* and the presence of the insert was determined by agarose gel electrophoresis. As shown in figure 25C, the 9 miniprep samples all contained the two expected bands; an upper band of 7350 bp which corresponds to the pmirGLO vector, and a lower band of 1783bp, which corresponds to the fragment (*CD44* 3’ UTR 2164-3947). As a result, all 9 clones tested positive, indicating that the fragment was successfully ligated into the vector. The 9 clones containing the insert were digested with *Xbal,* an enzyme with 1 restriction site in the vector and in the insert to identify the right (3’-5’) or wrong (5’-3’) orientation of the ligated insert with respect of the luciferase gene. By performing an in silico restriction study on the sequence of the plasmid pmirGLO *CD44* 3' UTR 2164-3947 using NEB Cutter 2.0, the location of the restriction sites and the size of the resultant fragments were pre-determined. As shown in figure 25D, 5 clones showed the insert cloned in the right orientation, which are clones 2, 3, 6, 7 and 9, whereas in clones 1, 4, 5 and 8 the insert was ligated in the wrong orientation. One

clone was selected among the five that were oriented correctly, and the Centro Nacional de Investigaciones Cardiovasculares CNIC in Madrid, Spain, used sequencing to confirm the accuracy of the amplified fragment's sequence. A plasmid maxipreparation using this clone was performed to obtain enough plasmid DNA for subsequent functional assays. The plasmid isolated by maxiprepation was checked again for presence of the insert (digestion with *XhoI* showing the size of insert 1783 bp) in the right orientation (digestion with *XbaI*) as shown in figure 25E. Following tests, the produced clone, known as pmirGLO-*CD44* 3'UTR (2164-3947), was used.

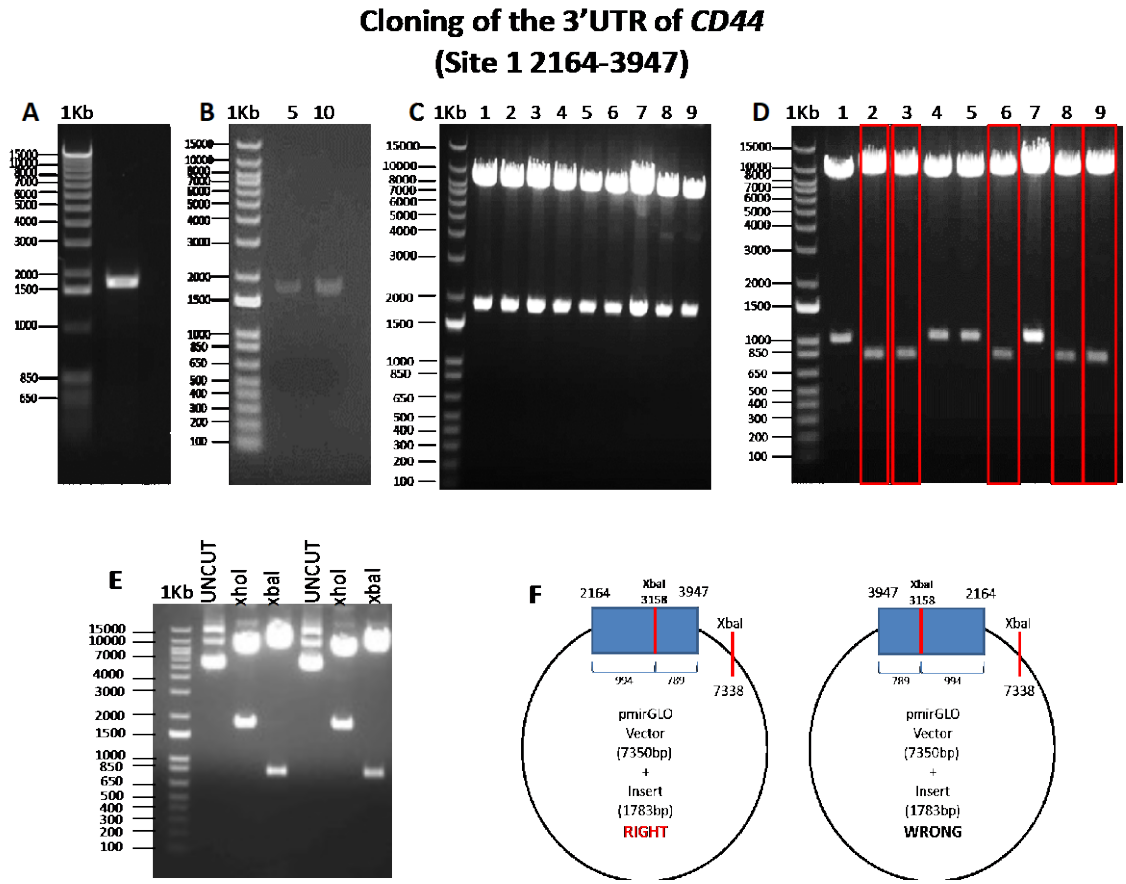

Figure 25. Overview of cloning the fragment 2164-3947 of the 3'UTR of *CD44* RNA. A) PCR amplification which shows the exact size of the insert which was 1783bp (3947-2164). B) Quantification of the purified fragment 2164-3947. C) Digestion with *XhoI* of plasmid miniprep samples isolated from colonies resulting from transformation of the ligation reaction. The presence of the two expected bands; 7350 (corresponding to the vector size) and 1783

corresponding to the insert size, denotes successful cloning of the insert into the vector. D) Restriction analysis of the direction of insertion fragment-vector. Clones with proven insert in part C), were digested with *XbaI* to identify the right (5'-3') orientation for insert ligation into the vector. Agarose gel analysis of the digestion revealed that the insert was placed in the right orientation in 5 samples (in red) and in the wrong orientation in 4. E) Digestion analysis of plasmid maxipreparation of the final clone selected for further functional analysis.

3.8.4 Generation of plasmid harbouring the region 3911-5725 of *CD44* 3' UTR mRNA

To generate the pmirGLO vector containing the 3'UTR *CD44* 3911-5725, which was the second half of 3'UTR *CD44*, PCR amplification was initially performed as previously described in chapter 3.8.3. DNA gel electrophoresis using 0.7% agarose gel was used to analyse the PCR product. A unique band was observed and shown in figure 26A, confirming the exact size of the fragment which was 1814bp (5725-3911), using a 1Kb plus ladder (ThermoFisher) as a marker for DNA length. The same process of quantification of the purified fragment shown in chapter 3.8.3 was performed as shown in figure 26B. The pmirGLO vector and the *CD44 3' UTR* 3911-5725 fragment were ligated at 15°C overnight in a thermal cycler. The ligated construct was transformed into JM109 competent *E. coli* cells. 4 ampicillin-resistant colonies were selected and inoculated to perform miniprep analysis. The miniprep samples were digested with *XhoI* and an agarose gel was performed to analyse the presence of the recombinant plasmid containing the *CD44* 3' UTR fragment with the correct size of 1814bp. As shown in figure 26C, the 4 miniprep samples all contained two unique bands, with the upper band of 7350bp which corresponds to the pmirGLO vector and a lower band of 1814bp, which corresponds to the fragment (*CD44 3' UTR* 3911-5725). Therefore all 4 clones were positive showing successful ligation of the fragment into the vector. The 4 clones containing the insert were digested with *SalI* and *ScaI*. *SalI* has 1 restriction site in the insert at position 4025 bp, and *ScaI* has 3 restriction sites in the vector, which are positions 3343 bp, 5055 bp and 5810 bp to identify the right (3'-5') or wrong (5'-3') orientation. The position of the

restriction sites and the size of resulting fragments were pre-determined by carrying out in silico restriction analysis of the sequence of plasmid pmirGLO *CD44 3' UTR* 3911-5725 using NEB Cutter 2.0. As shown in figure 26D, 2 clones were in the right orientation, which are clones 1 and 4, whereas clones 2 and 3 were in the wrong orientation. From the 2 clones in the right orientation, one clone was chosen and the fidelity of the sequence of the amplified fragment validated by sequencing in the department of Vascular Biology and Inflammation, Centro Nacional de Investigaciones Cardiovasculares CNIC, Madrid, Spain. A plasmid maxipreparation using this clone was performed to obtain enough plasmid DNA for subsequent functional assays. The plasmid isolated by maxiprepation was checked again for presence of the insert (digestion with *XhoI* showing the size of insert 1814 bp) in the right orientation (digestion with *SalI* and *ScaI*) as shown in figure 26E. The resulting clone was now named pmirGLO-*CD44* 3'UTR (3911-5725) and was used in subsequent experiments.

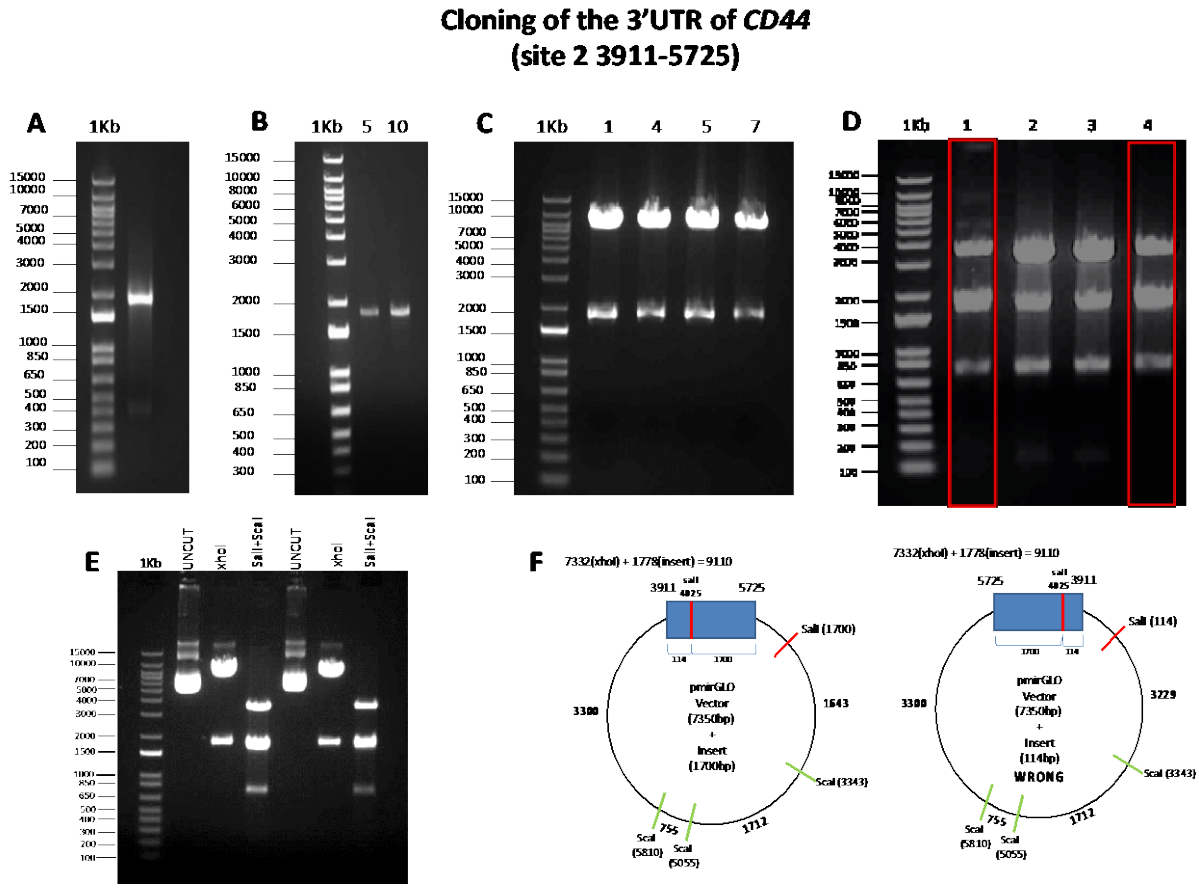

Figure 26. Overview of cloning the 3'UTR of *CD44,* site 2 position 3911-5725bp. A) PCR amplification which shows the exact size of the insert which was 1814bp (5725-3911). B) Quantification of the purified fragment 3911-5725. C) Digestion with *XhoI* of plasmid miniprep samples isolated from colonies resulting from transformation of the ligation reaction. The presence of the two expected bands; 7350 (corresponding to the vector size) and 1814 corresponding to the insert size, denotes successful cloning of the insert into the vector. D) Restriction analysis of the direction of insertion fragment-vector. Clones with proven insert in part C), were digested with *SalI* and *ScaI* to identify the right (5'-3') orientation for insert ligation into the vector. Agarose gel analysis of the digestion revealed that the insert was placed in the right orientation in 2 samples (in red) and 2 samples in the wrong orientation. E) Digestion analysis of plasmid maxipreparation of the final clone selected for further functional analysis. F) schematic diagram which illustrate the right and wrong orientation. The right orientation is determined by size of insert when digested with *SalI* 5725-4025 = 1700 bp, and *ScaI* 3343-1700 = 1643. The wrong orientation is determined by size of insert when digested with *SalI* 4025-3911 = 114, which is sample 2 and 3, which is faint, but there is a band around the region 114 in sample 2 and 3.

3.8.5 Generation of plasmid harbouring the region 2164-3026 of *CD44* 3' UTR mRNA

To further evaluate the functionality of the potential miR-133a-binding site, the fragment harbouring the region 2164-3947 of *CD44* 3'UTR, was split into two fragments, regions 2164-3026 and 3003-3947. As shown in figure 27 the plasmid harbouring the region 2164-3026 of *CD44* 3'UTR mRNA was successfully cloned using the same process as mentioned in chapter 3.8.3. To generate the pmirGLO vector containing the 3'UTR *CD44* 2164-3026, PCR amplification was initially performed as previously described in chapter 3.8.3. DNA gel electrophoresis using 0.7% agarose gel was used to analyse the PCR product. A unique band was observed and shown in figure 27A confirming the exact size of the fragments which was 862bp (3026-2164). The same process of quantification of the purified fragment shown in

chapter 3.8.3 was performed on this fragment as shown in figure 27B and ligated into the vector. The pmirGLO *CD44 3' UTR* 2164-3026 was incubated at 15°C overnight in a thermal cycler. The ligated construct was transformed into JM109 competent *E. coli* cells. The miniprep samples were digested with *XhoI* and an agarose gel was performed to analyse the presence of the recombinant plasmid containing the *CD44* 3' UTR fragment with the correct size of 862bp. As shown in figure 27C, all 10 miniprep samples all contained two unique bands, with the upper band of 7350bp which corresponds to the pmirGLO vector and a lower band of 862bp, which corresponds to the fragment (*CD44 3' UTR* 2164-3026). Therefore all 10 clones were positive showing successful ligation of the fragment into the vector. The 10 clones shown in figure 27C containing the insert were digested with *ApaI. ApaI* has 1 restriction site in the insert at position 2873 bp and has 1 restriction site in the vector, which is at position 5675 bp to identify the right (3'-5') or wrong (5'-3') orientation. As shown in figure 27D, in the red boxes are the clones in the right orientation. One clone was chosen and the fidelity of the sequence of the amplified fragment validated by sequencing in the department of Vascular Biology and Inflammation, Centro Nacional de Investigaciones Cardiovasculares CNIC, Madrid, Spain. The plasmid isolated by maxiprepation was checked again for presence of the insert (digestion with *XhoI* showing the size of insert 862 bp) in the right orientation (digestion with *ApaI* showing the size of 2424 bp) as shown in figure 27E. The resulting clone was now named pmirGLO-*CD44* 3'UTR (3911-5725) and was used in subsequent experiments.

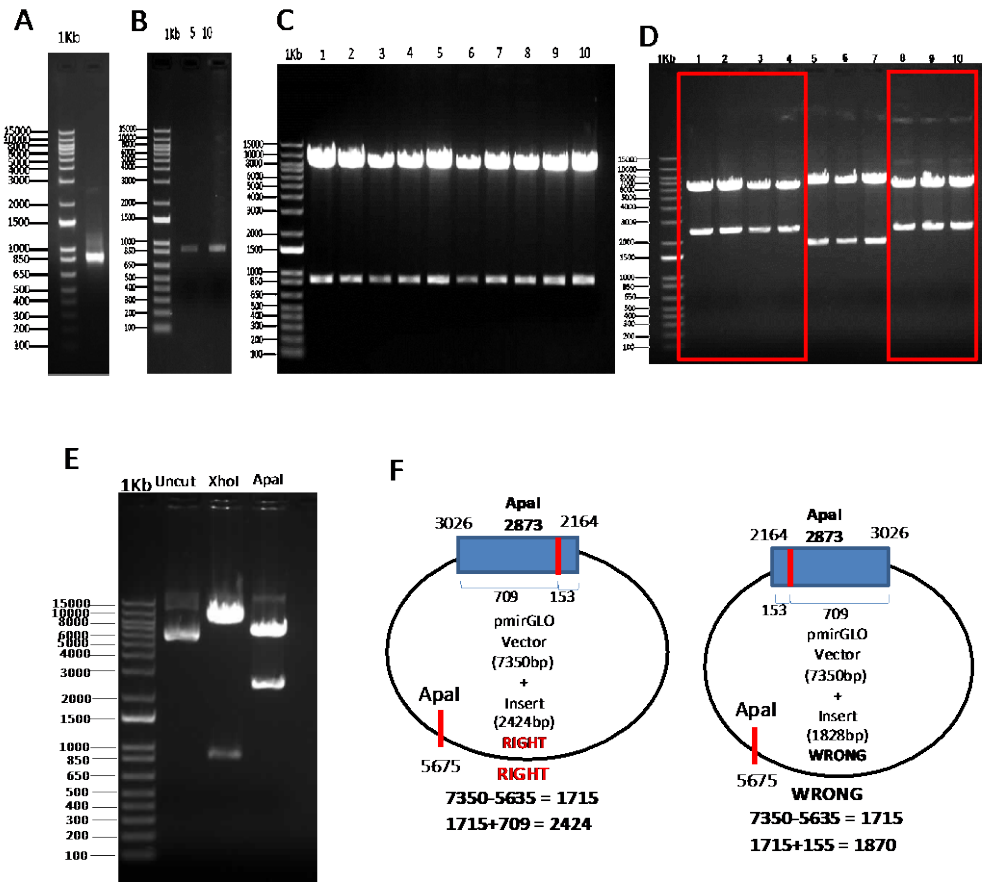

Figure 27. Overview of cloning the 3'UTR of *CD44,* clone 1 (site 1) position 2164-3026bp.

A) PCR amplification which shows the exact size of the insert which was 862bp (3026-2164). B) Quantification of the purified fragment 3911-5725. C) Digestion with *XhoI* of plasmid miniprep samples isolated from colonies resulting from transformation of the ligation reaction. The presence of the two expected bands; 7350 (corresponding to the vector size) and 862 corresponding to the insert size, denotes successful cloning of the insert into the vector. D) Restriction analysis of the direction of insertion fragment-vector. Clones with proven insert in part C), were digested with *ApaI* to identify the right (5'-3') orientation for insert ligation into the vector. Agarose gel analysis of the digestion revealed that the insert was placed in the right orientation in 7 samples (in red) and 3 samples in the wrong orientation. E) Digestion analysis of plasmid maxipreparation of the final clone selected for further functional analysis.

3.8.6 Generation of plasmid harbouring the region 3003-3947 of *CD44* 3' UTR mRNA

As shown in figure 28, the plasmid harbouring the region 3003-3947 of *CD44* 3'UTR mRNA was successfully cloned using the same procedure mentioned above. As shown in figure 28A, analysis of the PCR reaction confirming the exact size of the fragment which was 944 bp (3947-3003), using a 1Kb plus ladder (ThermoFisher) as a marker for DNA length circled in red as the first band was fragment pmirGLO-*CD44* 3'UTR (2164-3026). This amplified fragment was then precipitated, digested with *XhoI*, and purified/ extracted from an 0.7% agarose gel as shown in figure 28B and ligated into the pmirGLO vector. The pmirGLO *CD44 3' UTR* 3003-3947 was incubated at 15°C overnight in a thermal cycler. The ligated construct was transformed into JM109 competent *E. coli* cells. 6 colonies were inoculated to perform miniprep analysis. The miniprep samples were digested with *XhoI* and an agarose gel was performed to analyse the presence of the recombinant plasmid containing the *CD44* 3' UTR fragment with the correct size of 944 bp. As shown in figure 28C, colonies 5 out of the 6 samples contained two unique bands, with the upper band of 7350bp which corresponds to the pmirGLO vector and a lower band of 944 bp, which corresponds to the fragment (*CD44 3' UTR* 3003-3947). Therefore the 5 clones were positive showing successful ligation of the fragment into the vector. The 5 clones containing the insert were digested with *XbaI. XbaI* has 1 restriction site in the insert at position 3159 bp and has 1 restriction site in the vector, which is at position 7338 bp to identify the right (3'-5') or wrong (5'-3') orientation. By doing an in-silico restriction analysis of the plasmid pmirGLO *CD44* 3' UTR 3003-3947 sequence using NEB Cutter 2.0, the location of the restriction sites and the size of the resultant fragments were pre-determined. According to figure 28D, 1 clone was in the right orientation highlighted in a red box. This clone in the right orientation was validated by sequencing in the department of Vascular Biology and Inflammation, Centro Nacional de Investigaciones Cardiovasculares CNIC, Madrid, Spain. The DNA maxi-preparation of the plasmid was performed and was digested with *XhoI* to show the size of insert (944 bp), *XbaI* to show the right orientation, which was a band at 800 bp and uncut as a control to only show the pmirGLO vector. The resulting

clone was now named pmirGLO-*CD44* 3'UTR (3003-3947) and was used in subsequent experiments.

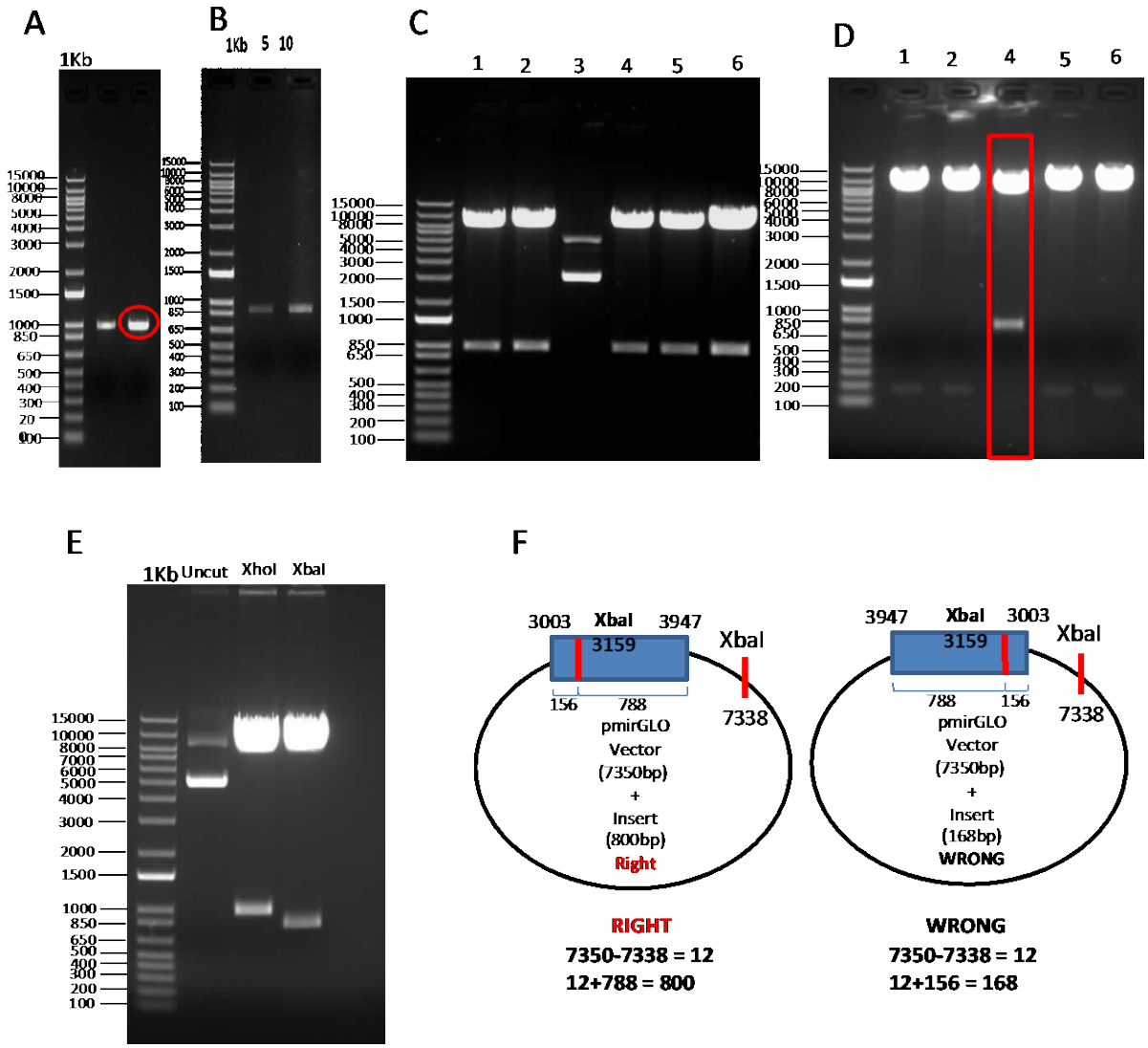

Figure 28. Overview of cloning the 3'UTR of *CD44,* clone 1 (site 2) position 3003-3947bp. A) PCR amplification which shows the exact size of the insert which was 944bp (3947-3003). B) Quantification of the purified fragment 3003-3947. C) Digestion with *XhoI* of plasmid miniprep samples isolated from colonies resulting from transformation of the ligation reaction. The presence of the two expected bands; 7350 (corresponding to the vector size) and 944 corresponding to the insert size, denotes successful cloning of the insert into the vector. D) Restriction analysis of the direction of insertion fragment-vector. Clones with proven insert in part C), were digested with *XbaI* to identify the right (5'-3') orientation for insert ligation into

the vector. Agarose gel analysis of the digestion revealed that the insert was placed in the right orientation in 1 sample (in red) and 4 samples in the wrong orientation. E) Digestion analysis of plasmid maxipreparation of the final clone selected for further functional analysis.

Table 9: The list of enzymes and corresponding buffers used for the constructs of the fragments for the insert size and orientation.

Plasmids	Digest for size	Corresponding Buffer	Digest for right orientation	Corresponding Buffer
2164 to 3947 (ALA 314-315)	*XhoI*	Buffer D	*XbaI*	buffer D
3911 to 5725 (ALA 319-318)	*XhoI*	Buffer D	*SalI + ScaI*	buffer D
2164 to 3026 (ALA 314-322)	*XhoI*	Buffer D	*ApaI*	buffer A
3003 to 3947 (ALA 323-315)	*XhoI*	Buffer D	*XbaI*	buffer D

When all fragments harbouring the 3'UTR of *CD44* were successfully cloned, the plasmids were transfected into HEK293A with miRNA-NC, miR-133a-3p and miR-133a-5p mimics and dual luciferase assay was performed to measure the activity of the firefly luciferase gene.

3.9. Determining how the firefly luciferase gene's activity is impacted by *CD44*'s 3'UTR fragments.

HEK 293A cells were used to investigate potential binding sites for miR-133a in the 3'UTR of *CD44,* as the RNA expression of *CD44* was inhibited in the presence of miR-133a-3p and miR-133a-5p in endothelial cells. Bioinformatic analysis predicted miR-133a-5p targets the

3’UTR of *CD44* mRNA. HEK 293A cells were seeded at a density of 2 x 10^5 cells/well in a 12 well plate pre-coated with gelatine. The next morning, cells were co-transfected with miR-NC, miR-133a-3p, and miR-133a-5p, as well as plasmids made from Promega's (USA) pmirGLO Dual-Luciferase MiRNA Target Expression Vector and containing various sections of *CD44*'s 3'UTR downstream of the Firefly luciferase reporter gene (*luc2*). After 24 hours incubation, transfection solutions were aspirated, and transfection medium replaced with fresh complete DMEM. A further 24 hours were spent incubating the transfected cells. To examine the impact of the *CD44* 3'UTR fragments on the stability of *luc2* RNA, Firefly luciferase activity was measured. *Renilla* luciferase activity was assessed to normalise any variations in each plasmid's transfection efficiency.

Co-transfection of pmirGLO empty vector, pmirGLO-*CD44* 3’UTR (2164-3947) and pmirGLO-*CD44* 3’UTR (3911-5725) with miR-NC, miR-133a-3p and miR-133a-5p was performed. As shown in figure 29 from one independent experiment, when pmirGLO empty vector was the control to demonstrate the effect of the mimics on both the fragments. As mentioned before, pmirGLO-*CD44* 3’UTR (2164-3947) contains the predicted site at position 3063-3070, where miR-133a-5p targets the 3’UTR of *CD44* mRNA. There was more reduction in HEK 293A transfected with pmirGLO-*CD44* 3’UTR (2164-3947) and miR-133a-5p, which was 67.5% when compared with the empty pmirGLO vector transfected with miR-133a-5p. This suggest the bioinformatic prediction database could possibly be true. To validate these data, a further experiment was performed on pmirGLO-*CD44* 3’UTR (2164-3026) and pmirGLO-*CD44* 3’UTR (3003-3947). The pmirGLO-*CD44* 3’UTR (3003-3947) fragment contains the predicted target site for miR-133a-5p in the 3’UTR of *CD44* mRNA at position 3063-3070. As shown in figure 30, HEK 293A cells co-transfection with miR-NC, miR-133a-3p or miR-133a-5p did not show inhibitory effect for any of the strand of miR-133a transfected.

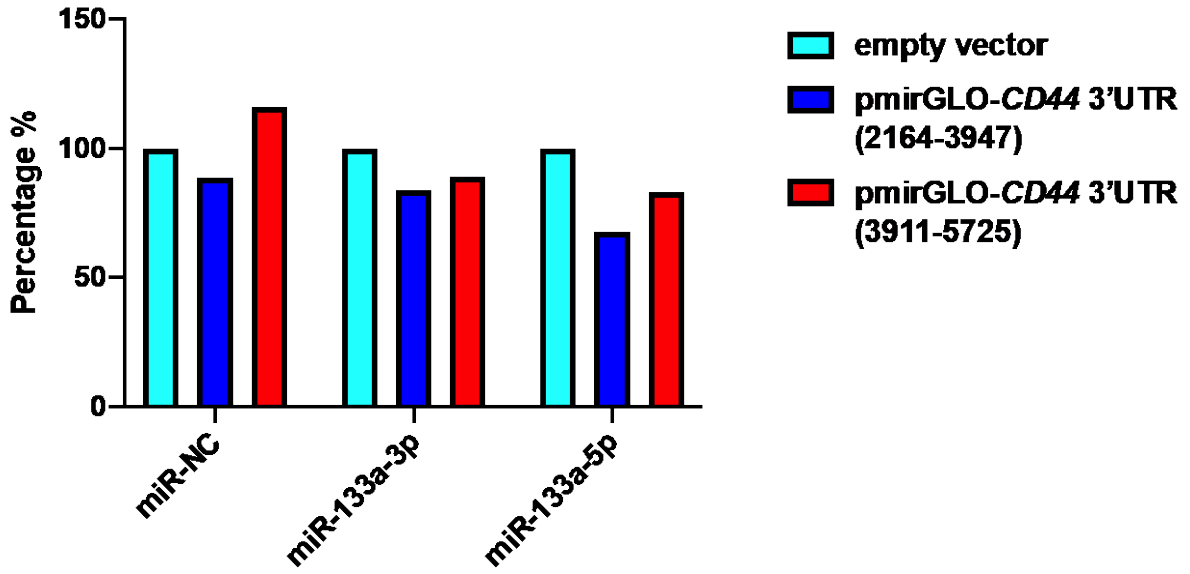

Figure 29. pmirGLO dual luciferase luminometer results after transfecting HEK293A with miR-mimics pmirGLO-*CD44* 3'UTR (2164-3947) and pmirGLO-*CD44* 3'UTR (3911-5725) and an empty vector as control. When the empty vector was the control, there was more reduction, 68% in site 1 (2164-3947) when transfected with miR-133a-5p compared to site 2 (3911-5725), 83.2%. Which suggested the database prediction could possibly be true, and mir-133a-5p targets the 3'UTR of *CD44* at this position.

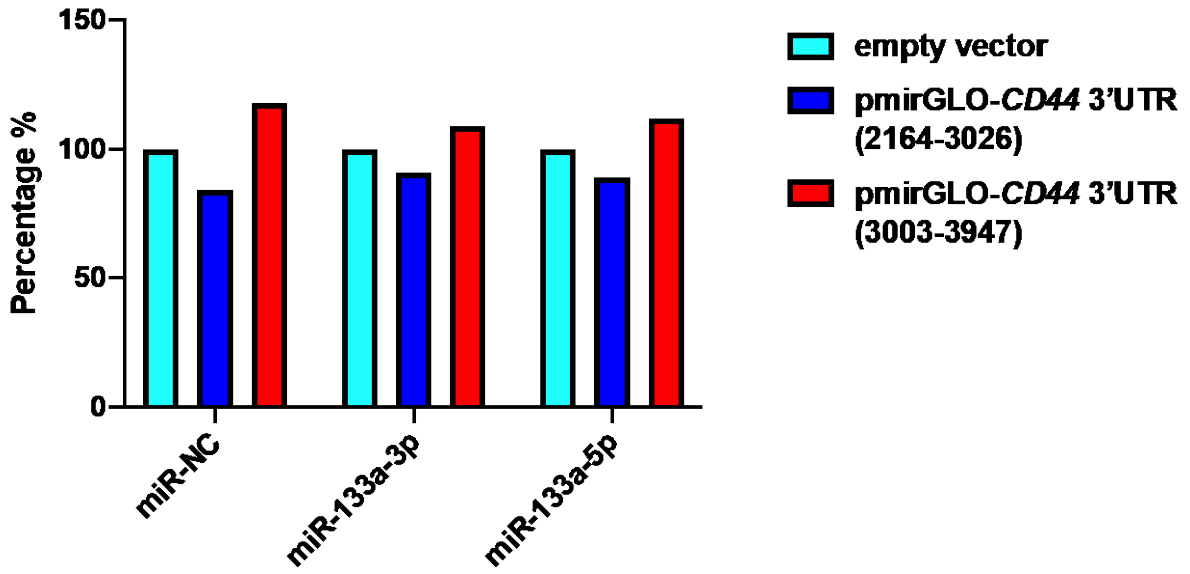

Figure 30: pmirGLO dual luciferase luminometer results after transfecting HEK293A with miR-mimics pmirGLO-*CD44* 3'UTR (2164-3026) and pmirGLO-*CD44* 3'UTR (3003-3947) and an empty vector as control. When the empty vector was the control, to demonstrate the effect of the mimics had on site 1, pmirGLO 314-322 (2164-3026), and site 2, pmirGLO 323-315 (3003-3947). miR-133a-5p had no effect on the 3 sites.

CHAPTER 4
DISCUSSION

4.1 Discussion

Angiogenesis is the formation of blood vessels from pre-existing ones. This multi-factorial physiological process is tightly regulated by a balance of pro-angiogenic and anti-angiogenic signals (Kazerounian and Lawler, 2018). An unbalance of this process will lead to human diseases characterised by excessive or insufficient blood vessel formation (Potente *et al.,* 2011). Among all pro-angiogenic factors, VEGF is the most prominent cytokine, which exerts its biological function by binding to its receptor VEGFR2, which plays a pivotal role as an inducer of both physiological and pathological angiogenesis. However further evidence of how intracellular regulators modulate VEGF-A induced signalling in endothelial cells is yet to be fully characterised (Koch *et al.,* 2011).

MicroRNAs (miRNAs) are single-stranded, small, non-coding RNA molecules that are roughly 22 nucleotides long. By attaching to certain regions in the 3'UTR of RNAs, they control gene expression by either inducing mRNA degradation or suppressing protein translation. In most cases, miRNAs interact with the 3′ untranslated region (3′ UTR) of target mRNAs to induce mRNA degradation and translational repression. However, interaction of miRNAs with other regions, including the 5′ UTR, coding sequence, and gene promoters, have also been reported (Broughton *et al.,* 2016). Increasing evidence points to miRNAs as important cytoplasmic regulators of angiogenesis. Inhibition of two endonucleases, Dicer and Drosha, which are necessary for the formation of mature miRNAs in the biogenesis of miRNA, has demonstrated the role of miRNAs in the biology of endothelial cells and vascular development both in vitro and in vivo (Ha and Kim, 2014). Important endothelial cell activities such as impaired postnatal angiogenesis and sprouting angiogenesis are impacted by the drop in miRNA levels (Suárez *et al.,* 2008). There has been more research done on the relationship between certain miRNAs and the elements of the VEGF signalling pathway. For instance, VEGF expression is suppressed by miR-15a and miR-16, among other miRNAs (Chamorro-Jorganes *et al.,* 2011; Dang *et al.,* 2013) while miR-126 stimulates VEGF signalling by directing its attention to the

downstream effector PIK3R2 (Fish *et al.,* 2008). A regulatory miRNA network regulates the phenotypic flip of endothelial cells during sprouting angiogenesis, as demonstrated by Rosano et al. important proliferative and migratory genes were shown to be down- and up-regulated by the miRNA network. A coordinated regulation of several biological processes, including extracellular matrix synthesis, deposition, cell migration, and proliferation, is necessary for the sprouting angiogenesis process. They showed in their studies that during the first stage of sprouting angiogenesis, miRNAs work together to strengthen the specification of the tip cell phenotype by upregulating the expression of genes related to cell migration and extracellular matrix remodelling and downregulating the expression of genes linked to cell-cycle progression and members of the mitogen-associated protein kinase (MAPK) cascade, which support VEGF-A-mediated cell proliferation (Rosano *et al.,* 2020).

miRNAs are mostly expressed ubiquitously, whereas others present a tissue restrictive pattern of expression. This is the case with miR-133a, a myo-miRNAs, which means this miRNA is muscle tissue specific. Cardiac specific and skeletal muscle specific miR-1 and miR-133 have shown their essential functions in controlling skeletal muscle proliferation and differentiation (Chen *et al.,* 2006). MiR-133a is normally expressed at modest levels in endothelial cells, however recent research by Li et al. has demonstrated that miR-133a expression levels significantly increased in diseased endothelium. MiR-133a was not found in the endothelium layer of normal rats' carotid arteries when miR-133a expression was examined using fluorescent in situ hybridization. However, miR-133a was expressed in the endothelium layer in rats given injections of streptozotocin (STZ) to mimic diabetes conditions (Li *et al.,* 2016). Studies on the topic of angiogenesis demonstrate the connection between miR-133a's action on endothelial cells and the prevention of angiogenesis. Peripheral arterial disease (PAD), which is caused by ischemia-induced impaired neovascularisation, was the focus of a study by Chen et al. (2018). When compared to non-diabetic mice, diabetic animals had greater levels of miR-133a expression in the ischemic muscle. Transfecting HUVEC cells with miR-133a mimics or miR-133a inhibitors allowed researchers to examine miR-133a's impact on

angiogenesis in vitro. Because diabetic animals had increased levels of miR-133a, miR-133a was knocked down using antagomirs, which enhanced angiogenesis and perfusion recovery.

As previously established, miRNAs are essential regulators of a variety of cellular activities by post-transcriptionally silencing the genes that they target. Recent research has revealed that miRNAs also control certain angiogenic environments and signalling pathways. In vitro endothelial cell migration, proliferation, and viability were all suppressed by miR-133a in HUVEC cells, as demonstrated by Soufi-Zomorrod et al., 2016. This suggests that miR-133a can directly target important angiogenesis-related factors to suppress them, and it also illustrates the potential therapeutic implications of using miR-133a-based interventions to treat a range of diseases that involve dysregulated angiogenesis (Soufi-Zomorrod et al., 2016).

Although these studies demonstrated that aberrant expression of miR-133a in endothelial cells inhibits angiogenesis, Zhu *et al* (2021) recently reported an opposite role for miR-133a as a positive regulator of endothelial cell angiogenesis. Zhu et al study showed exosomes from macrophage migration inhibitory factor (MIF) engineered ucMSCs (MIF-Exo) significantly improved cell survival, blood vessel formation and cell migration *in vitro* in HUVEC cells when compared to the control non-engineered ucMSCs (MSC-Exo). Comparing MIF-Exo to MSC-Exo, quantitative real time PCR (qRT-PCR) and miRNA sequencing revealed an increase in miR-133a-3p expression. Additionally, miR-133a-3p mimics enhanced the phosphorylation of AKT in HUVECs. Furthermore, MIF-Exo and miR-133a incubation reduced the biological effects of HUVECs (Zhu et al., 2021).

The miRNA biogenesis generates two mature strands, -3p and -5p. During the process of miR maturation either strand can be incorporated into the RISC complex and both strands can modulate gene expression (Daugaard and Hansen, 2017). Bioinformatic target gene predictions have shown that each miR-133a strand target different genes, however there are genes which might still be targeted by both -3p and -5p (Ohanian *et al.,* 2013). It has been reported that the expression of both miR-133a strands increase in cardiovascular settings. For example, miR-133a-5p expression is up-regulated in myocardial infarction studies as a key

selected apoptosis-associated miRNA (Ma *et al.,* 2018). strands up regulated in diabetic atherosclerosis (DA). Both miRNA-133a-3p and -5p strands, out of 9 differentially expressed miRNAs (DE-miRs), were targeting 3349 genes related to known functions and pathways for lipid and glucose metabolism (Li *et al.,* 2018). However, in the context of angiogenesis, the specific effect of the -3p and -5p strand has not fully been addressed.

This study looked at the practical implications of particular expression of each strand on the regulation of significant endothelial angiogenic processes in order to resolve the conflicting findings regarding the role of aberrant expression of miR-133a in angiogenesis and to investigate the molecular and cellular mechanisms regulated by each strand. In HUVEC cells, the impact of aberrant miR-133a-3p and -5p expression on the expression of genes encoding important regulators of angiogenesis was investigated. Previous research on the impact of miR-133a aberrant expression on endothelial cell angiogenesis has produced mixed findings (Soufi-Zomorrod et al., 2016; Chen et al., 2018; Zhu et al.,2021).

This work examined the tubular morphogenesis of HUVEC cells that were particularly overexpressing miR-133a-3p or -5p in order to further clarify the impact of aberrant miR-133a expression on endothelial cell angiogenesis. Cells were either left unstimulated (control) or stimulated with VEGF (50 ng/µl). When compared to the control, miR-NC, the Matrigel tube formation experiment showed that ectopic expression of miR-133a-3p significantly inhibited tubular morphogenesis of primary endothelial cells (HUVECs). While VEGF stimulation had no effect in cells transfected with miR-133a-3p, there was a significant increase in tube morphogenesis in VEGF-stimulated cells transfected with miR-NC. This finding suggests that aberrant expression of miR-133a-3p impaired both basal and VEGF-induced tubular morphogenesis. When compared to the control miR-NC, HUVECs transfected with miR-133a-5p showed a statistically significant decrease in tubular morphogenesis. Although the 5p strand's effect was weaker than the 3p strand's, VEGF stimulation still led to a statistically significant increase in the number of cells that overexpress miR-133a-5p. Our research demonstrates that the -3p and -5p strands suppress endothelial cell angiogenesis in separate

ways, indicating that they could each target a different biological mechanism for angiogenic cell growth. Our first research led us to hypothesise that miR-133a-3p may have a significant negative regulatory role in endothelial cell angiogenesis.

As a result, using the evidence from the literature as a springboard, the first step was to ascertain the impact of aberrant miR-133a expression on endothelial cell tubular morphogenesis, which was studied in HUVEC cells using adenovirus miR-133a (Ad-miR-133a) with a MOI of 200 and adenovirus miR control (Ad-miR NC). Because miR-133a was expressed in endothelial cells in diabetic rats but not in normal rats, as demonstrated in Chen et al (2018) publication, primary endothelium cells were infected with Ad-miR-133a in order to mimic a pathology. Infected cells were treated with bFGF (25 ng/μl) and left unstimulated as a control. Endothelial tubular morphogenesis was suppressed by miR-133a both with and without pro-angiogenic agents. This study concentrates on VEGF since it is the most prevalent pro-angiogenic factor, but by performing bFGF tests, this shows the impact of aberrant miR-133a expression in endothelial cells that have been stimulated by a variety of pro-angiogenic factors. This finding suggests that miR-133a-based therapeutics may have practical relevance in treating human disorders linked with angiogenesis that include several variables, such as tumour cells that are resistant to anti-VEGF treatment.

We transfected HUVEC cells with miR-133a-3p or miR-NC as a control and checked the expression of genes encoding components of the Notch signalling system following VEGF stimulation in light of the substantial inhibitory function of miR-133a-3p shown in endothelial cell tubular morphogenesis. Over the past few years, it has been abundantly obvious that VEGF-A facilitates endothelial cell differentiation, migration, and proliferation, as well as regulates endothelial cell-cell junctions. The angiogenic response is regulated by a variety of pathways, including Wnt, TGF/Alk1, Angiopoietin/Tie2, Notch, FGF, S1P/Edg1, Semaphorin/Plexin, Netrin/Unc5b, Slit/robo, cell matrix/integrin signalling, and others. However, a number of studies have demonstrated that participants in the Notch signalling pathway are crucial in coordinating a variety of endothelial cell behaviours throughout the

formation, patterning, and remodelling of the vascular network (Phng and Gerhardt, 2009). The expression of *JAG2, HEY1, NOTCH4, DLL4, HES4,* and *NRARP,* was considerably elevated by the ectopic expression of miR-133a-3p, as shown in (Figure 15). The intriguing finding regarding these Notch signalling pathway regulators is that they have anti-angiogenic properties. For instance, *DLL4*, a membrane-bound ligand for *Notch1* and *Notch4* that is activated by hypoxia and VEGF-A, is expressed only in growing endothelium. Strong angiogenesis inhibitor *DLL4* has been shown to prevent the production of cell tips and is necessary for the correct establishment of vascular networks throughout development (Williams et al., 2006; Suchting et al., 2007). Similar to this, migrating and proliferating endothelium cells lack the fundamental helix-loop-helix transcription factor HESR1 (HEY-1/HRT-1/CHF-2/gridlock). A negative involvement for this protein in the control of angiogenesis is suggested by the fact that overexpression of HESR1 in endothelial cells reduces VEGFR2 mRNA expression, which in turn prevents proliferation, migration, and network development (Henderson et al., 2001). The notch family of transmembrane receptors, which are expressed on endothelial cells, includes *Notch4*. Leong et al. (2002) used an in vitro endothelial-sprouting test to investigate the function of *Notch4* in angiogenesis. Human dermal microvascular endothelial cells (HMEC-1) that expressed *Notch 4* were unable to sprout new endothelial cells. They also demonstrated that VEGF-induced angiogenesis was reduced by activated *Notch4* (Leong et al., 2002). Our data suggests that increased expression of these genes is one of the factors mediating the inhibitory effect exerted by miR-133a-3p in angiogenesis. These findings, along with others (Leslie et al., 2007; Phng and Gerhardt, 2009), have shown that *DLL4*/Notch signalling negatively modulates sprouting angiogenesis.

Our findings further demonstrate that miR-133a-3p's aberrant expression suppressed *CD44* and *ID1* expression (Figure 15). In rat models of choroidal neovascularization, hindlimb ischemia, and cardiac ischemia, enhanced endothelial *CD44* expression has been shown, showing that *CD44* promotes angiogenesis in these pathological circumstances (Shen et al., 1998; van Royen et al., 2004; Cao et al., 2006; Wei et al., 2014). Additionally, *CD44*

encourages and controls a variety of endothelial cell activities, including proliferation, migration, adhesion, and invasion. Furthermore, abnormal angiogenesis and disease development would be hampered by *CD44* deficiency or its function (Chen et al., 2020). Helix-loop-helix transcription factor *ID1* is known to promote angiogenesis, according to published studies. The presence of *ID1* increased HUVEC migration, proliferation, and the development of capillary-like tubes, as demonstrated by Nishiyama et al. (2005) (Nishiyama et al., 2005). Our findings demonstrate that abnormal miR-133a expression in endothelial cells suppresses the expression of *CD44* and *ID1*. The documented pro-angiogenic properties of these genes coincide with the detrimental impact of miR-133a on the tubular morphogenesis of endothelial cells found in our work.

The proliferation of endothelial cells in response to pro-angiogenic stimuli is a critical stage in the process of angiogenesis. Here, we demonstrate that both the -3p and -5p strands limit the proliferation of endothelial cells, while the impact of miR-133a-3p is stronger than that observed with the -5p strand (Figure 16). Further tests showed that miR-133a-3p downregulated the expression of *CDK1, CCNA2, CCNB1, MCM2,* and *MCM4* when it was expressed ectopically (Figure 16). The advancement of DNA replication during the cell cycle and entrance into the S phase, which is where endothelial cell proliferation occurs, are significantly regulated by cyclins and the minichromosome maintenance protein (MCM) (Yeeles et al., 2015). Therefore, we looked at whether abnormal miR-133a-3p expression prevented cells from entering the S phase. A flow cytometer examination of the miR-133a-3p-transfected HUVEC population was done. Results demonstrated that compared to cells transfected with miR-NC, the G0/G1 phase of the cell cycle had more cells, but fewer in the S and G2.M stages (Figure 16). Gao et al 2019 study looked at *CDK1*'s impact on angiogenesis. The authors' extremely intriguing findings corroborate our findings. Initially, they used *CDK1* siRNAs on HUVEC to examine the function of *CDK1* in angiogenesis. The outcomes showed that the *CDK1* siRNAs drastically decreased *CDK1*'s mRNA expression. In contrast to what was discovered in this study, miR-133a-3p overexpression suppressed *CDK1* expression.

Second, in HUVEC cells, the impact of *CDK1* siRNAs on endothelial cell proliferation was examined. According to their findings, cells exposed to *CDK1* siRNAs multiplied more slowly than cells from the control and scramble groups. We may conclude from these observations and our findings that aberrant miR-133a-3p expression prevents endothelium growth by suppressing *CDK1* expression. The authors further demonstrate that silencing *CDK1* prevents HUVEC from forming tubes, which is consistent with the reduction of endothelial cell tubular morphogenesis observed when miR-133a is transfected into HUVECs (Gao et al., 2019).

Cell migration was investigated since it is another area where miR-133a-3p could inhibit angiogenesis. As already noted, the Notch signalling system is essential for controlling the development of tip and stalk cells. Furthermore, through controlling the expression of essential regulators of cell motility, it also plays a significant role in the migration of endothelial cells. When there is a wound, VEGF is raised in the skin and contributes to cell migration, which encourages endothelial cell migration to seal the wound (Johnson and Wilgus, 2014). Our findings shown that miR-133a-3p ectopic expression slows the migration of endothelial cells after 24 hours. After 24 hours, miR-133a-5p-transfected cells showed no statistically significant change in endothelial cell movement. The research from Gao et al. (2019) revealed that silencing of *CDK1* decreased vascular endothelial cell migration, which is thought to be an important mechanism for angiogenesis. They demonstrated that silencing of *CDK1* hindered the migration of HUVECs (Gao et al., 2019). When compared to our findings, this evidence suggests that endothelial cell overexpression of miR-133a-3p inhibits *CDK1* expression, supporting the observed suppression of endothelial cell migration. Here, we also show that overexpressing miR-133a-3p in HUVEC decreased the expression of the genes for *PLAUR* (also known as *uPAR*) and Moesin (*MSN*). The primary regulator that stimulates *uPAR*, which in turn activates tip cell migration, is *MSN*, a regulator of receptor signalling and a promoter of cell migration. Therefore, downregulation of this gene also supports miR-133a's inhibitory role in endothelial cell migration. *RCAN1.4* expression was also evaluated in addition. *RCAN1.4* is a critical negative regulator of angiogenesis that is activated by VEGF

stimulation in endothelial cells (Minami et al., 2004). While there was no difference in the RNA expression of this gene in cells transfected with miR-133a-5p, it was evident that HUVECs transfected with miR-133a-3p and stimulated with VEGF at different time points increased the RNA expression of this gene in comparison to the control, indicating that this gene is a key mediator of the inhibitory effect of miR-133a-3p on angiogenesis. Overall, our findings show that aberrant miR-133a-3p expression prevents the migration of endothelial cells by suppressing the RNA production of the pro-angiogenic genes *PLAUR* and *MSN*. *RCAN1.4*, which is encoded as an inhibitor of angiogenesis, is expressed more highly when miR-133a-3p is overexpressed in endothelial cells.

This pathway is crucial for angiogenesis because the remodelling of the extracellular matrix (ECM) brought about by secreted proteases in the region surrounding vessel branching is the only way for endothelial cell migration, tube formation, and the ability of a new vessel sprout to move toward pro-angiogenic signal (Adams and Alitalo, 2007). Therefore, we looked at whether abnormal miR-133a expression in endothelial cells affects the expression of ECM and protease degraders. In both unstimulated and VEGF-stimulated cells, ectopic expression of miR-133a-3p increased the expression of *SPARC, ITGA6*, and *THBS1* to the same extent, indicating that the impact was not reliant on VEGF stimulation. The ectopic expression of miR-133a-3p also increased the expression of ADAMTS1, but only after VEGF stimulation. These genes were not affected by cells transfected with miR-133a-5p, indicating that they are miR-133a-3p-specific. Previous studies have indicated that these genes act as angiogenic inhibitors. Zhang et al. (2012), for instance, showed that *SPARC* inhibits angiogenesis by preventing proliferation and invasion. According to their findings, *SPARC* silencing enhanced the expression of VEGF and angiogenesis whereas *SPARC* overexpression decreased the expression of VEGF (Zhang et al., 2012). Other research has shown that *ADAMTS1* lowers endothelial cell growth in vitro and decreases angiogenesis in vivo. In the work of Xu et al., the researchers used siRNA knockdown to examine the impact of *ADAMTS1* on endothelial cell growth. Their findings demonstrated that *ADAMTS1* knockdown increased endothelial cell

proliferation (Xu et al., 2006). *TIMP3* (tissue inhibitor of metalloproteinases 3) has been shown in several studies to be a powerful inhibitor of angiogenesis. It achieves its anti-angiogenic activity by direct contact with VEGFR2, which in turn prevents endothelial cell proliferation, migration, and tube formation. This research reveals that *TIMP3* reduces downstream signalling and angiogenesis by preventing the binding of VEGF to VEGFR2 (Qi and Anand-Apte, 2015). According to our findings, miR-133a-3p transfected HUVECs increased *TIMP3* expression both at basal levels and in response to VEGF stimulation. Canine endothelial colony-forming cells (ECFCs) were identified and cultivated in a recent work by Liao et al. (2022). Using a lentiviral vector, the expression of *THBS1* in these cells was suppressed. To examine the impact of exosomes on the angiogenic activity of HUVECs, the exosomes released by ECFCs were separated and purified. Their findings demonstrated that ECFC-Exo increased HUVECs proliferation, migration, and tube formation, which was made possible by ECFC-inhibition Exo's of *THBS1* expression. Additionally, they showed that suppressing *THBS1* expression in ECFCs-Exo stimulated PI3K, AKT, and ERK phosphorylation levels in HUVECs, promoting the production of VEGF and bFGF (Liao et al., 2022). Our findings show that increased miR-133a-3p expression in endothelial cells increases the expression of genes encoding angiogenesis-inhibiting proteins, supporting the negative influence that miR-133a-3p has on angiogenesis. This is supported by data from other studies and data from our own research.

Evaluations of gene arrays that take into consideration ECM-CAM, Notch signalling regulators, or cell cycle, as was previously found, revealed that endothelial cells overexpressing miR-133a-3p displayed differential expression of 25 genes. We investigated whether the differential gene expression profile of these 25 genes supported the inhibitory effect on angiogenesis brought on by the overexpression of miR-133a-3p in endothelial cells. The IPA analysis revealed that the following categories have enhanced biological processes: "Cell cycle," "DNA replication, recombination, and repair," and "Cardiovascular system development and function." According to the activation Z-scored prediction, cellular activities such as

"proliferation of endothelial cells," “branching of vasculature," "tubulation of endothelial cells," "entry into S phase," "DNA replication," "cell cycle progression," "synthesis of DNA," and "mitosis" were all suppressed. Our findings on the inhibitory activity of miR-133a-3p in angiogenic cellular processes are supported by the decrease in these cellular activities.

Overall, our study has shown that aberrant miR-133a-3p expression increases the expression of genes that have inhibitory roles in angiogenesis while lowering the expression of genes that have pro-angiogenic activities in primary HUVECs. The research published by Soufi-Zomorrod et al., 2016 and Chen et al., 2018, provide support for our findings. They disagree with the research reported by Zhu et al. in 2021, which characterise miR-133a-3p as having a beneficial regulatory effect in angiogenesis. In their investigation, in order to create exosomes that were enriched in miR-133a-3p, Zhu et al. used mesenchymal stem cells that had been exposed to a lentivirus that overexpressed the macrophage migration inhibitory factor protein. The disagreement regarding the impact of miR-133a-3p on angiogenesis may thus be caused by different exosomal cargo components. As far as we are aware, miR-133a-3p is exclusively expressed in endothelial cells under pathological circumstances and is muscle-specific. Because of transcriptional stimulation of the miR-133a promoter in Li et al., 2016 investigations, we found the influence of direct transfection of miR-133a-3p into endothelial cells. Our experiments supported this finding. With this discovery, we tried to reproduce the circumstances present in the ailing endothelium.

We hypothesise that miR-133a-3p's direct binding to complimentary motifs in the targeted gene's sequence, which is how miR-133a binds to target genes, may be the source of the decrease in gene expression. This was inferred from in silico research that predicted the direct miR-133a-3p binding sites in the 3'UTR of *MSN* (Kinoshita et al., 2012). Additionally, we have demonstrated that miR-133a increases the expression of angiogenesis inhibitors such *THBS1*. A lentiviral vector containing siTHBS1 (THBS1-shRNA) exosomes as opposed to con-shRNA exosomes was utilised to analyse HUVECs angiogenesis, according to a research by Liao et al. (2022). They found that decreasing *THBS1* expression in ECFC-Exo improved the

capacity of HUVECs to proliferate, migrate, and form tubes (Liao et al., 2022). Our results validate the inhibition of angiogenesis that miR-133a-3p has been demonstrated to produce by increasing the expression of the gene that encodes for an angiogenesis inhibitor. However, these findings could point to a side effect brought on by the suppression of a repressor of the increased RNA by miR-133a. Some miR-1 effects have been linked to this method. According to Lin et al (2013) research, miR-1 specifically targets the mRNA that encodes seryl-tRNA synthetase (SARS). In embryos with miR-1 knockdown, SARS expression is elevated. Reduced VEGFaa expression and impaired blood vessel development was caused by either SARS overexpression or miR-1 knockdown. SARS knockdown caused aberrant vessel branching and an increase in VEGFaa expression, research demonstrated that miR-1 enhances angiogenesis by inhibiting SARS and exhibited behaviours that were comparable to those of embryos with VEGFaa overexpression (Lin et al., 2013).

Alternatively, miR-133a may target other areas of the gene apart from the 3'UTR such as the promoter. Place et al. (2008) demonstrated that the expression of genes with complementary promoter sequences is boosted by miR-373 which supports the notion that miRNAs may target promoter sequences and in doing so, regulate the expression of the target genes (Place *et al.,* 2008).

As previously indicated, the 3p strand directly binds and targets the 3'UTR of *MSN*, which accounts for the suppression of RNA levels we see. Bioinformatic analysis utilising databases like miRWalk, miRDB, and Target-Scan was carried out to ascertain if the decrease in gene expression is the consequence of direct miR-133a binding to complementary motifs in the sequence of the target genes. No other genes had any possible binding sites predicted by at least two databases, with the exception of *MSN*, where potential sites were found by miRDB and TargetScan with a prediction score more than 90%. However, it is plausible that miR-133a might suppress by identifying sequences that databases have not yet predicted, gene expression. By attaching to specific areas in the promoters of target genes as well as cytoplasmic target RNAs, for instance, Catalanotto et al. (2016) demonstrate that miRNAs

may contribute to the transcriptional regulation of gene expression in the nucleus (Catalanotto et al., 2016). According to research by Di Mauro et al (2019) Through the traditional mRNA suppression process, which occurs in the cytoplasm, miR-133a controls the expression of certain of its target genes. But the researchers also showed that miR-133a translocate to the nucleus of cardiac cells when the canonical Wnt pathway is turned off. MiR-133a inhibits the transcription of de novo DNA methyltransferase 3B (Dnmt3b) in the nucleus by recognising a complementary region in its promoter (Di Mauro et al., 2019). These findings suggest that miR-133a may inhibit gene expression by means other than targeting the 3'UTR of target genes.

A bioinformatic investigation using Target-Scan revealed a strong prediction for miR-133a-5p to bind the 3'UTR of *CD44*, returning to the conventional mode of miR activity. We cloned the 3'UTR of *CD44* since it is a pro-angiogenic gene that encourages angiogenesis, and in our tests, overexpression of both the -3p and -5p stands inhibits the production of this gene. In order to look into a potential inhibition in the production of firefly luciferase, we successfully cloned a number of segments of the *CD44* 3'UTR and carried out dual luciferase tests. However, luciferase activity was unaffected whether miR-133a-3p or miR-133a-5p were co-transfected with the luciferase reporter construct. It's likely that miR-133a does not target the 3'UTR of *CD44* and that other mechanisms are at work when miR-133a reduces *CD44* expression. In actuality, miR-133a binding to the 3'UTR of *CD44* was predicted to have a prediction score of 21% on the target scan database, which is notably low when compared to binding to a previously described location in the 3'UTR of *MSN*, which exhibited a score of 98%.

In conclusion, abnormal expression of miR-133a in endothelial cells prevents angiogenesis with or without VEGF.

The -3p strand has a higher inhibitory effect than the -5p strand on the morphogenesis, proliferation, and migration of endothelial cell tubes. Key regulators of angiogenesis are encoded by target genes that miR-133a modifies in terms of expression. Our results suggest that miR-133a alteration in diseased endothelial cells, namely the -3p strand, may have important therapeutic ramifications for the management of human illnesses related to angiogenesis. For instance, delivering -3p strand to the diseased endothelium of conditions characterised by excessive angiogenesis may provide patients new therapeutic alternatives. However, this potential would need to be verified using pathological angiogenesis-related pre-clinical animal models.

4.1.1 Conclusion

Both strands of miR-133a inhibit endothelial cell angiogenesis, with the -3p having exerted a more profound effect than -5p. Aberrant expression of miR-133a-3p in primary endothelial cells up-regulate the expression of anti-angiogenic genes and downregulates the expression of pro-angiogenic genes. miR-133a-3p attenuated endothelial cell proliferation. Through reducing the expression of genes encoding cell cycle regulators. miR-133a-3p significantly reduced endothelial cell migration. Our findings indicate that specific delivery of miR-133a-3p mimics to endothelial cells within tumours that are resistant to anti-VEGF treatment or the neo-vasculature of diseased diabetic eyes, might open new therapeutic interventions to treat these patients. Although the potential therapeutic delivery of miR-133a-3p requires validation using animal models of pathological angiogenesis, our results warrant further investigations into this possibility.

References

Adams, R.H. and Alitalo, K. (2007) “Molecular regulation of angiogenesis and lymphangiogenesis,” *Nature Reviews Molecular Cell Biology*, 8(6), pp. 464–478. Available at: https://doi.org/10.1038/nrm2183.

Ahmadi, M. and Rezaie, J. (2020) ‘Tumor cells derived-exosomes as angiogenenic agents: Possible therapeutic implications’, Journal of Translational Medicine, 18(1). doi:10.1186/s12967-020-02426-5.

Andersson, E.R., Sandberg, R. and Lendahl, U. (2011) “Notch signaling: Simplicity in design, versatility in function,” *Development*, 138(17), pp. 3593–3612. Available at: https://doi.org/10.1242/dev.063610.

Aquila, G. *et al.* (2019) “The notch pathway: A novel therapeutic target for cardiovascular diseases?,” *Expert Opinion on Therapeutic Targets*, 23(8), pp. 695–710. Available at: https://doi.org/10.1080/14728222.2019.1641198.

Arany, Z. *et al.* (2008) “HIF-independent regulation of VEGF and angiogenesis by the transcriptional coactivator pgc-1α,” *Nature*, 451(7181), pp. 1008–1012. Available at: https://doi.org/10.1038/nature06613.

Baig, M.U. and Bodle, J. (2022) *Thrombolytic Therapy*, *Baig Mu, Bodle J. (2021). thrombolytic therapy. in: Statpearls [internet]. treasure island (FL): Statpearls Publishing; PP: 1-10.* Available at: http://www.sciepub.com/reference/396697 (Accessed: December 12, 2022).

Bartel, D.P. (2004) “MicroRNAs: genomics, biogenesis, mechanism, and function,” *Cell*, 116(2), pp. 281–297. Available at: https://doi.org/10.1016/s0092-8674(04)00045-5.

Bauer, S.M., Bauer, R.J. and Velazquez, O.C. (2005) “Angiogenesis, Vasculogenesis, and Induction of Healing in Chronic Wounds,” *Vascular and Endovascular Surgery*, 39(4), pp. 293–306. Available at: https://doi.org/10.1177/153857440503900401.

Benedito, R. *et al.* (2009) “The notch ligands *DLL4* and Jagged1 have opposing effects on angiogenesis,” *Cell*, 137(6), pp. 1124–1135. Available at: https://doi.org/10.1016/j.cell.2009.03.025.

Blanco, R. and Gerhardt, H. (2012) “VEGF and notch in tip and stalk cell selection,” *Cold Spring Harbor Perspectives in Medicine*, 3(1). Available at: https://doi.org/10.1101/cshperspect.a006569.

Boštjančič, E. *et al.* (2018) “Down-regulation of Mir-133A/B in patients with myocardial infarction correlates with the presence of ventricular fibrillation,” *Biomedicine & Pharmacotherapy*, 99, pp. 65–71. Available at: https://doi.org/10.1016/j.biopha.2018.01.019.

Broughton, J.P. *et al.* (2016) “Pairing beyond the seed supports MicroRNA targeting specificity,” *Molecular Cell*, 64(2), pp. 320–333. Available at: https://doi.org/10.1016/j.molcel.2016.09.004.

Burri, P.H. and Djonov, V. (2002) “Intussusceptive angiogenesis—the alternative to capillary sprouting,” *Molecular Aspects of Medicine*, 23(6), pp. 1–27. Available at: https://doi.org/10.1016/s0098-2997(02)00096-1.

Cao, G. *et al.* (2006) “Involvement of endothelial *CD44* during in vivo angiogenesis,” *The American Journal of Pathology*, 169(1), pp. 325–336. Available at: https://doi.org/10.2353/ajpath.2006.060206.

Caporali, A. and Emanueli, C. (2011) “MicroRNA-503 and the extended MicroRNA-16 family in angiogenesis,” *Trends in Cardiovascular Medicine*, 21(6), pp. 162–166. Available at: https://doi.org/10.1016/j.tcm.2012.05.003.

Caporali, A. *et al.* (2011) “Deregulation of microrna-503 contributes to diabetes mellitus–induced impairment of endothelial function and reparative angiogenesis after limb ischemia,” *Circulation*, 123(3), pp. 282–291. Available at: https://doi.org/10.1161/circulationaha.110.952325.

Carmeliet, P. (2005) “Angiogenesis in life, disease and medicine,” *Nature*, 438(7070), pp. 932–936. Available at: https://doi.org/10.1038/nature04478.

Carmeliet, P. and Jain, R.K. (2011) “Molecular mechanisms and clinical applications of angiogenesis,” *Nature*, 473(7347), pp. 298–307. Available at: https://doi.org/10.1038/nature10144.

Carpentier, G. *et al.* (2020) “Angiogenesis analyzer for imagej — a comparative morphometric analysis of ‘Endothelial Tube Formation Assay’ and ‘Fibrin bead assay,’” *Scientific Reports*, 10(1). Available at: https://doi.org/10.1038/s41598-020-67289-8.

Catalanotto, C., Cogoni, C. and Zardo, G. (2016) “MicroRNA in control of gene expression: An overview of nuclear functions,” *International Journal of Molecular Sciences*, 17(10), p. 1712. Available at: https://doi.org/10.3390/ijms17101712.

Chamorro-Jorganes, A. *et al.* (2011) “Microrna-16 and MicroRNA-424 regulate cell-autonomous angiogenic functions in endothelial cells via targeting vascular endothelial growth factor receptor-2 and fibroblast growth factor receptor-1,” *Arteriosclerosis, Thrombosis, and Vascular Biology*, 31(11), pp. 2595–2606. Available at: https://doi.org/10.1161/atvbaha.111.236521.

Chen, J.-F. *et al.* (2006) “The role of microrna-1 and microrna-133 in skeletal muscle proliferation and differentiation,” *Nature Genetics*, 38(2), pp. 228–233. Available at: https://doi.org/10.1038/ng1725.

Chen, L. *et al.* (2018) “MicroRNA-133A impairs perfusion recovery after hindlimb ischemia in diabetic mice,” *Bioscience Reports*, 38(4). Available at: https://doi.org/10.1042/bsr20180346.

Chen, L. *et al.* (2020) “The role of *CD44* in pathological angiogenesis,” *The FASEB Journal*, 34(10), pp. 13125–13139. Available at: https://doi.org/10.1096/fj.202000380rr.

Cheung, N., Mitchell, P. and Wong, T.Y. (2010) “Diabetic retinopathy,” *The Lancet*, 376(9735), pp. 124–136. Available at: https://doi.org/10.1016/s0140-6736(09)62124-3.

Dang, L.T., Lawson, N.D. and Fish, J.E. (2013) “MicroRNA control of vascular endothelial growth factor signaling output during vascular development,” *Arteriosclerosis, Thrombosis, and Vascular Biology*, 33(2), pp. 193–200. Available at: https://doi.org/10.1161/atvbaha.112.300142.

Daugaard, I. and Hansen, T.B. (2017) “Biogenesis and function of ago-associated RNAS,” *Trends in Genetics*, 33(3), pp. 208–219. Available at: https://doi.org/10.1016/j.tig.2017.01.003.

Davis, G.E. and Senger, D.R. (2005) “Endothelial extracellular matrix,” *Circulation Research*, 97(11), pp. 1093–1107. Available at: https://doi.org/10.1161/01.res.0000191547.64391.e3.

de Rie, D. *et al.* (2017) “An integrated expression atlas of mirnas and their promoters in human and mouse,” *Nature Biotechnology*, 35(9), pp. 872–878. Available at: https://doi.org/10.1038/nbt.3947.

De Smet, F. *et al.* (2009) “Mechanisms of Vessel Branching,” *Arteriosclerosis, Thrombosis, and Vascular Biology*, 29(5), pp. 639–649. Available at: https://doi.org/10.1161/atvbaha.109.185165.

Degryse, B. *et al.* (2017) “Moesin and Merlin regulate urokinase receptor-dependent endothelial cell migration, adhesion and angiogenesis,” *The International Journal of Biochemistry & Cell Biology*, 88, pp. 14–22. Available at: https://doi.org/10.1016/j.biocel.2017.04.012.

del Zoppo, G.J. and Mabuchi, T. (2003) “Cerebral Microvessel Responses to Focal Ischemia,” *Journal of Cerebral Blood Flow & Metabolism*, 23(8), pp. 879–894. Available at: https://doi.org/10.1097/01.wcb.0000078322.96027.78.

Di Mauro, V. *et al.* (2019) “Wnt signalling mediates Mir-133a nuclear re-localization for the transcriptional control of dnmt3b in cardiac cells,” *Scientific Reports*, 9(1). Available at: https://doi.org/10.1038/s41598-019-45818-4.

Ding, L. *et al.* (2020) “The roles of cyclin-dependent kinases in cell-cycle progression and therapeutic strategies in human breast cancer,” *International Journal of Molecular Sciences*, 21(6), p. 1960. Available at: https://doi.org/10.3390/ijms21061960.

DiPietro, L.A. (2016) “Angiogenesis and wound repair: when enough is enough,” *Journal of Leukocyte Biology*, 100(5), pp. 979–984. Available at: https://doi.org/10.1189/jlb.4mr0316-102r.

Djonov, V., Baum, O. and Burri, P.H. (2003) “Vascular remodeling by intussusceptive angiogenesis,” *Cell and Tissue Research*, 314(1), pp. 107–117. Available at: https://doi.org/10.1007/s00441-003-0784-3.

Duh, E.J., Sun, J.K. and Stitt, A.W. (2017) “Diabetic retinopathy: current understanding, mechanisms, and treatment strategies,” *JCI Insight*, 2(14). Available at: https://doi.org/10.1172/jci.insight.93751.

Duval, M. *et al.* (2007) “Src-mediated phosphorylation of hsp90 in response to vascular endothelial growth factor (VEGF) is required for VEGF receptor-2 signaling to endothelial no synthase,” *Molecular Biology of the Cell*, 18(11), pp. 4659–4668. Available at: https://doi.org/10.1091/mbc.e07-05-0467.

Ecker, D.M., Jones, S.D. and Levine, H.L. (2015) “The therapeutic monoclonal antibody market,” *mAbs*, 7(1), pp. 9–14. Available at: https://doi.org/10.4161/19420862.2015.989042.

Egginton, S. and Bicknell, R. (2011) “Advances in the Cellular and Molecular Biology of Angiogenesis,” *Biochemical Society Transactions*, 39(6), pp. 1551–1555. Available at: https://doi.org/10.1042/bst20110749.

Fantin, A. *et al.* (2010) “Tissue macrophages act as cellular chaperones for vascular anastomosis downstream of VEGF-mediated endothelial tip cell induction,” *Blood*, 116(5), pp. 829–840. Available at: https://doi.org/10.1182/blood-2009-12-257832.

Farber, A. and Eberhardt, R.T. (2016) “The Current State of Critical Limb Ischemia,” *JAMA Surgery*, 151(11), p. 1070. Available at: https://doi.org/10.1001/jamasurg.2016.2018.

Farghaly, T.A., Al-Hasani, W.A. and Abdulwahab, H.G. (2021) “An updated patent review of VEGFR-2 inhibitors (2017-present),” *Expert Opinion on Therapeutic Patents*, 31(11), pp. 989–1007. Available at: https://doi.org/10.1080/13543776.2021.1935872.

Ferrara, N. (2004) “Vascular Endothelial Growth Factor: Basic Science and Clinical Progress,” *Endocrine Reviews*, 25(4), pp. 581–611. Available at: https://doi.org/10.1210/er.2003-0027.

Ferrara, N. (2016) “Commentary on ‘Humanization of an anti-vegf monoclonal antibody for the therapy of solid tumors and other disorders,’” *Cancer Research*, 76(17), pp. 4913–4915. Available at: https://doi.org/10.1158/0008-5472.can-16-1973.

Ferrara, N. *et al.* (2004) “Discovery and development of bevacizumab, an anti-VEGF antibody for treating cancer,” *Nature Reviews Drug Discovery*, 3(5), pp. 391–400. Available at: https://doi.org/10.1038/nrd1381.

Ferrara, N., Gerber, H.-P. and LeCouter, J. (2003) “The biology of VEGF and its receptors,” *Nature Medicine*, 9(6), pp. 669–676. Available at: https://doi.org/10.1038/nm0603-669.

Fish, J.E. *et al.* (2008) “Mir-126 regulates angiogenic signaling and Vascular integrity,” *Developmental Cell*, 15(2), pp. 272–284. Available at: https://doi.org/10.1016/j.devcel.2008.07.008.

Fu, G. *et al.* (2013) “MicroRNAs in human placental development and pregnancy complications,” *International Journal of Molecular Sciences*, 14(3), pp. 5519–5544. Available at: https://doi.org/10.3390/ijms14035519.

Ganta, V.C. *et al.* (2019) “Antiangiogenic VEGF ₁₆₅ B regulates macrophage polarization via S100A8/S100A9 in peripheral artery disease,” *Circulation*, 139(2), pp. 226–242. Available at: https://doi.org/10.1161/circulationaha.118.034165.

Gao, X. *et al.* (2019) “Cyclin-dependent kinase 1 disruption inhibits angiogenesis by inducing cell cycle arrest and apoptosis,” *Experimental and Therapeutic Medicine* [Preprint]. Available at: https://doi.org/10.3892/etm.2019.7883.

Garcia, J. *et al.* (2020) “Bevacizumab (Avastin®) in cancer treatment: A review of 15 years of clinical experience and future outlook,” *Cancer Treatment Reviews*, 86, p. 102017. Available at: https://doi.org/10.1016/j.ctrv.2020.102017.

Garcia, R. *et al.* (2019) “VEGF-A plasma levels are associated with microvascular obstruction in patients with st-segment elevation myocardial infarction,” *International Journal of Cardiology*, 291, pp. 19–24. Available at: https://doi.org/10.1016/j.ijcard.2019.02.067.

Giuliari, G., Guel, D. and Gonzalez, V. (2009) “Pegaptanib sodium for the treatment of proliferative diabetic retinopathy and diabetic macular edema,” *Current Diabetes Reviews*, 5(1), pp. 33–38. Available at: https://doi.org/10.2174/157339909787314158.

Goldie, L.C., Nix, M.K. and Hirschi, K.K. (2008) “Embryonic vasculogenesis and hematopoietic specification,” *Organogenesis*, 4(4), pp. 257–263. Available at: https://doi.org/10.4161/org.4.4.7416.

Gotink, K.J. and Verheul, H.M. (2009) “Anti-angiogenic tyrosine kinase inhibitors: What is their mechanism of action?,” *Angiogenesis*, 13(1), pp. 1–14. Available at: https://doi.org/10.1007/s10456-009-9160-6.

Greaves, N.S. *et al.* (2013) “Current understanding of molecular and cellular mechanisms in fibroplasia and angiogenesis during acute wound healing,” *Journal of Dermatological Science*, 72(3), pp. 206–217. Available at: https://doi.org/10.1016/j.jdermsci.2013.07.008.

Griffiths, C.E.M. and Barker, J.N.W.N. (2007) “Pathogenesis and clinical features of psoriasis,” *The Lancet*, 370(9583), pp. 263–271. Available at: https://doi.org/10.1016/s0140-6736(07)61128-3.

Guerard, S. and Pouliot, R. (2014) “The Role of Angiogenesis in the Pathogenesis of Psoriasis: Mechanisms and Clinical Implications,” *Journal of Clinical & Experimental Dermatology Research*, 4(3). Available at: https://doi.org/10.4172/2155-9554.s2-007.

Ha, M. and Kim, V.N. (2014) “Regulation of microrna biogenesis,” *Nature Reviews Molecular Cell Biology*, 15(8), pp. 509–524. Available at: https://doi.org/10.1038/nrm3838.

Hajar, R. (2017) “Risk factors for coronary artery disease: Historical perspectives,” *Heart Views*, 18(3), p. 109. Available at: https://doi.org/10.4103/heartviews.heartviews_106_17.

Han, J. *et al.* (2004) “The drosha-DGCR8 complex in primary microrna processing,” *Genes & Development*, 18(24), pp. 3016–3027. Available at: https://doi.org/10.1101/gad.1262504.

Haringman, J.J. *et al.* (2005) “Synovial tissue macrophages: a sensitive biomarker for response to treatment in patients with rheumatoid arthritis,” *Annals of the Rheumatic Diseases*, 64(6), pp. 834–838. Available at: https://doi.org/10.1136/ard.2004.029751.

Harper, S.J. and Bates, D.O. (2008) “VEGF-A splicing: The key to anti-angiogenic therapeutics?,” *Nature Reviews Cancer*, 8(11), pp. 880–887. Available at: https://doi.org/10.1038/nrc2505.

Harris, S. *et al.* (2012) “Do anti-angiogenic VEGF (VEGFXXXB) isoforms exist? A cautionary tale,” *PLoS ONE*, 7(5). Available at: https://doi.org/10.1371/journal.pone.0035231.

Hayes, J., Peruzzi, P.P. and Lawler, S. (2014) “MicroRNAs in cancer: Biomarkers, functions and therapy,” *Trends in Molecular Medicine*, 20(8), pp. 460–469. Available at: https://doi.org/10.1016/j.molmed.2014.06.005.

He, N. *et al.* (2020) “Exosomes: Cell-Free Therapy for Cardiovascular Diseases,” *Journal of Cardiovascular Translational Research*, 13(5), pp. 713–721. Available at: https://doi.org/10.1007/s12265-020-09966-7.

Henderson, A.M. *et al.* (2001) “The basic helix-loop-helix transcription factor HESR1 regulates endothelial cell tube formation,” *Journal of Biological Chemistry*, 276(9), pp. 6169–6176. Available at: https://doi.org/10.1074/jbc.m008506200.

Henno, A. *et al.* (2010) “Histological and transcriptional study of angiogenesis and lymphangiogenesis in uninvolved skin, acute pinpoint lesions and established psoriasis plaques: An approach of vascular development chronology in psoriasis,” *Journal of Dermatological Science*, 57(3), pp. 162–169. Available at: https://doi.org/10.1016/j.jdermsci.2009.12.006.

Herbert, S.P. and Stainier, D.Y.R. (2011) “Molecular control of endothelial cell behaviour during blood vessel morphogenesis,” *Nature Reviews Molecular Cell Biology*, 12(9), pp. 551–564. Available at: https://doi.org/10.1038/nrm3176.

Hlushchuk, R. *et al.* (2008) “Tumor Recovery by Angiogenic Switch from Sprouting to Intussusceptive Angiogenesis after Treatment with PTK787/ZK222584 or Ionizing

Radiation," *The American Journal of Pathology*, 173(4), pp. 1173–1185. Available at: https://doi.org/10.2353/ajpath.2008.071131.

Holmes, K. *et al.* (2007) "Vascular endothelial growth factor receptor-2: Structure, function, intracellular signalling and therapeutic inhibition," *Cellular Signalling*, 19(10), pp. 2003–2012. Available at: https://doi.org/10.1016/j.cellsig.2007.05.013.

Horvitz, H.R. and Sulston, J.E. (1980) "Isolation and genetic characterization of cell-lineage mutants of the nematode Caenorhabditis elegans," *Genetics*, 96(2), pp. 435–454. Available at: https://doi.org/10.1093/genetics/96.2.435.

Huang, W. (2017) "MicroRNAs: Biomarkers, diagnostics, and therapeutics," *Bioinformatics in MicroRNA Research*, pp. 57–67. Available at: https://doi.org/10.1007/978-1-4939-7046-9_4.

Hurwitz, H. *et al.* (2004) "Bevacizumab plus irinotecan, Fluorouracil, and Leucovorin for metastatic colorectal cancer," *New England Journal of Medicine*, 350(23), pp. 2335–2342. Available at: https://doi.org/10.1056/nejmoa032691.

Iadecola, C. (2013) "The Pathobiology of Vascular Dementia," *Neuron*, 80(4), pp. 844–866. Available at: https://doi.org/10.1016/j.neuron.2013.10.008.

Iruela-Arispe, M.L. and Davis, G.E. (2009) "Cellular and Molecular Mechanisms of Vascular Lumen Formation," *Developmental Cell*, 16(2), pp. 222–231. Available at: https://doi.org/10.1016/j.devcel.2009.01.013.

Ji, Y. *et al.* (2016) "Evaluation of in vivo antitumor effects of low-frequency ultrasound-mediated Mirna-133a Microbubble delivery in breast cancer," *Cancer Medicine*, 5(9), pp. 2534–2543. Available at: https://doi.org/10.1002/cam4.840.

Jiang, B.H. and Liu, L.Z. (2009) "PI3K/PTEN signaling in angiogenesis and tumorigenesis," *Advances in Cancer Research*, pp. 19–65. Available at: https://doi.org/10.1016/s0065-230x(09)02002-8.

Jin, F. *et al.* (2019) "Impairment of hypoxia-induced angiogenesis by LDL involves a HIF-centered signaling network linking inflammatory tnfα and angiogenic VEGF," *Aging*, 11(2), pp. 328–349. Available at: https://doi.org/10.18632/aging.101726.

Johnson, K.E. and Wilgus, T.A. (2014) “Vascular Endothelial Growth Factor and angiogenesis in the regulation of cutaneous wound repair,” *Advances in Wound Care*, 3(10), pp. 647–661. Available at: https://doi.org/10.1089/wound.2013.0517.

Kamba, T. and McDonald, D.M. (2007) “Mechanisms of adverse effects of anti-VEGF therapy for cancer,” *British Journal of Cancer*, 96(12), pp. 1788–1795. Available at: https://doi.org/10.1038/sj.bjc.6603813.

Kamei, M. *et al.* (2006) “Endothelial tubes assemble from intracellular vacuoles in vivo,” *Nature*, 442(7101), pp. 453–456. Available at: https://doi.org/10.1038/nature04923.

Kangsamaksin, T., Tattersall, I.W. and Kitajewski, J. (2014) “Notch functions in developmental and tumour angiogenesis by diverse mechanisms1,” *Biochemical Society Transactions*, 42(6), pp. 1563–1568. Available at: https://doi.org/10.1042/bst20140233.

Kazerounian, S. and Lawler, J. (2017) “Integration of pro- and anti-angiogenic signals by endothelial cells,” *Journal of Cell Communication and Signaling*, 12(1), pp. 171–179. Available at: https://doi.org/10.1007/s12079-017-0433-3.

Keck, P.J. *et al.* (1989) “Vascular permeability factor, an endothelial cell mitogen related to PDGF,” *Science*, 246(4935), pp. 1309–1312. Available at: https://doi.org/10.1126/science.2479987.

Kelly-Goss, M.R. *et al.* (2014) “Targeting Pericytes for Angiogenic Therapies,” *Microcirculation*, 21(4), pp. 345–357. Available at: https://doi.org/10.1111/micc.12107.

Kim, K.J. *et al.* (1993) “Inhibition of vascular endothelial growth factor-induced angiogenesis suppresses tumour growth in vivo,” *Nature*, 362(6423), pp. 841–844. Available at: https://doi.org/10.1038/362841a0.

Kim, Y.-K. and Kim, V.N. (2007) “Processing of intronic micrornas,” *The EMBO Journal*, 26(3), pp. 775–783. Available at: https://doi.org/10.1038/sj.emboj.7601512.

Kinoshita, T. *et al.* (2012) “Tumor suppressive microrna-133a regulates novel targets: Moesin contributes to cancer cell proliferation and invasion in head and neck squamous cell

carcinoma," *Biochemical and Biophysical Research Communications*, 418(2), pp. 378–383. Available at: https://doi.org/10.1016/j.bbrc.2012.01.030.

Koch, S. and Claesson-Welsh, L. (2012) "Signal transduction by vascular endothelial growth factor receptors," *Cold Spring Harbor Perspectives in Medicine*, 2(7). Available at: https://doi.org/10.1101/cshperspect.a006502.

Kong, B. *et al.* (2021) "MicroRNA-133A-3p inhibits cell proliferation, migration and invasion in colorectal cancer by targeting AQP1," *Oncology Letters*, 22(3). Available at: https://doi.org/10.3892/ol.2021.12910.

Kong, D.-H. *et al.* (2017) "A review of anti-angiogenic targets for monoclonal antibody cancer therapy," *International Journal of Molecular Sciences*, 18(8), p. 1786. Available at: https://doi.org/10.3390/ijms18081786.

Korhonen, A. *et al.* (2021) "Proliferative diabetic retinopathy transcriptomes reveal angiogenesis, anti-angiogenic therapy escape mechanisms, fibrosis and lymphatic involvement," *Scientific Reports*, 11(1). Available at: https://doi.org/10.1038/s41598-021-97970-5.

KOURLAS, H. and ABRAMS, P. (2007) "Ranibizumab for the treatment of neovascular age-related Macular degeneration: A review," *Clinical Therapeutics*, 29(9), pp. 1850–1861. Available at: https://doi.org/10.1016/j.clinthera.2007.09.008.

KOURLAS, H. and ABRAMS, P. (2007) "Ranibizumab for the treatment of neovascular age-related macular degeneration: A review," *Clinical Therapeutics*, 29(9), pp. 1850–1861. Available at: https://doi.org/10.1016/j.clinthera.2007.09.008.

Kumar, P. *et al.* (2015) "Role of angiogenesis and angiogenic factors in acute and chronic wound healing," *Plastic and Aesthetic Research*, 2(5), p. 243. Available at: https://doi.org/10.4103/2347-9264.165438.

Kurusamy, S. A novel selective inhibitor for plasma membrane calcium ATPase 4 improves VEGF-mediated angiogenesis. (2017) PhD Thesis. University of Wolverhampton.

Kuwabara, Y. *et al.* (2011) “Increased microrna-1 and microrna-133a levels in serum of patients with cardiovascular disease indicate myocardial damage,” *Circulation: Cardiovascular Genetics*, 4(4), pp. 446–454. Available at: https://doi.org/10.1161/circgenetics.110.958975.

Lamalice, L., Le Boeuf, F. and Huot, J. (2007) “Endothelial cell migration during angiogenesis,” *Circulation Research*, 100(6), pp. 782–794. Available at: https://doi.org/10.1161/01.res.0000259593.07661.1e.

Larsson, E. *et al.* (2009) “Discovery of microvascular mirnas using public gene expression data: Mir-145 is expressed in pericytes and is a regulator of FLI1,” *Genome Medicine*, 1(11), p. 108. Available at: https://doi.org/10.1186/gm108.

Lee, R.C., Feinbaum, R.L. and Ambros, V. (1993) “The C. elegans heterochronic gene lin-4 encodes small RNAS with antisense complementarity to lin-14,” *Cell*, 75(5), pp. 843–854. Available at: https://doi.org/10.1016/0092-8674(93)90529-y.

Lee, S.J. *et al.* (2017) “Phase I trial and pharmacokinetic study of tanibirumab, a fully human monoclonal antibody to vascular endothelial growth factor receptor 2, in patients with refractory solid tumors,” *Investigational New Drugs*, 35(6), pp. 782–790. Available at: https://doi.org/10.1007/s10637-017-0463-y.

Lee, Y. *et al.* (2004) “MicroRNA genes are transcribed by RNA polymerase II,” *The EMBO Journal*, 23(20), pp. 4051–4060. Available at: https://doi.org/10.1038/sj.emboj.7600385.

Leong, K.G. *et al.* (2002) “Activated *NOTCH4* inhibits angiogenesis: Role of β1-Integrin Activation,” *Molecular and Cellular Biology*, 22(8), pp. 2830–2841. Available at: https://doi.org/10.1128/mcb.22.8.2830-2841.2002.

Leslie, J.D. *et al.* (2007) “Endothelial signalling by the notch ligand delta-like 4 restricts angiogenesis,” *Development*, 134(5), pp. 839–844. Available at: https://doi.org/10.1242/dev.003244.

Li, D. *et al.* (2016) “Dual blockade of vascular endothelial growth factor (VEGF) and basic fibroblast growth factor (FGF-2) exhibits potent anti-angiogenic effects,” *Cancer*

Letters, 377(2), pp. 164–173. Available at: https://doi.org/10.1016/j.canlet.2016.04.036.

Li, P. *et al.* (2016) “Inhibition of aberrant microrna-133a expression in endothelial cells by statin prevents endothelial dysfunction by targeting GTP cyclohydrolase 1 in vivo,” *Circulation*, 134(22), pp. 1752–1765. Available at: https://doi.org/10.1161/circulationaha.116.017949.

Li, Y. *et al.* (2009) “MicroRNA-221 regulates high glucose-induced endothelial dysfunction,” *Biochemical and Biophysical Research Communications*, 381(1), pp. 81–83. Available at: https://doi.org/10.1016/j.bbrc.2009.02.013.

Li, Y. *et al.* (2018) “MicroRNA profiling of diabetic atherosclerosis in a rat model,” *European Journal of Medical Research*, 23(1). Available at: https://doi.org/10.1186/s40001-018-0354-5.

Liao, F. *et al.* (2022) “ECFC-derived exosomal *THBS1* mediates angiogenesis and osteogenesis in distraction osteogenesis via the PI3K/AKT/erk pathway,” *Journal of Orthopaedic Translation*, 37, pp. 12–22. Available at: https://doi.org/10.1016/j.jot.2022.08.004.

Lin, C.-Y. *et al.* (2013) “Mir-1 and Mir-206 target different genes to have opposing roles during angiogenesis in zebrafish embryos,” *Nature Communications*, 4(1). Available at: https://doi.org/10.1038/ncomms3829.

Lohela, M. *et al.* (2009) “VEGFs and receptors involved in angiogenesis versus lymphangiogenesis,” *Current Opinion in Cell Biology*, 21(2), pp. 154–165. Available at: https://doi.org/10.1016/j.ceb.2008.12.012.

Lugano, R., Ramachandran, M. and Dimberg, A. (2019) “Tumor angiogenesis: Causes, consequences, challenges and opportunities,” *Cellular and Molecular Life Sciences*, 77(9), pp. 1745–1770. Available at: https://doi.org/10.1007/s00018-019-03351-7.

Ma, H. *et al.* (2018) “Modulation of apoptosis-related microRNAs following myocardial infarction in fat-1 transgenic mice vs wild-type mice,” *Journal of Cellular and Molecular Medicine*, 22(11), pp. 5698–5707. Available at: https://doi.org/10.1111/jcmm.13846.

Mack, J.J. and Iruela-Arispe, M.L. (2018) “Notch regulation of the Endothelial Cell Phenotype,” *Current Opinion in Hematology*, 25(3), pp. 212–218. Available at: https://doi.org/10.1097/moh.0000000000000425.

Makanya, A.N., Hlushchuk, R. and Djonov, V.G. (2009) “Intussusceptive angiogenesis and its role in vascular morphogenesis, patterning, and remodeling,” *Angiogenesis*, 12(2), pp. 113–123. Available at: https://doi.org/10.1007/s10456-009-9129-5.

Malecic, N. and Young, H.S. (2017) “Excessive angiogenesis associated with psoriasis as a cause for cardiovascular ischaemia,” *Experimental Dermatology*, 26(4), pp. 299–304. Available at: https://doi.org/10.1111/exd.13310.

Malumbres, M. (2014) “Cyclin-dependent kinases,” *Genome Biology*, 15(6), p. 122. Available at: https://doi.org/10.1186/gb4184.

Marrelli, A. *et al.* (2011) “Angiogenesis in rheumatoid arthritis: A disease specific process or a common response to chronic inflammation?,” *Autoimmunity Reviews*, 10(10), pp. 595–598. Available at: https://doi.org/10.1016/j.autrev.2011.04.020.

Mazzone, M. *et al.* (2009) “Heterozygous Deficiency of PHD2 Restores Tumor Oxygenation and Inhibits Metastasis via Endothelial Normalization,” *Cell*, 136(5), pp. 839–851. Available at: https://doi.org/10.1016/j.cell.2009.01.020.

Meybosch, S. *et al.* (2019) “Epidermal growth factor and its influencing variables in healthy children and adults,” *PLOS ONE*, 14(1), p. e0211212. Available at: https://doi.org/10.1371/journal.pone.0211212.

Minami, T. *et al.* (2004) “Vascular endothelial growth factor- and thrombin-induced termination factor, down syndrome critical region-1, attenuates endothelial cell proliferation and angiogenesis,” *Journal of Biological Chemistry*, 279(48), pp. 50537–50554. Available at: https://doi.org/10.1074/jbc.m406454200.

Mukherjee, A. *et al.* (2020) “Recent advancements of nanomedicine towards antiangiogenic therapy in cancer,” *International Journal of Molecular Sciences*, 21(2), p. 455. Available at: https://doi.org/10.3390/ijms21020455.

Naito, H., Iba, T. and Takakura, N. (2020) “Mechanisms of New Blood-vessel formation and proliferative heterogeneity of endothelial cells,” *International Immunology*, 32(5), pp. 295–305. Available at: https://doi.org/10.1093/intimm/dxaa008.

Nicoli, S. *et al.* (2010) “MicroRNA-mediated integration of haemodynamics and VEGF signalling during angiogenesis,” *Nature*, 464(7292), pp. 1196–1200. Available at: https://doi.org/10.1038/nature08889.

Nishiyama, K. *et al.* (2005) “*ID1* gene transfer confers angiogenic property on fully differentiated endothelial cells and contributes to therapeutic angiogenesis,” *Circulation*, 112(18), pp. 2840–2850. Available at: https://doi.org/10.1161/circulationaha.104.516898.

O'Brien, J. *et al.* (2018) “Overview of microrna biogenesis, mechanisms of actions, and circulation,” *Frontiers in Endocrinology*, 9. Available at: https://doi.org/10.3389/fendo.2018.00402.

Ohanian, M. *et al.* (2013) “A heterozygous variant in the human cardiac Mir-133 gene, MIR133A2, alters MIRNA duplex processing and Strand Abundance,” *BMC Genetics*, 14(1). Available at: https://doi.org/10.1186/1471-2156-14-18.

Ohr, M. and Kaiser, P.K. (2012) “Aflibercept in wet age-related macular degeneration: A perspective review,” *Therapeutic Advances in Chronic Disease*, 3(4), pp. 153–161. Available at: https://doi.org/10.1177/2040622312446007.

Okada, C. *et al.* (2009) “A high-resolution structure of the pre-microrna nuclear export machinery,” *Science*, 326(5957), pp. 1275–1279. Available at: https://doi.org/10.1126/science.1178705.

Olsson, A.-K. *et al.* (2006) “VEGF receptor signalling ? in control of vascular function,” *Nature Reviews Molecular Cell Biology*, 7(5), pp. 359–371. Available at: https://doi.org/10.1038/nrm1911.

Otto, T. and Sicinski, P. (2017) “Cell cycle proteins as promising targets in cancer therapy,” *Nature Reviews Cancer*, 17(2), pp. 93–115. Available at: https://doi.org/10.1038/nrc.2016.138.

Peach, C. *et al.* (2018) “Molecular pharmacology of VEGF-A isoforms: Binding and signalling at VEGFR2,” *International Journal of Molecular Sciences*, 19(4), p. 1264. Available at: https://doi.org/10.3390/ijms19041264.

Phng, L.-K. and Gerhardt, H. (2009) “Angiogenesis: A team effort coordinated by notch,” *Developmental Cell*, 16(2), pp. 196–208. Available at: https://doi.org/10.1016/j.devcel.2009.01.015.

Pieramici, D.J. and Rabena, M.D. (2008) “Anti-VEGF therapy: Comparison of current and future agents,” *Eye*, 22(10), pp. 1330–1336. Available at: https://doi.org/10.1038/eye.2008.88.

Place, R.F. *et al.* (2008) “MicroRNA-373 induces expression of genes with complementary promoter sequences,” *Proceedings of the National Academy of Sciences*, 105(5), pp. 1608–1613. Available at: https://doi.org/10.1073/pnas.0707594105.

Poliseno, L. *et al.* (2006) “MicroRNAs modulate the angiogenic properties of huvecs,” *Blood*, 108(9), pp. 3068–3071. Available at: https://doi.org/10.1182/blood-2006-01-012369.

Poole, R.M. and Vaidya, A. (2014) “Ramucirumab: First global approval,” *Drugs*, 74(9), pp. 1047–1058. Available at: https://doi.org/10.1007/s40265-014-0244-2.

Potente, M., Gerhardt, H. and Carmeliet, P. (2011) “Basic and therapeutic aspects of angiogenesis,” *Cell*, 146(6), pp. 873–887. Available at: https://doi.org/10.1016/j.cell.2011.08.039.

Qi, J.H. *et al.* (2013) “Tissue inhibitor of metalloproteinases-3 peptides inhibit angiogenesis and choroidal neovascularization in mice,” *PLoS ONE*, 8(3). Available at: https://doi.org/10.1371/journal.pone.0055667.

Ralapanawa, U. and Sivakanesan, R. (2021) “Epidemiology and the Magnitude of Coronary Artery Disease and Acute Coronary Syndrome: A Narrative Review,” *Journal of Epidemiology and Global Health*, 11(2), p. 169. Available at: https://doi.org/10.2991/jegh.k.201217.001.

Reichholf, B. *et al.* (2019) “Time-resolved small RNA sequencing unravels the molecular principles of MicroRNA homeostasis,” *Molecular Cell*, 75(4). Available at: https://doi.org/10.1016/j.molcel.2019.06.018.

Ribatti, D. (2019) “The discovery of the fundamental role of VEGF in the development of the vascular system,” *Mechanisms of Development*, 160, p. 103579. Available at: https://doi.org/10.1016/j.mod.2019.103579.

Ribatti, D. and Crivellato, E. (2012) “‘Sprouting angiogenesis’, a reappraisal,” *Developmental Biology*, 372(2), pp. 157–165. Available at: https://doi.org/10.1016/j.ydbio.2012.09.018.

Rosano, S. *et al.* (2020) “A regulatory microRNA network controls endothelial cell phenotypic switch during sprouting angiogenesis,” *eLife*, 9. Available at: https://doi.org/10.7554/elife.48095.

Ruby, J.G., Jan, C.H. and Bartel, D.P. (2007) “Intronic microrna precursors that bypass Drosha Processing,” *Nature*, 448(7149), pp. 83–86. Available at: https://doi.org/10.1038/nature05983.

Saetan, N. *et al.* (2013) “Relationship of plasma and synovial fluid vascular endothelial growth factor with radiographic severity in primary knee osteoarthritis,” *International Orthopaedics*, 38(5), pp. 1099–1104. Available at: https://doi.org/10.1007/s00264-013-2192-y.

Schafer, K.A. (1998) “The cell cycle: A Review,” *Veterinary Pathology*, 35(6), pp. 461–478. Available at: https://doi.org/10.1177/030098589803500601.

Seghezzi, G. *et al.* (1998) “Fibroblast growth factor-2 (FGF-2) induces vascular endothelial growth factor (VEGF) expression in the endothelial cells of forming capillaries: An autocrine mechanism contributing to angiogenesis,” *Journal of Cell Biology*, 141(7), pp. 1659–1673. Available at: https://doi.org/10.1083/jcb.141.7.1659.

Selvin, E. and Erlinger, T.P. (2004) “Prevalence of and Risk Factors for Peripheral Arterial Disease in the United States,” *Circulation*, 110(6), pp. 738–743. Available at: https://doi.org/10.1161/01.cir.0000137913.26087.f0.

Shaik, F. *et al.* (2020) “Structural basis for vascular endothelial growth factor receptor activation and implications for disease therapy,” *Biomolecules*, 10(12), p. 1673. Available at: https://doi.org/10.3390/biom10121673.

Shen, W.Y. *et al.* (1998) “Expression of cell adhesion molecules and vascular endothelial growth factor in experimental choroidal neovascularisation in the rat,” *British Journal of Ophthalmology*, 82(9), pp. 1063–1071. Available at: https://doi.org/10.1136/bjo.82.9.1063.

Shi, L. *et al.* (2019) “Effect of microrna-133a-3p/matrix metalloproteinase-9 axis on the growth of atherosclerotic vascular smooth muscle cells,” *Experimental and Therapeutic Medicine* [Preprint]. Available at: https://doi.org/10.3892/etm.2019.8070.

Shibuya, M. and Claesson-Welsh, L. (2006) “Signal transduction by VEGF receptors in regulation of angiogenesis and lymphangiogenesis,” *Experimental Cell Research*, 312(5), pp. 549–560. Available at: https://doi.org/10.1016/j.yexcr.2005.11.012.

Shih, T. and Lindley, C. (2006) “Bevacizumab: An angiogenesis inhibitor for the treatment of solid malignancies,” *Clinical Therapeutics*, 28(11), pp. 1779–1802. Available at: https://doi.org/10.1016/j.clinthera.2006.11.015.

Shin, E.S., Sorenson, C.M. and Sheibani, N. (2014) “Diabetes and retinal vascular dysfunction,” *J Ophthalmic Vis Res*, 9(3), pp. 362–373. Available at: https://doi.org/10.4103/2008-322X.143378.

Soufi-zomorrod, M. *et al.* (2016) “MicroRNAs modulating angiogenesis: MIR-129-1 and Mir-133 act as Angio-Mir in huvecs,” *Tumor Biology*, 37(7), pp. 9527–9534. Available at: https://doi.org/10.1007/s13277-016-4845-0.

Stacker, S.A. *et al.* (2001) “VEGF-D promotes the metastatic spread of tumor cells via the lymphatics,” *Nature Medicine*, 7(2), pp. 186–191. Available at: https://doi.org/10.1038/84635.

Stavast, C. and Erkeland, S. (2019) “The non-canonical aspects of micrornas: Many roads to gene regulation,” *Cells*, 8(11), p. 1465. Available at: https://doi.org/10.3390/cells8111465.

Stuttfeld, E. and Ballmer-Hofer, K. (2009) “Structure and function of VEGF receptors,” *IUBMB Life*, 61(9), pp. 915–922. Available at: https://doi.org/10.1002/iub.234.

Suchting, S. *et al.* (2007) “The notch ligand delta-like 4 negatively regulates endothelial tip cell formation and vessel branching,” *Proceedings of the National Academy of Sciences*, 104(9), pp. 3225–3230. Available at: https://doi.org/10.1073/pnas.0611177104.

Suárez, Y. *et al.* (2008) “Dicer-dependent endothelial microrna s are necessary for postnatal angiogenesis,” *Proceedings of the National Academy of Sciences*, 105(37), pp. 14082–14087. Available at: https://doi.org/10.1073/pnas.0804597105.

Szekanecz, Z. and Koch, A.E. (2008) “Vascular involvement in rheumatic diseases: 'vascular rheumatology',” *Arthritis Research & Therapy*, 10(5), p. 224. Available at: https://doi.org/10.1186/ar2515.

Takahashi, H. and Shibuya, M. (2005) “The vascular endothelial growth factor (VEGF)/VEGF receptor system and its role under physiological and pathological conditions,” *Clinical Science*, 109(3), pp. 227–241. Available at: https://doi.org/10.1042/cs20040370.

Tang, P.A. and Moore, M.J. (2013) “AFLIBERCEPT in the treatment of patients with metastatic colorectal cancer: Latest findings and interpretations,” *Therapeutic Advances in Gastroenterology*, 6(6), pp. 459–473. Available at: https://doi.org/10.1177/1756283x13502637.

Tang, R. *et al.* (2021) ‘Proanthocyanidins as a potential novel way for the treatment of Hemangioma’, *BioMed Research International*, 2021, pp. 1–10. doi:10.1155/2021/5695378.

Tanzer, A. and Stadler, P.F. (2004) “Molecular evolution of a MicroRNA cluster,” *Journal of Molecular Biology*, 339(2), pp. 327–335. Available at: https://doi.org/10.1016/j.jmb.2004.03.065.

Thu, K.L. *et al.* (2018) “Targeting the cell cycle in breast cancer: Towards the next phase,” *Cell Cycle*, 17(15), pp. 1871–1885. Available at: https://doi.org/10.1080/15384101.2018.1502567.

Trichonas, G. and Kaiser, P.K. (2013) “Aflibercept for the treatment of age-related macular degeneration,” *Ophthalmology and Therapy*, 2(2), pp. 89–98. Available at: https://doi.org/10.1007/s40123-013-0015-2.

Ucuzian, A.A. *et al.* (2010) “Molecular Mediators of Angiogenesis,” *Journal of Burn Care & Research*, 31(1), pp. 158–175. Available at: https://doi.org/10.1097/bcr.0b013e3181c7ed82.

van Royen, N. *et al.* (2004) “*CD44* regulates arteriogenesis in mice and is differentially expressed in patients with poor and good collateralization,” *Circulation*, 109(13), pp. 1647–1652. Available at: https://doi.org/10.1161/01.cir.0000124066.35200.18.

Vanchinathan, V. *et al.* (2015) “The vascular marker CD31 also highlights histiocytes and histiocyte-like cells within cutaneous tumors,” *American Journal of Clinical Pathology*, 143(2), pp. 177–185. Available at: https://doi.org/10.1309/ajcprhm8czh5emfd.

Voellenkle, C. *et al.* (2012) “Deep-sequencing of endothelial cells exposed to hypoxia reveals the complexity of known and novel micrornas,” *RNA*, 18(3), pp. 472–484. Available at: https://doi.org/10.1261/rna.027615.111.

Walayat, A., Yang, M. and Xiao, D.L. (2019) “Therapeutic implication of Mirna in human disease,” *Antisense Therapy* [Preprint]. Available at: https://doi.org/10.5772/intechopen.82738.

Wang, J., Chen, J. and Sen, S. (2015) “MicroRNA as biomarkers and Diagnostics,” *Journal of Cellular Physiology*, 231(1), pp. 25–30. Available at: https://doi.org/10.1002/jcp.25056.

Wang, Q. *et al.* (2016) “Role of moesin in advanced glycation end products-induced angiogenesis of human umbilical vein endothelial cells,” *Scientific Reports*, 6(1). Available at: https://doi.org/10.1038/srep22749.

Wang, S. and Olson, E.N. (2009) “Angiomirs—key regulators of angiogenesis,” *Current Opinion in Genetics & Development*, 19(3), pp. 205–211. Available at: https://doi.org/10.1016/j.gde.2009.04.002.

Wang, X. *et al.* (2020) “Molecular bases of VEGFR-2-mediated physiological function and pathological role,” *Frontiers in Cell and Developmental Biology*, 8. Available at: https://doi.org/10.3389/fcell.2020.599281.

Ward, D.S. *et al.* (2010) “Expression and Localization of Angiogenic Growth Factors in Developing Porcine Mesonephric Glomeruli,” *Journal of Histochemistry & Cytochemistry*, 58(12), pp. 1045–1056. Available at: https://doi.org/10.1369/jhc.2010.956557.

Wei, Q. *et al.* (2014) “CD82 restrains pathological angiogenesis by altering lipid raft clustering and *CD44* trafficking in endothelial cells,” *Circulation*, 130(17), pp. 1493–1504. Available at: https://doi.org/10.1161/circulationaha.114.011096.

Wietecha, M.S. *et al.* (2011) “Sprouty2 downregulates angiogenesis during mouse skin wound healing,” *American Journal of Physiology-Heart and Circulatory Physiology*, 300(2), pp. H459–H467. Available at: https://doi.org/10.1152/ajpheart.00244.2010.

Wightman, B., Ha, I. and Ruvkun, G. (1993) “Posttranscriptional regulation of the heterochronic Gene Lin-14 by lin-4 mediates temporal pattern formation in C. elegans,” *Cell*, 75(5), pp. 855–862. Available at: https://doi.org/10.1016/0092-8674(93)90530-4.

Williams, C.K. *et al.* (2006) “Up-regulation of the notch ligand delta-like 4 inhibits VEGF-induced endothelial cell function,” *Blood*, 107(3), pp. 931–939. Available at: https://doi.org/10.1182/blood-2005-03-1000.

Witjas, F.M. *et al.* (2018) “Concise review: The Endothelial cell extracellular matrix regulates tissue homeostasis and repair,” *Stem Cells Translational Medicine*, 8(4), pp. 375–382. Available at: https://doi.org/10.1002/sctm.18-0155.

Wu, F., Yang, Z. and Li, G. (2009) “Role of specific microrna for endothelial function and angiogenesis,” *Biochemical and Biophysical Research Communications*, 386(4), pp. 549–553. Available at: https://doi.org/10.1016/j.bbrc.2009.06.075.

Xiao, Y. *et al.* (2019) “MicroRNA-133A and myocardial infarction,” *Cell Transplantation*, 28(7), pp. 831–838. Available at: https://doi.org/10.1177/0963689719843806.

Xie, M. *et al.* (2013) “Mammalian 5′-capped MicroRNA precursors that generate a single MicroRNA,” *Cell*, 155(7), pp. 1568–1580. Available at: https://doi.org/10.1016/j.cell.2013.11.027.

Xu, Z., Yu, Y. and Duh, E.J. (2006) “Vascular endothelial growth factor upregulates expression of *ADAMTS1* in endothelial cells through protein kinase C signaling,” *Investigative Opthalmology & Visual Science*, 47(9), p. 4059. Available at: https://doi.org/10.1167/iovs.05-1528.

Yang, B., Lu, Y. and Wang, Z. (2008) “Control of cardiac excitability by microrna s,” *Cardiovascular Research*, 79(4), pp. 571–580. Available at: https://doi.org/10.1093/cvr/cvn181.

Yeeles, J.T. *et al.* (2015) “Regulated eukaryotic DNA replication origin firing with purified proteins,” *Nature*, 519(7544), pp. 431–435. Available at: https://doi.org/10.1038/nature14285.

Zachary, I. and Morgan, R.D. (2010) “Therapeutic angiogenesis for cardiovascular disease: biological context, challenges, prospects,” *Heart*, 97(3), pp. 181–189. Available at: https://doi.org/10.1136/hrt.2009.180414.

Zhang, H. *et al.* (2004) “Single Processing Center models for human dicer and bacterial RNase III,” *Cell*, 118(1), pp. 57–68. Available at: https://doi.org/10.1016/j.cell.2004.06.017.

Zhang, J.-L. *et al.* (2012) “Secreted protein acidic and rich in cysteine (*SPARC*) suppresses angiogenesis by down-regulating the expression of VEGF and MMP-7 in gastric cancer,” *PLoS ONE*, 7(9). Available at: https://doi.org/10.1371/journal.pone.0044618.

Zhang, Q. *et al.* (2019) “ACE2 inhibits breast cancer angiogenesis via suppressing the VEGFA/VEGFR2/erk pathway,” *Journal of Experimental & Clinical Cancer Research*, 38(1). Available at: https://doi.org/10.1186/s13046-019-1156-5.

Zhou, Y. *et al.* (2021) “The role of the VEGF family in coronary heart disease,” *Frontiers in Cardiovascular Medicine*, 8. Available at: https://doi.org/10.3389/fcvm.2021.738325.

Zhu, H. *et al.* (2021) “Inflammation-Mediated Angiogenesis in Ischemic Stroke,” *Frontiers in Cellular Neuroscience*, 15. Available at: https://doi.org/10.3389/fncel.2021.652647.

Zhu, W. *et al.* (2021) “Macrophage migration inhibitory factor facilitates the therapeutic efficacy of mesenchymal stem cells derived exosomes in acute myocardial infarction through upregulating mir-133a-3p,” *Journal of Nanobiotechnology*, 19(1). Available at: https://doi.org/10.1186/s12951-021-00808-5.

Zirlik, K. and Duyster, J. (2018) “Anti-Angiogenics: Current Situation and Future Perspectives,” *Oncology Research and Treatment*, 41(4), pp. 166–171. Available at: https://doi.org/10.1159/000488087.

Appendix

Position	Gene Symbol	AVG ΔC_t		$2^{-\Delta C_t}$		Fold Change	p-value
		miR133a-3p VEGF 1h	miR-NC VEGF 1h	miR133a-3p VEGF 1h	miR-NC VEGF 1h	miR133a-3p VEGF 1h/miR-NC VEGF 1h	miR133a-3p VEGF 1h / miR-NC VEGF 1h
A01	ADAM10	2.37	2.87	0.19382	0.136999	1.41	0.010688
A02	ADAM17	4.33	4.38	0.049602	0.047931	1.03	0.967439
A03	AES	2.39	2.54	0.191036	0.172458	1.11	0.573270
A04	AXIN1	6.09	6.06	0.014722	0.01497	0.98	0.883499
A05	CBL	6	6.03	0.015596	0.015344	1.02	0.862729
A06	CCND1	3.04	2.06	0.121559	0.23953	0.51	0.032068
A07	CCNE1	7.54	6.74	0.005356	0.009343	0.57	0.003687
A08	CD44	4.81	3.01	0.035679	0.124391	0.29	0.002287
A09	CDKN1A	1.98	2.12	0.254345	0.229741	1.11	0.622333
A10	CFLAR	3.68	4.29	0.078231	0.051042	1.53	0.001997
A11	CHUK	4.52	5.16	0.043592	0.028058	1.55	0.474799
A12	CTNNB1	2.52	3.11	0.174498	0.116168	1.5	0.165019
B01	DLL1	7.63	7.76	0.005062	0.004599	1.1	0.868859
B02	DLL3	13.89	14.94	0.000066	0.000032	2.08	0.500788
B03	DLL4	3.54	6.41	0.086118	0.01174	7.34	0.002103
B04	EP300	5.11	5.08	0.028991	0.029642	0.98	0.744398
B05	ERBB2	6	6.48	0.015619	0.011181	1.4	0.084305
B06	FIGF	12.68	12.13	0.000152	0.000224	0.68	0.427723
B07	FOS	7.3	7.76	0.006344	0.004614	1.37	0.312468
B08	FOSL1	3.97	3.84	0.063655	0.069966	0.91	0.347284
B09	FZD7	11.95	12.28	0.000253	0.000201	1.26	0.608977
B10	GLI1	11.23	12.12	0.000415	0.000225	1.85	0.430816
B11	GSK3B	4.14	4.15	0.056579	0.056255	1.01	0.985468
B12	HDAC1	3.91	4.37	0.066313	0.04834	1.37	0.042302
C01	HES1	4.06	3.9	0.059933	0.066897	0.9	0.748074
C02	HEY1	6.71	8.12	0.009553	0.003606	2.65	0.003644
C03	HOXB4	8.25	8.04	0.003276	0.00381	0.86	0.663624
C04	HR	11.48	13.02	0.00035	0.000121	2.9	0.280384
C05	ID1	6.15	5.02	0.014127	0.030772	0.46	0.011025
C06	IFNG	15.93	16.78	0.000016	0.000009	1.81	0.333035
C07	IL2RA	15.83	16.69	0.000017	0.000009	1.81	0.358301
C08	JAG1	4.13	5.18	0.056924	0.027556	2.07	0.060391
C09	JAG2	4.1	5.45	0.058398	0.022886	2.55	0.008049
C10	KRT1	16.16	16.78	0.000014	0.000009	1.55	0.308032
C11	LFNG	6.84	6.92	0.00875	0.008239	1.06	0.840951
C12	LMO2	2.91	3.61	0.133194	0.081731	1.63	0.038285
D01	LOR	16.15	16.31	0.000014	0.000012	1.12	0.688941
D02	LRP5	7.55	7.59	0.005347	0.00519	1.03	0.851724
D03	MAML1	6.31	5.87	0.012626	0.017067	0.74	0.198066
D04	MAML2	6.44	6.51	0.011547	0.010951	1.05	0.889567
D05	MFNG	3.07	2.83	0.119359	0.140923	0.85	0.021107
D06	MMP7	8.32	8.22	0.003136	0.003351	0.94	0.664009
D07	NCOR2	4.53	4.27	0.04326	0.052003	0.83	0.495544
D08	NCSTN	3.27	3.61	0.103865	0.081666	1.27	0.000225
D09	NFKB1	5.71	6.01	0.01913	0.015483	1.24	0.441816
D10	NFKB2	5.4	5.68	0.023755	0.019526	1.22	0.387127
D11	NOTCH1	5.99	6.37	0.015696	0.012083	1.3	0.521508
D12	NOTCH2	6.14	5.67	0.014193	0.019697	0.72	0.141066
E01	NOTCH3	9.74	9.88	0.001168	0.001064	1.1	0.905228
E02	NOTCH4	4.5	5.81	0.044197	0.017865	2.47	0.011842
E03	NUMB	4.29	4.21	0.051166	0.054054	0.95	0.124417
E04	PAX5	15.62	16.36	0.00002	0.000012	1.67	0.426859
E05	POFUT1	7.7	7.9	0.0048	0.004199	1.14	0.366457
E06	PPARG	8.36	10.18	0.003044	0.000865	3.52	0.000338
E07	PSEN1	4.63	4.42	0.040491	0.046872	0.86	0.032367
E08	PSEN2	6	6.02	0.015611	0.0154	1.01	0.928805
E09	PSENEN	4.33	4.4	0.049687	0.047374	1.05	0.626692
E10	PTCRA	14.15	15.3	0.000055	0.000025	2.22	0.400245
E11	RBPJL	15.59	15.66	0.00002	0.000019	1.05	0.763113
E12	RFNG	5.21	5.44	0.027062	0.023039	1.17	0.088466
F01	RUNX1	6.81	6.06	0.008936	0.014977	0.6	0.033440
F02	SEL1L	3.35	3.84	0.097817	0.069881	1.4	0.006913
F03	SHH	11.97	11.35	0.00025	0.000382	0.65	0.007158
F04	SMO	7.62	7.37	0.005075	0.00603	0.84	0.105797
F05	SNW1	5.2	4.82	0.027124	0.035378	0.77	0.170943
F06	STAT6	4.16	3.93	0.055907	0.065676	0.85	0.108075
F07	TLE1	4.7	4.75	0.03838	0.037252	1.03	0.761570
F08	WISP1	12.63	15.4	0.000158	0.000023	6.83	0.000754
F09	ADA	4.92	4.89	0.033064	0.033743	0.98	0.912166
F10	AFAP1L2	9.3	12.01	0.001592	0.000242	6.57	0.056412
F11	DTX1	15.26	16.07	0.000025	0.000015	1.75	0.428849
F12	H19	11.49	13.47	0.000347	0.000088	3.93	0.032924
G01	Hes4	4.95	6.64	0.032401	0.010001	3.24	0.044112
G02	HES5	13.99	15.62	0.000062	0.00002	3.11	0.407130
G03	HEY2	10.02	10.17	0.000966	0.000868	1.11	0.872676
G04	HEYL	16	16.68	0.000015	0.00001	1.6	0.230238
G05	NRARP	5.7	7.11	0.019182	0.007259	2.64	0.046670
G06	SCGB1A1	15.64	16.78	0.00002	0.000009	2.22	0.048320
G07	SERPINA3	13.27	13.9	0.000101	0.000065	1.55	0.348460
G08	SLC6A12	16.66	16.78	0.00001	0.000009	1.09	0.629893
G09	SNAI2	10.11	9.59	0.000902	0.001301	0.69	0.321168
G10	TFF1	16.3	16.58	0.000012	0.00001	1.21	0.481258
G11	TNFSF10	4.19	4.23	0.054855	0.053357	1.03	0.877834
G12	UBD	10.53	10.94	0.000678	0.00051	1.33	0.547084
H01	ACTB	-2.73	-2.65	6.644773	6.274732	1.06	0.419120
H02	B2M	-0.76	-0.36	1.698719	1.28043	1.33	0.182271
H03	GAPDH	-1.15	-1.33	2.222983	2.508923	0.89	0.269595
H04	HPRT1	5.96	5.59	0.016051	0.020728	0.77	0.007666
H05	RPLP0	-1.31	-1.26	2.48292	2.393297	1.04	0.704859

Appendix 1: Differential gene expression analysis of RT2 ProfilerTM PCR Array Human Notch Signalling Pathway Plus Kit. HUVEC transfected with miR-133a-3p, or negative control miR-NC were stimulated with VEGF-A 165 for 1hour. Upregulated and down regulated genes are highlighted in red and green, respectively. Genes showing values of AVG ΔCt ≥10 indicating high number of amplification cycles required in the PCR analysis were not considered in further experiments to improve accuracy and reproducibility of data

Position	Gene Symbol	AVG ΔC_t		$2^{-\Delta C_t}$		Fold Change	p-value
		miR133a-3p VEGF 1h	miR-NC VEGF 1h	miR133a-3p VEGF 1h	miR-NC VEGF 1h	miR133a-3p VEGF 1h/miR-NC VEGF 1h	miR133a-3p VEGF 1h / miR-NC VEGF 1h
A01	ABL1	5.34	6.03	0.024615	0.015268	1.61	0.370162
A02	ANAPC2	6.51	7.12	0.011003	0.007179	1.53	0.163561
A03	ATM	7.71	7.98	0.004776	0.003964	1.2	0.872675
A04	ATR	8.28	8.4	0.003218	0.002964	1.08	0.764299
A05	AURKA	6.76	5.73	0.009201	0.018801	0.49	0.193957
A06	AURKB	9.17	7.13	0.001741	0.007153	0.24	0.117954
A07	BCCIP	4.74	4.44	0.037322	0.046224	0.81	0.358242
A08	BCL2	8.81	10.45	0.002229	0.000715	3.12	0.002742
A09	BIRC5	12.19	10.18	0.000215	0.000863	0.25	0.113655
A10	BRCA1	10.06	8.42	0.000936	0.00291	0.32	0.128632
A11	BRCA2	9.49	9.05	0.001395	0.001889	0.74	0.518049
A12	CASP3	4.08	4.58	0.05904	0.041737	1.41	0.568454
B01	CCNA2	7.19	4.63	0.006844	0.040408	0.17	0.007077
B02	CCNB1	6.88	4.77	0.008602	0.036538	0.23	0.014929
B03	CCNB2	8.04	5.97	0.003788	0.015924	0.24	0.101765
B04	CCNC	6.14	6.9	0.014182	0.008399	1.69	0.310672
B05	CCND1	2.69	2.97	0.155198	0.127381	1.22	0.750967
B06	CCND2	6.84	8.46	0.008759	0.00283	3.09	0.280935
B07	CCND3	3.61	5.03	0.082101	0.030607	2.68	0.029723
B08	CCNE1	7.52	7.47	0.005459	0.005632	0.97	0.907534
B09	CCNF	7.33	7.27	0.006214	0.006487	0.96	0.575306
B10	CCNG1	1.48	3.26	0.358697	0.104205	3.44	0.037099
B11	CCNG2	5.08	5.59	0.029486	0.020746	1.42	0.704174
B12	CCNH	6.44	7.4	0.011521	0.00594	1.94	0.576288
C01	CCNT1	6.45	7.22	0.011417	0.006717	1.7	0.805782
C02	CDC16	4.48	5.2	0.044827	0.027234	1.65	0.533739
C03	CDC20	8.37	6.42	0.003019	0.011709	0.26	0.08117
C04	CDC25A	8.32	8.1	0.00313	0.003657	0.86	0.57382
C05	CDC25C	12.28	10.35	0.000201	0.000764	0.26	0.260847
C06	CDC34	5.74	6.49	0.018661	0.011092	1.68	0.240041
C07	CDC6	7.66	6.54	0.004951	0.010772	0.46	0.223849
C08	CDK1	6.57	3.44	0.010508	0.0921	0.11	0.000581
C09	CDK2	6.22	6.2	0.013418	0.013595	0.99	0.983534
C10	CDK4	4.09	4.72	0.058805	0.038073	1.54	0.545356
C11	CDK5R1	9.49	9.87	0.001387	0.001067	1.3	0.530816
C12	CDK5RAP1	9.72	10.39	0.001187	0.000743	1.6	0.590426
D01	CDK6	4.61	6.94	0.04084	0.008172	5	0.067356
D02	CDK7	5.02	5.13	0.030758	0.028553	1.08	0.98645
D03	CDK8	7.4	7.42	0.005916	0.005848	1.01	0.912495
D04	CDKN1A	2.25	3.54	0.209834	0.085955	2.44	0.157594
D05	CDKN1B	4.96	5.77	0.032056	0.018345	1.75	0.489002
D06	CDKN2A	11.48	12.12	0.000349	0.000224	1.55	0.482616
D07	CDKN2B	7.18	8.71	0.00689	0.002394	2.88	0.094351
D08	CDKN3	7.19	6.41	0.006888	0.011727	0.59	0.33057
D09	CHEK1	7.44	6.66	0.00574	0.009899	0.58	0.283328
D10	CHEK2	8.09	8.63	0.003857	0.00253	1.45	0.432738
D11	CKS1B	6.14	4.94	0.014219	0.032558	0.44	0.159196
D12	CKS2	4.19	4.44	0.054895	0.046006	1.19	0.766768
E01	CUL1	5.12	5.19	0.02682	0.027368	1.05	0.918052
E02	CUL2	5.1	5.55	0.029246	0.02138	1.37	0.205873
E03	CUL3	3.82	4.62	0.070815	0.040534	1.75	0.448347
E04	E2F1	8.13	7.39	0.003577	0.005964	0.6	0.307408
E05	E2F4	4.36	5.41	0.048604	0.023558	2.06	0.501406
E06	GADD45A	6.33	5.55	0.012446	0.021391	0.58	0.133284
E07	GTSE1	8.37	6.45	0.003024	0.011404	0.27	0.087604
E08	HUS1	5.28	6.23	0.025811	0.013311	1.94	0.541133
E09	KNTC1	8.79	8.1	0.002266	0.003652	0.62	0.428603
E10	KPNA2	2.09	2.75	0.234331	0.148965	1.57	0.794139
E11	MAD2L1	7.9	6.16	0.004173	0.014016	0.3	0.130544
E12	MAD2L2	9.12	8.91	0.001795	0.002077	0.86	0.564985
F01	MCM2	7.9	6.7	0.004176	0.009641	0.43	0.060139
F02	MCM3	6.32	5.57	0.012524	0.021659	0.59	0.182968
F03	MCM4	7.4	6.29	0.005925	0.012761	0.46	0.007047
F04	MCM5	6.28	5.84	0.012686	0.017422	0.74	0.579795
F05	MDM2	2.68	3.82	0.155521	0.070568	2.2	0.104164
F06	MKI67	7	5.16	0.007788	0.0279	0.28	0.245959
F07	MNAT1	6.4	7.08	0.011809	0.007386	1.6	0.551554
F08	MRE11A	6.51	6.8	0.010994	0.008984	1.22	0.966266
F09	NBN	4.84	5.69	0.034921	0.019365	1.8	0.092656
F10	RAD1	6.49	7.16	0.01111	0.006969	1.59	0.476448
F11	RAD17	6.4	7.3	0.011843	0.006341	1.87	0.241411
F12	RAD51	9.4	8.35	0.001478	0.003064	0.48	0.238363
G01	RAD9A	8.4	8.51	0.002954	0.002752	1.08	0.936191
G02	RB1	5.49	5.56	0.022225	0.021268	1.05	0.933481
G03	RBBP8	8.25	8.15	0.00329	0.003516	0.94	0.936822
G04	RBL1	7.71	7.21	0.004772	0.006754	0.71	0.415562
G05	RBL2	5.35	5.93	0.024592	0.016415	1.5	0.548759
G06	SERTAD1	6.5	7.16	0.011049	0.006976	1.58	0.267238
G07	SKP2	7.09	7.14	0.007348	0.007102	1.03	0.73783
G08	STMN1	2.5	1.52	0.176889	0.348554	0.51	0.032378
G09	TFDP1	4.22	3.63	0.053894	0.080782	0.66	0.455342
G10	TFDP2	7.18	7.67	0.006887	0.004909	1.4	0.922733
G11	TP53	3.04	3.74	0.121287	0.074857	1.62	0.614892
G12	WEE1	5.01	5.49	0.0311	0.022296	1.39	0.373908
H01	ACTB	-2.49	-2.53	5.637138	5.76735	0.98	0.847387
H02	B2M	-0.12	0.22	1.087523	0.8606	1.26	0.432388
H03	GAPDH	-1.18	-1.71	2.269593	3.269933	0.7	0.385742
H04	HPRT1	4.65	4.97	0.039753	0.032014	1.24	0.485624
H05	RPLP0	-0.85	-0.96	1.807953	1.929933	0.94	0.734311

Appendix 2: Differential gene expression analysis of RT2 ProfilerTM PCR Array Human Cell Cycle Kit. HUVEC transfected with miR-133a-3p, or negative Control miR-NC were stimulated with VEGF-A165 for 1hour. Upregulated and downregulated genes are highlighted in red and green, respectively. Genes showing values of AVG ΔCt≥10 indicating high number of amplification cycles required in the PCR analysis were not considered in further experiments to improve accuracy and reproducibility of data.

Position	Gene Symbol	AVG ΔC_t		$2^{-\Delta C_t}$		Fold Change	p-value
		miR133a-3p VEGF 1h	miR-NC VEGF 1h	miR133a-3p VEGF 1h	miR-NC VEGF 1h	miR133a-3p VEGF 1h/miR-NC VEGF 1h	miR133a-3p VEGF 1h / miR-NC VEGF 1h
A01	ADAMTS1	3.51	4.63	0.087613	0.040452	2.17	0.009728
A02	ADAMTS13	12.76	13.14	0.000145	0.000111	1.30	0.425539
A03	ADAMTS8	16.85	16.41	0.000008	0.000011	0.73	0.557347
A04	CD44	3.12	2.32	0.115321	0.200883	0.57	0.032911
A05	CDH1	16.85	17.27	0.000008	0.000006	1.33	0.752087
A06	CLEC3B	13.88	13.13	0.000067	0.000112	0.60	0.642833
A07	CNTN1	14.66	13.55	0.000039	0.000084	0.46	0.347898
A08	COL11A1	14.94	16.46	0.000032	0.000011	2.87	0.291711
A09	COL12A1	6.17	7.21	0.013842	0.006753	2.05	0.153185
A10	COL14A1	12.18	11.44	0.000215	0.000359	0.60	0.288410
A11	COL15A1	14.64	15.9	0.000039	0.000016	2.40	0.472659
A12	COL16A1	11.86	11.62	0.000269	0.000318	0.85	0.625143
B01	COL1A1	14.86	12.47	0.000034	0.000176	0.19	0.054788
B02	COL4A2	0.35	1.17	0.785597	0.44353	1.77	0.185808
B03	COL5A1	2.22	3.33	0.214854	0.099275	2.16	0.141926
B04	COL6A1	5.58	6.02	0.020913	0.015454	1.35	0.467034
B05	COL6A2	10.59	10.13	0.000651	0.000892	0.73	0.975068
B06	COL7A1	14.68	14.35	0.000038	0.000048	0.80	0.765503
B07	COL8A1	4.25	3.45	0.05246	0.09175	0.57	0.521567
B08	CTGF	-0.35	-0.8	1.272852	1.735088	0.73	0.601233
B09	CTNNA1	2.02	1.99	0.245921	0.251472	0.98	0.961821
B10	CTNNB1	2.57	3.55	0.168494	0.085373	1.97	0.024149
B11	CTNND1	3.42	3	0.093283	0.125032	0.75	0.264605
B12	CTNND2	16.8	15.62	0.000009	0.00002	0.44	0.336888
C01	ECM1	9.44	9.05	0.001437	0.001885	0.76	0.640300
C02	FN1	-2.43	-1.94	5.375817	3.837224	1.40	0.256214
C03	HAS1	13.49	13.91	0.000087	0.000065	1.34	0.941511
C04	ICAM1	3.17	4	0.111119	0.062604	1.77	0.116271
C05	ITGA1	7.13	8.1	0.00716	0.003652	1.96	0.251296
C06	ITGA2	3.84	3.48	0.069607	0.089804	0.78	0.014392
C07	ITGA3	3.25	2.89	0.105097	0.134514	0.78	0.497416
C08	ITGA4	6.49	7.9	0.011127	0.004184	2.66	0.345427
C09	ITGA5	0.44	0.9	0.739286	0.535757	1.38	0.188920
C10	ITGA6	2.1	3.27	0.232914	0.103672	2.25	0.004711
C11	ITGA7	13.45	13.93	0.00009	0.000064	1.40	0.191173
C12	ITGA8	11.79	15.66	0.000282	0.000019	14.60	0.001639
D01	ITGAL	15.52	16.38	0.000021	0.000012	1.81	0.231277
D02	ITGAM	16.59	16.47	0.00001	0.000011	0.92	0.850826
D03	ITGAV	1.72	2.31	0.302769	0.202065	1.50	0.097940
D04	ITGB1	-0.32	-0.06	1.250113	1.039281	1.20	0.095719
D05	ITGB2	10.98	12.45	0.000495	0.000179	2.76	0.153679
D06	ITGB3	4.55	4.41	0.042643	0.046962	0.91	0.731497
D07	ITGB4	6.89	6.58	0.008432	0.010462	0.81	0.652303
D08	ITGB5	2.54	3.01	0.171767	0.123782	1.39	0.366620
D09	ANOS1	14.11	12.67	0.000056	0.000154	0.37	0.124574
D10	LAMA1	15.86	17.27	0.000017	0.000006	2.65	0.229367
D11	LAMA2	9.66	10.19	0.001232	0.000854	1.44	0.430870
D12	LAMA3	9.18	8.99	0.001719	0.001964	0.88	0.678911
E01	LAMB1	1.13	1.58	0.456631	0.334105	1.37	0.201049
E02	LAMB3	9.75	8.26	0.001163	0.003255	0.36	0.256610
E03	LAMC1	0.89	1.36	0.538577	0.389106	1.38	0.056254
E04	MMP1	-0.53	-0.02	1.4419	1.017202	1.42	0.238318
E05	MMP10	4.56	4.12	0.041799	0.057384	0.73	0.637562
E06	MMP11	7.68	7.11	0.00487	0.007256	0.67	0.424430
E07	MMP12	10.63	14.78	0.00063	0.000036	17.71	0.373191
E08	MMP13	16.48	16.23	0.000011	0.000013	0.84	0.628353
E09	MMP14	2.4	2.19	0.189256	0.218687	0.87	0.871463
E10	MMP15	12.49	13.47	0.000174	0.000088	1.98	0.231498
E11	MMP16	5.69	6.27	0.019349	0.012915	1.59	0.183187
E12	MMP2	1.11	0.97	0.462092	0.50978	0.91	0.573546
F01	MMP3	13.73	13.89	0.000074	0.000066	1.12	0.731364
F02	MMP7	10.01	9.54	0.000971	0.001345	0.72	0.818732
F03	MMP8	16.38	16.57	0.000012	0.00001	1.13	0.813477
F04	MMP9	16.32	15.66	0.000012	0.000019	0.63	0.402307
F05	NCAM1	13.29	15.91	0.0001	0.000016	6.17	0.046454
F06	PECAM1	3.31	3.93	0.100651	0.065422	1.54	0.621359
F07	SELE	5.1	5.97	0.029148	0.015907	1.83	0.402759
F08	SELL	9.08	7.93	0.001846	0.004089	0.45	0.074673
F09	SELP	7.77	6.92	0.004583	0.00828	0.55	0.205867
F10	SGCE	4.99	5.51	0.031477	0.021938	1.43	0.251018
F11	SPARC	-1.58	-0.56	2.994117	1.47936	2.02	0.001120
F12	SPG7	5.56	5.51	0.021163	0.021955	0.96	0.954220
G01	SPP1	9.38	10.76	0.001504	0.000578	2.60	0.302247
G02	TGFBI	4.75	5.62	0.037102	0.020382	1.82	0.287751
G03	THBS1	-3.9	-2.88	14.896099	7.376909	2.02	0.015251
G04	THBS2	10.27	11.16	0.000811	0.000437	1.85	0.406394
G05	THBS3	9.68	8.72	0.001221	0.002372	0.51	0.121761
G06	TIMP1	4.58	4.18	0.041804	0.055082	0.76	0.243837
G07	TIMP2	0.64	0.84	0.642926	0.559352	1.15	0.565337
G08	TIMP3	7.99	11.04	0.003943	0.000476	8.29	0.386948
G09	TNC	16.46	14.38	0.000011	0.000047	0.24	0.288267
G10	VCAM1	9.01	8.13	0.001942	0.00357	0.54	0.812977
G11	VCAN	14.3	11.39	0.000049	0.000373	0.13	0.242396
G12	VTN	11.24	13.16	0.000413	0.000109	3.77	0.325615
H01	ACTB	-2.91	-2.88	7.510101	7.375274	1.02	0.827371
H02	B2M	-0.27	-0.37	1.207778	1.288915	0.94	0.742064
H03	GAPDH	-1.44	-1.29	2.718774	2.444897	1.11	0.601017
H04	HPRT1	5.66	5.36	0.019746	0.024336	0.81	0.299149
H05	RPLP0	-1.04	-0.82	2.05343	1.767995	1.16	0.667373

Appendix 3: Differential gene expression analysis of RT2 ProfilerTM PCR Array Human Extracellular Matrix and Cell Adhesion Molecules Kit. HUVEC transfected with miR-133a-3p, or negative control miR-NC were stimulated with VEGF-A165 for 4hour. Upregulated and downregulated genes are highlighted in red and green, respectively. Genes showing values of AVG ΔCt≥10 indicating high number of amplification cycles required in the PCR analysis were not considered in further experiments to improve accuracy and reproducibility of data.

Genes	miR-133a-3p/5p	position	MIR WALK/ Score %	Targetscan/ Score %	MiRDB/ Score %	predicted binding sites
MSN	3p	3UTR	no	yes/ 98%	yes/ 92%	Position 140-147 of MSN 3' UTR
PLAUR	3p	3UTR	yes/ 92%	no	no	Position 241 and position 732 of PLAUR 3' UTR
CCND3	5p	3UTR	no	yes/ 18% and 23%	yes/ 61%	Position 226 and position 294 of CCND3 3' UTR
CD44	5p	3UTR	yes/ 92%	yes/ 21%	no	Position 3063-3070 of CD44 3' UTR
CCNE1	3P	3UTR	yes/ 85%	no	no	Position 1828- 1846 of CCNE1 3' UTR
CCND1	3P	CDS	yes/ 92%	no	no	Position 427-472 of CCND1 CDS
DLL4	3P	3UTR	yes/ 92%	no	no	Position 1794-2838 3'UTR position 2184-2209 CDS
HEY1	3P	3UTR	yes/ 85%	no	no	Position 1482-1532 of HEY1 3' UTR
JAG2	3P	CDS	yes/ 100%	no	no	Position 1616-1650 of JAG2 CDS
NOTCH4	3P	CDS	yes/ 100%	no	no	Position 2179-2200 of NOTCH4 CDS
HES4	3P	CDS	yes/ 85%	no	no	Position 230-264 of HES4 CDS
TIMP3	3P	CDS	yes/ 85%	no	no	Position 332-356 of TIMP3 CDS
ITGA6	5P	3UTR	yes/ 85%	no	no	Position 3729-3749 of ITGA6 3' UTR
ADAMTS1	3P	3UTR	yes/ 82%	no	no	Position 3405-3445 of ADAMTS1 3' UTR
THBS1	3P	CDS	yes/ 85%	no	no	Position 183-203 of THBS1 CDS
SPARC	3P	3UTR	yes/ 85%	no	no	Position 2589-2622 of SPARC 3' UTR
CCNB1	3P	CDS	yes/ 92%	no	no	Position 845-868 of CCNB1 CDS
MCM2	5P	CDS	yes/ 85%	no	no	Position 1062-1081 of MCM2 CDS

Appendix 4: List of the predicted score of the differentiated genes which have miR-133a-3p or -5p binding sites in either the coding region (CDS) or 3'UTR of the 3 bioinformatic databases, miRWalk, miRDB or Target Scan. The 3'UTR of *CD44's* RNA was cloned as 2 out 3 bioinformatic databases predicted miR-133a-5p directly binding to the 3'UTR of *CD44's* RNA at position 3063-3070, with a prediction score of 92% on miRWalk and 21% on target scan.